

POLY(LACTIC ACID) BLENDS, COMPOSITES AND FIBERS  
AND  
DIRECT PYROLYSIS MASS SPECTROMETRY FOR NANOCCLAY COMPOSITES

A THESIS SUBMITTED TO  
THE GRADUATE SCHOOL OF NATURAL AND APPLIED SCIENCES  
OF  
MIDDLE EAST TECHNICAL UNIVERSITY

BY

ESRA ÖZDEMİR

IN PARTIAL FULFILLMENT OF THE REQUIREMENTS  
FOR  
THE DEGREE OF DOCTOR OF PHILOSOPHY  
IN  
POLYMER SCIENCE AND TECHNOLOGY

NOVEMBER 2017



Approval of the thesis:

**POLY(LACTIC ACID) BLENDS, COMPOSITES AND FIBERS  
AND DIRECT PYROLYSIS MASS SPECTROMETRY FOR NANOCCLAY  
COMPOSITES**

submitted by **ESRA ÖZDEMİR** in partial fulfillment of the requirements for the degree  
of **Doctor of Philosophy in Polymer Science and Technology Department, Middle  
East Technical University** by,

Prof. Dr. Gülbin Dural Ünver  
Dean, Graduate School of **Natural and Applied Sciences**

\_\_\_\_\_

Prof. Dr. Necati Özkan  
Head of Department, **Polymer Science and Technology**

\_\_\_\_\_

Prof. Dr. Jale Hacaloğlu  
Supervisor, **Chemistry Dept., METU**

\_\_\_\_\_

Prof. Dr. Ceyhan Kayran İşçi  
Co-supervisor, **Chemistry Dept., METU**

\_\_\_\_\_

**Examining Committee Members:**

Prof. Dr. Nursel Dilsiz  
Chemical Engineering Dept., Gazi University

\_\_\_\_\_

Prof. Dr. Jale Hacaloğlu  
Chemistry Dept., METU

\_\_\_\_\_

Prof. Dr. Necati Özkan  
Polymer Science and Technology Dept., METU

\_\_\_\_\_

Assoc. Prof. Dr. Emren Nalbant Esentürk  
Chemistry Dept., METU

\_\_\_\_\_

Assoc. Prof. Dr. Tamer Uyar  
UNAM, Bilkent University

\_\_\_\_\_

Date: 09/11/2017

**I hereby declare that all information in this document has been obtained and presented in accordance with academic rules and ethical conduct. I also declare that, as required by these rules and conduct, I have fully cited and referenced all material and results that are not original to this work.**

Name, Last name: Esra ÖZDEMİR

Signature:

## **ABSTRACT**

### **POLY(LACTIC ACID) BLENDS, COMPOSITES AND FIBERS AND DIRECT PYROLYSIS MASS SPECTROMETRY FOR NANOCCLAY COMPOSITES**

Özdemir, Esra

Ph.D., Polymer Science and Technology Department

Supervisor : Prof. Dr. Jale Hacaloğlu

Co-Supervisor : Prof. Dr. Ceyhan Kayran İşçi

November 2017, 171 pages

In the first part of this study, poly(lactic acid)-poly(ethylene glycol), PLA-PEG, blends, composites and electrospun fibers of PLA and PLA composites, PLA-PEG blends and PLA-PEG, blends composites were prepared and characterized. X-ray Diffractometer (XRD), Scanning Electron Microscope (SEM), Transmission Electron Microscope (TEM), Gel Permeation Chromatography (GPC), Simultaneous Thermal Analyzer (STA) and Direct Pyrolysis Mass Spectrometer (DP-MS) techniques were used for characterization studies.

Both TGA and DP-MS analyses of PLA-PEG blends involving 10, 15 and 20 wt% PEG pointed out that the thermal decomposition occurred mainly in two steps. An interaction between COOH groups of PLA and ether linkages of PEG due to

blending process was detected. Addition of 20 wt% PEG decreased the tensile strength and tensile modulus of PLA while improving its ductility due to its plasticization effect. Enhancement in the chemical interactions between PLA and PEG in the presence of Cloisite 30B (C30B) was observed. Also, tensile strength, %elongation at break and Young's modulus were increased compared to the corresponding blends. Fiber formation not only effected thermal degradation behaviors of PLA, PLA-PEG blends and corresponding composites but also affected the morphology. The intermolecular trans-esterification reactions were enhanced upon fiber formation. Better delamination and intercalation of PLA chains into clay layers of Cloisite 15A (C15A), Cloisite 20A (C20A) and C30B were detected. On the other hand, the interaction between PLA and PEG decreased and phase separation during the electrospinning process was recorded upon fiber generation. On the contrary, in the presence of C30B, the interactions between PLA and PEG were enhanced and the phase separation was not detected for PLA-PEG composite fibers.

In the second part of this study, the use of direct pyrolysis mass spectrometry to characterize polymer/organoclay systems was discussed. DP-MS analyses of poly(lactic acid) (PLA), poly(methyl methacrylate), (PMMA) and poly(ethylene) (PE) composites involving organically modified montmorillonites C15A, C20A, C25A (Cloisite 25A), C93A, (Cloisite 93A) or C30B showed that the technique supplies strong evidences for the extent and type of dispersion of clay layers in the polymer matrices. In addition, the technique allows identification of possible interactions between the polymer and the organic modifier.

**Keywords:** Poly(lactic acid), Poly(ethylene glycol), Blends, Composites, Electrospun Fibers.

## ÖZ

# **POLİ(LAKTİK ASİT) KARIŞIMLARI, KOMPOZİTLERİ VE LİFLERİ VE DİREKT PİROLİZ KÜTLE SPEKTROMETRESİNİN NANOKİL KOMPOZİTLERİNDE KULLANIMI**

Özdemir, Esra

Doktora, Polimer Bilimi ve Teknolojisi Bölümü

Tez Yöneticisi : Prof. Dr. Jale Hacaloğlu

Ortak Tez Yöneticisi : Prof. Dr. Ceyhan Kayran İşçi

Kasım 2017, 171 sayfa

Bu tez çalışmasının ilk kısmında, poli(laktik asit)-poli(etilen glikol), PLA-PEG karışımları, kompozitleri ve PLA'nın, PLA kompozitlerinin, PLA-PEG karışımlarının ve kompozitlerinin elektroçirme lifleri hazırlanıp karakterize edilmiştir. Karakterizasyon çalışmaları; X-ışınları difraksiyonu (XRD), taramalı elektron mikroskobu (SEM), geçirimli elektron mikroskobu (TEM), jel geçirgenlik kromatografisi (GPC), simultane termal analizör (STA), direkt piroliz kütle spektrometresi (DP-MS) yöntemleriyle yapılmıştır.

Kütlece 10, 15 ve %20 PEG içeren PLA-PEG karışımlarının TGA ve DP-MS analizleri termal bozunumun iki basamakta gerçekleştiğini ortaya çıkarmıştır. PLA'nın COOH gruplarıyla PEG'in eter grupları arasında karışım sırasında etkileşim olduğu gözlenmiştir. Kütlece %20 PEG eklenmesi PLA'nın çekme gücü ve Young

modülünü azaltırken plastikleştirme etkisi sebebiyle sünekliğini arttırmıştır. PLA ve PEG arasındaki etkileşim Cloisite 30B (C30B)'nin varlığında artmıştır. Ayrıca, çekme gücü, çekmede uzama ve Young modülü C30B'nin varlığında saf karışımlara oranla artmıştır. PLA'nın, PLA-PEG karışımlarının ve PLA kompozitlerinin lifleştirilmesi ise hem termal hem de morfolojik özellikleri etkilemiştir. PLA'nın lifleştirilmesi sonucunda moleküller arası trans-esterifikasyon reaksiyonlarında artış olduğu gözlenmiştir. PLA'nın Cloisite 15A, (C15A), Cloisite 20A, (C20A) ve C30B içeren kompozitlerinin lifleri incelendiğinde ise, kil tabakalarının lif yapılarında yapraklanma ya da saçılma oranlarının arttığı farkedilmiştir. PLA-PEG liflerine bakılınca ise PLA ve PEG arasındaki etkileşimin azaldığı ve elektroğirme prosesi esnasında faz ayrımı yaşandığı gözlemlenmiştir. C30B'nin varlığında ise PLA ve PEG arasındaki etkileşim tekrar artarken faz ayrımı ortadan kalkmıştır.

Bu çalışmanın ikinci kısmında ise, direkt piroliz kütle spektrometresinin polimer/organokil sistemlerinin karakterizasyonunda kullanılması çalışmaları araştırılmıştır. Poli(laktik asit) (PLA), poli(metil metakrilat) (PMMA) ve poli(etilen) (PE)'nin C15A, C20A, C25A (Cloisite 25A), C93A, (Cloisite 93A) veya C30B içeren kompozitlerinin DP-MS analizleri, bu tekniğin kil tabakalarının polimer matrisi içerisindeki dağılım seviyesi hakkında bilgi sağladığı tespit edilmiştir. Bu teknik ayrıca polimer zincirleri ve killerin sahip olduğu organik düzenleyici arasındaki olası reaksiyonu da ortaya koymaktadır.

**Anahtar kelimeler:** Poli(laktik asit), Poli(etilen glikol), Karışımlar, Kompozitler, Elektroğirme Lifler.



*To my mother,  
without whom none of my success would be possible..*

## ACKNOWLEDGEMENTS

I would like to express my sincere thanks to my supervisor Prof. Dr. Jale Hacalođlu for her support. Without her guidance I could not accomplish this journey.

I want to thank to my co-supervisor Prof. Dr. Ceyhan Kayran İřçi for her support through the work.

I thank to Dr. Ümit Tayfun not only for his help for preparation and characterization of blends and composites used in this work but also his mentorship and friendship.

I want to express my feelings to Nehir Utku and Melis Kesik how I feel blessed with their friendship. Thank you for sharing my happiness and sadness since 2008, and more importantly for being my family in Ankara.

I want to thank my dear friend Seza Göker for her precious friendship and constant supports and for showing me how to be strong against difficulties.

I would also extend my deep gratitude to Baki Er for his constant motivations and lovely patience against my whining. I cannot thank him enough and I am glad to have him in my life.

I also want to thank my dear lab mates, Ayşegül Hisar Telli and Halil İpek for their friendships and motivations.

I would also express my deep gratitude to my brother Kađan Özdemir who made me thinking about for starting to the graduate education and made me believe in myself.

Finally, I would like to present my deepest thanks to my mother, Nurten Özdemir, and my father, Ali Özdemir, for their endless supports, encouragements and patience.

Thank you for believing me.

## TABLE OF CONTENTS

ABSTRACT.....	v
ÖZ .....	vii
ACKNOWLEDGEMENTS .....	x
TABLE OF CONTENTS .....	xi
LIST OF TABLES .....	xv
LIST OF FIGURES .....	xvii
LIST OF SCHEMES.....	xxiii
LIST OF ABBREVIATIONS .....	xxiv
CHAPTERS	
1.INTRODUCTION .....	1
1.1. Poly(lactic acid) .....	1
1.2. Polymer Blends .....	4
1.2.1. Blending Techniques.....	6
1.2.2. PLA Based Blends .....	7
1.3. Polymer Composites .....	11
1.3.1. Nanoclays.....	12
1.3.2. Nanoclay-Polymer Interaction .....	14
1.3.3. Structural Characterization of Composites .....	15
1.3.4. Nanoclay Based Composites.....	17

1.3.4.1.Composites of PLA with Nanoclays .....	18
1.3.4.2.Composites of PLA-PEG Blends with Nanoclays .....	20
1.4. Polymer Fibers .....	20
1.4.1. Electrospinning.....	21
1.4.2. Electrospun Fibers.....	23
1.4.2.1.PLA Fibers .....	25
1.5. Aim of Work .....	28
2.EXPERIMENTAL.....	31
2.1. Materials.....	31
2.2. Preparation Methods .....	33
2.2.1. Preparation of PLA Based Blends, Composites and Electrospun Fibers.....	33
2.2.1.1.Preparation of PLA-PEG Blends with 90/10, 85/15 and 80/20 Blend Ratios and Their Composites Involving Cloisite 30B .....	33
2.2.1.2.Preparation of Electrospun Fibers .....	35
2.2.1.2.1.Preparation of Electrospun Fibers of PLA Composites Involving Cloisite 15A, Cloisite 20A and Cloisite 30B .....	36
2.2.1.2.2.Preparation of Electrospun Fibers of PLA-PEG Blends and Fibers of Blend Composites Involving Cloisite 30B .....	37
2.2.2. Preparation of PLA, PMMA and PE Composites Involving Several Organoclays for Morphological Characterization Studies of Polymer/Clay Composite Systems via DP-MS .....	37
2.3. Characterization Techniques .....	39
2.3.1. X-ray Diffractometer (XRD).....	39

2.3.2. Transmission Electron Microscope (TEM).....	39
2.3.3. Scanning Electron Microscope (SEM).....	40
2.3.4. Molecular Masses and Polydispersity .....	40
2.3.5. Mechanical Analyses .....	40
2.3.5.1.Simultaneous Thermal Analyses (STA) .....	41
2.3.5.2.Direct Pyrolysis Mass Spectrometer (DP-MS) .....	42
3.RESULTS AND DISCUSSIONS.....	45
3.1. PLA Based Blends, Composites and Fibers.....	45
3.1.1. PLA-PEG Blends And Composites Involving Cloisite 30B.....	46
3.1.1.1.Poly(lactic acid)-poly(ethylene glycol), PLA-PEG Blends .....	46
3.1.1.1.1.Thermal Analyses.....	46
3.1.1.1.2.Mechanical Properties .....	58
3.1.1.2.PLA-PEG Composites Involving Cloisite 30B .....	59
3.1.1.2.1.Morphological Analyses .....	59
3.1.1.2.2.Thermal Analyses.....	63
3.1.1.2.3.Mechanical Properties .....	74
3.1.1.2.4.Molecular Masses and Dispersity .....	75
3.1.2. Electrospun Fibers of PLA Based Systems.....	76
3.1.2.1.Electrospun Fibers of PLA.....	77
3.1.2.1.1.Morphological Analyses .....	77
3.1.2.1.2.Thermal Analyses.....	79
3.1.2.2.Electrospun Fibers of PLA Composites Involving Cloisite 15A, Cloisite 20A and Cloisite 30B.....	81

3.1.2.2.1.Morphological Analyses .....	81
3.1.2.2.2.Thermal Analyses.....	87
3.1.2.3.Electrospun Fibers of PLA-PEG Blends.....	94
3.1.2.3.1.Morphological Analyses .....	95
3.1.2.3.2.Thermal Analyses.....	96
3.1.2.4.Electrospun Fibers of PLA-PEG Composites Involving C30B..	102
3.1.2.4.1.Morphological Analyses .....	103
3.1.2.4.2.Thermal Analyses.....	105
3.2. Direct Pyrolysis Mass Spectrometry to Characterize Morphology of The Polymer/Organoclay Systems .....	112
3.2.1. X-Ray Diffractometry Analysis .....	116
3.2.2. Direct Pyrolysis Mass Spectrometry Analyses .....	119
3.2.2.1.Organoclays; C15A, C20A, C25A, C93A and C30B .....	119
3.2.2.2.Polymers; PLA, PMMA and PE .....	122
3.2.2.3.PLA, PMMA and PE Composites.....	124
4.CONCLUSION.....	137
REFERENCES.....	143
CURRICULUM VITAE .....	167

## LIST OF TABLES

### TABLES

<b>Table 1:</b> Properties of montmorillonites.....	32
<b>Table 2:</b> Mixing methods and process parameters of composites involving 3-5 wt% organoclay.....	38
<b>Table 3:</b> TGA data of neat PLA, neat PEG, PLA-PEG blends with 10 wt%, 15wt% and 20 wt% PEG.....	49
<b>Table 4:</b> Tensile test results of neat PLA, PLA-PEG blends with 10 wt%, 15wt% and 20 wt% PEG.....	59
<b>Table 5:</b> DTA results of PLA-PEG blends and composites involving C30B detected during the second heating cycles.....	66
<b>Table 6:</b> TGA data of neat PLA, neat PEG, PLA-PEG blends and their composites involving C30B.....	67
<b>Table 7:</b> Tensile test results of neat PLA, PLA-PEG blends and their composites involving C30B.....	75
<b>Table 8:</b> Number averaged and weight averaged molecular weights and polydispersity indexes of neat PLA, PLA-PEG blends and composites involving C30B.....	76
<b>Table 9:</b> TGA data of neat PLA, PLA composites involving C15A, C20A and C30B and their corresponding fibers.....	90
<b>Table 10:</b> TGA data of neat PLA, neat PEG, and fibers of PLA and PLA-PEG blends.....	99
<b>Table 11:</b> TGA data of neat PLA, neat PEG, PLA fiber, PLA-PEG blends and composites involving C30B and their corresponding fibers.....	108

**Table 12:** DP-MS and XRD data for the organoclays and corresponding composites.  
..... 127



## LIST OF FIGURES

### FIGURES

<b>Figure 1:</b> Chemical structure of poly(lactic acid), PLA.....	2
<b>Figure 2:</b> Chemical structure of poly(ethylene glycol), PEG.....	8
<b>Figure 3:</b> Schematic of ion-exchange reactions including (a) monolayer, (b) bilayer or (c), (d) inclined paraffin structures. ....	14
<b>Figure 4:</b> Types of composite structures: a) microcomposite b) intercalated nanocomposites c) exfoliated nanocomposites. ....	15
<b>Figure 5:</b> Structure of electrospun fibers. ....	23
<b>Figure 6:</b> Representation of dog-bone specimen.....	34
<b>Figure 7:</b> Electrospinning setup used for generation of fibers. ....	35
<b>Figure 8:</b> DTA curves of neat PLA, neat PEG, PLA-PEG blends with 10 wt%, 15wt% and 20 wt% PEG.....	47
<b>Figure 9:</b> a) TGA b) DTG curves of neat PLA, neat PEG, PLA-PEG blends with 10 wt%, 15wt% and 20 wt% PEG. ....	48
<b>Figure 10:</b> Total ion current curves and recorded mass spectrum of neat PLA, neat PEG and PLA-PEG blends at the recorded peak maxima. ....	50
<b>Figure 11:</b> Single ion evolution profiles of some selected products recorded during the pyrolysis of a) neat PLA, b) PLA-PEG blend with 10 wt% PEG, PLA90-PEG10 and c) neat PEG.....	51
<b>Figure 12:</b> Single ion evolution profiles of some selected products recorded during the pyrolysis of a) PLA90-PEG10, b) PLA85-PEG15, c) PLA80-PEG20 blends. ...	54
<b>Figure 13:</b> Single ion evolution profiles of selected products recorded during the pyrolysis of solution mixed PLA80-PEG20 blends having a) 1 h, b) 12 h, and c) 24 h mixing time and the pyrolysis of d) melt mixed PLA80-PEG20 blend.....	57

<b>Figure 14:</b> XRD diffractogram of C30B and PLA-PEG blend composites involving C30B.....	60
<b>Figure 15:</b> TEM images of a) neat PEG, b) neat PLA, and PLA-PEG blend composites with c,d) 10 wt%, e,f) 15 wt%, g,h) 20 wt% PEG amounts at low (bar scale= 500 nm) and high (bar scale= 100 nm) magnifications. ....	62
<b>Figure 16:</b> DTA curves of neat PLA, neat PEG, PLA-PEG blends with 10 wt%, 15wt% and 20 wt% PEG and their composites involving C30B. ....	64
<b>Figure 17:</b> DTA curves of PLA80-PEG20 blend recorded during first heating, slow cooling and second heating cycles .....	66
<b>Figure 18:</b> a) TGA and b) DTG curves of neat PLA, neat PEG, PLA-PEG blends and their composites.....	68
<b>Figure 19:</b> i. TIC curves and ii. the mass spectrum recorded at the peak maxima and low temperature shoulder of neat PLA, neat PEG, PLA-PEG blend composites involving C30B. ....	70
<b>Figure 20:</b> Single ion evolution profiles of a) neat PLA, b)10 wt% PEG plasticized PLA, PLA90-PEG10, c) its composite involving C30B, PLA90-PEG10-C30B and d) neat PEG. ....	71
<b>Figure 21:</b> Single ion evolution pyrograms of selected ion of PLA-PEG-C30B blend composites having a) 10, b) 15, c) 20 wt% PEG content, respectively. ....	72
<b>Figure 22:</b> SEM images of 7 wt% PLA nanofibers at high and low magnifications in CHCl <sub>3</sub> /DMF solvent systems with volume ratios 70:30, 80:20 and 90:10 (v/v). ....	78
<b>Figure 23:</b> SEM images of 10 wt% PLA nanofibers at high and low magnifications in CHCl <sub>3</sub> /DMF solvent systems with volume ratios 70:30, 80:20 and 90:10 (v/v). ..	78
<b>Figure 24:</b> SEM images of 7 wt%, 10 wt% and 15 wt% PLA nanofibers in CHCl <sub>3</sub> /DMF 90:10 (v/v) solvent systems. ....	79
<b>Figure 25:</b> (a) Total ion current curve, (b) pyrolysis mass spectrum at 350 °C, and (c) single ion evolution profiles of some selected products recorded during the pyrolysis of 15% (w/v) PLA fiber CHCl <sub>3</sub> /DMF 90:10 solution system. ....	80

<b>Figure 26:</b> a. XRD diffractograms of C15A, C20A, C30B montmorillonites, PLA composites and composite fibers and b. TEM images of PLA composites involving 3wt% C15A, C20A and C30B. ....	82
<b>Figure 27:</b> SEM images of 15% (w/v) PLA/nanoclay fibers involving 3 and 5wt% C15A. ....	83
<b>Figure 28:</b> SEM images of 15% (w/v) PLA/nanoclay fibers involving 1, 3 and 5wt% C20A. ....	84
<b>Figure 29:</b> SEM images of 15% (w/v) PLA/nanoclay fibers involving 1, 3 and 5wt% C30B. ....	85
<b>Figure 30:</b> SEM images of 15% (w/v) PLA fiber and PLA composite fibers involving 3 wt% C15A, C20A or C30B (bar scales= 10 $\mu$ m, 3 $\mu$ m and 1 $\mu$ m from left to right, respectively). ....	86
<b>Figure 31:</b> DTA curves of PLA, PLA fiber and composite fibers involving 3wt% C15A, C20A and C30B. ....	88
<b>Figure 32:</b> TGA curves of PLA and PLA composite fibers involving 3wt% C15A, C20A and C30B. ....	89
<b>Figure 33:</b> a) The TIC curves and b) the pyrolysis mass spectra recorded at peak maxima detected during the pyrolysis of 15% (w/v) PLA composite fibers involving 3 wt% I. C15A, II. C20A or III. C30B.....	91
<b>Figure 34:</b> Single ion evolution profiles of selected products of a) PLA, b) PLA fiber and PLA composite fibers involving 3wt% c) C15A, d) C20A and e) C30B. ....	92
<b>Figure 35:</b> Single ion evolution profiles of characteristic fragment with m/z= 296 Da of a) C15A b) C20A c) C30B recorded during the pyrolysis of pure organoclay, PLA/organoclay composite or composite fibers. ....	94
<b>Figure 36:</b> SEM images of electrospun fibers of a) PLA and PLA-PEG blends involving b) 10, c) 15 and d) 20 wt % PEG. ....	96
<b>Figure 37:</b> DTA curves of neat PLA, PLA-PEG blends and fibers of PLA-PEG. ...	97
<b>Figure 38:</b> TGA curves of neat PLA and electrospun fibers of PLA-PEG blends. ..	98

<b>Figure 39:</b> The TIC curves and the pyrolysis mass spectra recorded at peak maxima detected during the pyrolysis of 15% (w/v) PLA-PEG fibers involving a) 10 wt% b) 15 wt% c) 20 wt% PEG.....	100
<b>Figure 40:</b> Single ion evolution profiles of the selected products of electrospun fibers of PLA-PEG blends involving a) 10 wt% b) 15 wt% c) 20 wt% PEG. ....	102
<b>Figure 41:</b> XRD diffractogram of C30B and PLA-PEG composite fibers involving C30B.....	103
<b>Figure 42:</b> SEM images of a) PLA fibers, b) PEG beads and electrospun fibers of PLA-PEG blends and composites involving c,d) 10wt%, e,f) 15wt% and g,h) 20 wt% PEG. ....	104
<b>Figure 43:</b> Size distributions of 19 randomly selected fibers of blends and composites.....	105
<b>Figure 44:</b> DTA curves of neat PLA, PLA-PEG blends, PLA-PEG fibers and composite fibers involving 3 wt% C30B. ....	107
<b>Figure 45:</b> TGA curves of electrospun fibers PLA-PEG blends and composites involving C30B. ....	107
<b>Figure 46:</b> The TIC curves and the pyrolysis mass spectra recorded at peak maxima detected during the pyrolysis of PLA-PEG-C30B composite fibers involving a) 10 wt% b) 15 wt% c) 20 wt% PEG.....	109
<b>Figure 47:</b> Single ion evolution profiles of the selected products of electrospun fibers of PLA-PEG-C30B composites involving a) 10 wt%, b) 15 wt% and c) 20 wt% PEG.....	110
<b>Figure 48:</b> Single ion evolution profiles of the selected products of electrospun fibers of PLA-PEG a) blend and b) composite involving 20 wt% PEG. ....	111
<b>Figure 49:</b> TEM images of PLA composite involving C20A and C15A, and PMMA and PE composites involving C15A.....	113
<b>Figure 50:</b> TEM images of PLA, PMMA and PE composites involving C25A. ....	114
<b>Figure 51:</b> TEM images of PLA, PMMA and PE composites involving C93A. ....	115
<b>Figure 52:</b> TEM images of PLA, PMMA and PE composites involving C30B. ....	116

<b>Figure 53:</b> X-ray diffractogram of composites of PLA, PMMA and PE involving a) C15A, b) C20A, c) C25A, d) C93A and e) C30B. ....	118
<b>Figure 54:</b> i. the TIC curves, ii. pyrolysis mass spectra at peak maxima and iii. single ion pyrograms of abundant fragments recorded during the pyrolysis of a) organic modifier of C15A and C20A, b) C15A, c) C20A, d) C25A, e) C93A and f) C30B.	120
<b>Figure 55:</b> The TIC curves, pyrolysis mass spectra at peak maxima and single ion pyrograms of abundant fragments recorded during the pyrolysis of a) PLA, b) PMMA and c) PE. ....	123
<b>Figure 56:</b> Single ion evolution profiles of the organic modifier and the polymers detected during the pyrolysis of a) PLA-C15A, b) PLA-C20A, c) PMMA-C15A and d) PE-C15A. ....	125
<b>Figure 57:</b> Single ion evolution profiles of the organic modifier and the polymers detected during the pyrolysis of a) PLA-C25A, b) PMMA-C25A and c) PE-C25A. ....	125
<b>Figure 58:</b> Single ion evolution profiles of the organic modifier and the polymers detected during the pyrolysis of a) PLA-C93A, b) PMMA-C93A and c) PE-C93A. ....	126
<b>Figure 59:</b> Variation of $T_{max}$ as a function of inter-layer spacing for C15A, C20A and for the composites involving C15A and C20A. ....	129
<b>Figure 60:</b> Variation of $T_{max}$ as a function of inter-layer spacing for C25A and for the composites involving C25A. ....	129
<b>Figure 61:</b> Variation of $T_{max}$ as a function of inter-layer spacing for C93A and for the composites involving C93A. ....	130
<b>Figure 62:</b> Single ion profiles of selected products detected during the pyrolysis of a)PMMA, b)PMMA-C15A, c) PMMA-C25A and d)PMMA-C93A.....	132
<b>Figure 63:</b> Single ion evolution profiles of the organic modifier and the polymers detected during the pyrolysis of a) PLA-C30B, b) PMMA-C30B and c) PE- C30B. ....	133

**Figure 64:** Single ion profiles of selected products detected during the pyrolysis of  
a)PMMA, b)PMMA-C30B. .... 134

**Figure 65:** Single ion profiles of selected products detected during the pyrolysis of  
a)PLA, b) PLA-C30B..... 134

## LIST OF SCHEMES

### SCHEMES

<b>Scheme I:</b> Acid decomposition of ether linkages.....	55
<b>Scheme II:</b> Possible thermal degradation products of PLA chains involving ethylene oxide units as the end groups. ....	56
<b>Scheme III:</b> Trans-esterification reactions between the organic modifier of C30B and PLA. ....	73
<b>Scheme IV:</b> Generation of amide units by interaction of fragments of the organic modifier with ester groups of PMMA.....	131
<b>Scheme V:</b> Trans-esterification reaction between the hydroxyl groups of the organic modifier and the ester groups of PMMA. ....	135
<b>Scheme VI:</b> Crosslinking reactions due to trans-esterification reactions between the hydroxyl groups of the organic modifier and the ester groups of PMMA.....	135

## LIST OF ABBREVIATIONS

<b>PLA</b>	Poly(lactic acid), Polylactide
<b>SnOct<sub>2</sub></b>	Stannous octoate
<b>PLLA</b>	Poly(L-lactide)
<b>PDLA</b>	Poly(D-lactide)
<b>PDLLA</b>	Poly(D,L-lactide)
<b>X<sub>c</sub></b>	Degree of crystallinity
<b>T<sub>g</sub></b>	Glass transition temperature
<b>T<sub>m</sub></b>	Melting temperature
<b>T<sub>max</sub></b>	Maximum degradation temperature
<b>ΔG<sub>M</sub></b>	Free energy of mixing
<b>ΔH<sub>M</sub></b>	Enthalpy of mixing
<b>PEG</b>	Poly(ethylene glycol)
<b>PEO</b>	Poly(ethylene oxide)
<b>T<sub>cc</sub></b>	Cold crystallization temperature
<b>PCL</b>	Poly(ε-caprolactone)
<b>DSC</b>	Differential scanning calorimetry
<b>DMA</b>	Dynamic mechanical analyses
<b>SEM</b>	Scanning electron microscope
<b>PMMA</b>	Poly(methyl methacrylate)
<b>MDI</b>	Methylenediphenyl diisocyanate
<b>PMCs</b>	Polymer matrix composites
<b>XRD</b>	X-Ray diffractometer
<b>TEM</b>	Transmission electron microscope
<b>NMR</b>	Solid-state nuclear magnetic resonance
<b>SANS</b>	Small-angle neutron scattering
<b>USANS</b>	Ultra small-angle neutron scattering
<b>SAXS</b>	Small-angle X-ray scattering
<b>FTIR</b>	Fourier transform infrared spectroscopy
<b>ET</b>	Electron tomography
<b>PS</b>	Polystyrene
<b>AlPi</b>	Aluminium diethylphosphinate



<b>Ac</b>	Acetone
<b>THF</b>	Tetrahydrofuran
<b>DCM</b>	Dichloromethane
<b>DMF</b>	Dimethylformamide
<b>CNTs</b>	Carbon nanotubes
<b>C30B</b>	Cloisite 30B
<b>DPMS</b>	Direct pyrolysis mass spectrometry
<b>STA</b>	Simultaneous thermal analysis
<b>C15A</b>	Cloisite 15A
<b>C20A</b>	Cloisite 20A
<b>C25A</b>	Cloisite 25A
<b>C93A</b>	Cloisite 93A
<b>TIC</b>	Total ion current
<b>DTG</b>	Differential thermal gravimetry



## CHAPTER 1

### 1. INTRODUCTION

#### 1.1.Poly(lactic acid)

Petroleum based synthetic polymers are used in almost all fields of industry, especially in automotive, plastic and aerospace industries. Nevertheless, as a result of sustainable environmental and economic concerns, the use of biodegradable polymers instead of synthetic polymers has been the interest of scientists during the last decade [1]–[4].

Among all biodegradable polymers, Poly(lactic acid), PLA, has drawn the most attention for its distinct and comparable properties with other conventional petroleum based polymers like compatibility, resorbability, high strength, high modulus and transparency [5]–[7]. PLA, a promising polyester, is produced from renewable resources like sugar beet, starch, corn, etc. and highlighted as “green” polymer due to its biodegradability [1], [2]. In Figure 1, chemical formula of PLA is shown.

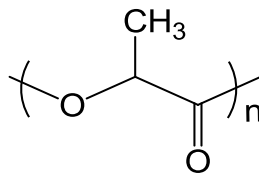


**Figure 1:** Chemical structure of poly(lactic acid), PLA

PLA or poly-lactide was discovered in 1932 by Carothers (at DuPont). He was only able to produce a low molecular weight PLA by heating lactic acid under vacuum while removing the condensed water. The problem at that time was to increase the molecular weight of the products; and, finally, by ring-opening polymerization of the lactide, high-molecular weight PLA was synthesized.

Poly(lactic acid), also known as polylactide, was first introduced by Wallace Carothers in 1932 when he was working at DuPont. He heated the lactic acid under vacuum, removed the condensed water from reaction medium, and obtained low molecular weight PLA by condensation reaction. Later, in 1954, high-molecular weight PLA successfully synthesized by ring opening polymerization of cyclic lactide. First, lactic acid is synthesized from corn starch via a fermentation process. Condensation reaction of the lactic acid results in low molecular weight polylactide. Then, depolymerization of low molecular weight PLA forms cyclic lactide. Finally, ring opening polymerization of lactide is carried out with an initiator, generally stannous octoate, SnOct<sub>2</sub> is preferred [2].

Since lactic acid is a chiral molecule and has two optically active isomers as L and D-lactic acid, PLA can be synthesized as Poly(L-lactide), PLLA, Poly(D-lactide), PDLA, and Poly(D,L-lactide), PDLLA. As chemical configurations affect the physical properties of polymers, both PLLA and PDLA shows semicrystalline property and semicrystalline pellets are opaque. In contrast, PDLLA behaves as an

amorphous polymer and it is transparent [2]. Amorphous polylactide is used especially for biomedical devices and in drug release studies and semicrystalline PLA is preferred generally for industrial applications in which higher thermal and mechanical properties are needed [8]. Also, in nature, even though both L and D forms of lactic acid are present, most of the lactic acid is in L form [9], [10].

It is known that molecular structure and crystallinity affects mechanical properties including tensile strength, modulus, and percent elongation at break, strongly. Semicrystalline PLA shows efficient mechanical properties with tensile strength of 50–70 MPa and elastic modulus of 3000–4000 MPa. However, low elongation at break typically, 2–10%, limits its industrial applications. Mechanical orientation by drawing sometimes applied to improve the mechanical properties of rigid PLA by changing its morphology to meet the different applications like packaging, coating, textile, etc. [8], [11].

On the other hand, Dorgan et al. searched the rheological properties of PLA and they claimed that branching affects melt flow properties significantly. The group pointed out that linear PLA obeys the Cox-Merz rule that relates steady viscosity versus shear rate curve to complex viscosity versus angular frequency curve; whereas branched PLA deviates from the rule. They also said that as the extent of branching PLA increases, zero shear viscosity increases and polymer shear thins more strongly [12].

Since one of the most important applications of PLA is in packaging industry, scientists have also studied its barrier properties against water vapor, atmospheric gases etc. Lehermeier et al. investigated gas permeation properties of PLA. The group claimed that branching and stereochemical (L,D) content did not affect the gas permeation properties [13]. In another research, Tsuji and coworkers investigated the effect of stereochemical content and degree of crystallinity on water vapor permeation. They said that water vapor transfer rate decreased with increasing degree of crystallinity,  $X_c$ , and remained unchanged with changing D unit content [14].

Finally, thermal properties of PLA has also been investigated. Poly(lactic acid) has a glass transition temperature,  $T_g$ , of about 60-70 °C and a melting temperature,  $T_m$ , of about 130-180 °C. Several mechanisms are suggested in the literature for degradation mechanisms of PLA including random chain scission, intramolecular and intermolecular trans-esterifications, cis-elimination, depolymerization, hydrolysis, oxidative degradation and radical reactions [4], [15]–[18]. Thermal degradation of PLA is mainly dominated by intramolecular trans-esterification reactions and maximum decomposition temperature,  $T_{max}$ , is at around 360 °C [15]. Even though its maximum degradation temperature is quite high, molecular weight reduction starts at low temperatures due to cyclic monomer formations upon thermal processing [18].

As mentioned above, although there are many unique properties of PLA, problematic properties such as high brittleness and low thermal stability restricts its applications. To improve the deficient properties different techniques are employed including copolymerization, incorporation of filler materials, plasticization with biocompatible plasticizer, and blending with other polymers [19]–[25].

## **1.2.Polymer Blends**

Polymer blends can be described as a mixture of two or more macromolecular substances that employed to create a new material with different physical properties than the original materials. Performances of polymers can be tailored by changing the component ratios and as a result, desired properties can be obtained easily. Since blending of polymers is a simple and an economical method, it has drawn much attention to manipulate the properties of materials for different commercial

applications including household plastic products, automotive components and biomedical devices etc. [26].

In general, polymer blends are separated into two main categories as miscible and immiscible. Apart from that, mixture of partially miscible systems can also be obtained. Miscible blends are single phase, homogeneous, transparent and generally presents improved properties compared to the blend components. In the characterization studies, observation of single a  $T_g$  is considered as a strong evidence for the creation of miscible blend. On the other hand, immiscible blends are heterogeneous and phase separated so preserve glass transition and/or melting temperatures of the original components [26]. Absence of interaction between the blend components, large differences in their chemical structures and viscosities are some of the significant reasons of immiscibility [27]. Generally, unstable phase morphology of immiscible blends leads to poor mechanical properties. To stabilize the phases and enhance the properties of blends compatibilization via reactive polymers, coupling agents and copolymers that contains miscible segments with each component, etc. are generally conducted. Compatibilizers improve the adhesion between immiscible polymers by locating to the interface of phases [26], [28].

Since miscibility is similar to thermodynamic solubility, free energy of mixing,  $\Delta G_{mix}$ , must be negative to obtain a miscible blend system. Since entropic contributions are negligible for polymers, enthalpy of mixing,  $\Delta H_{mix}$ , is another critical point for miscibility. Exothermic enthalpy of mixing, which can be provided by the interactions between the components, should be generated. If there is an interaction between materials such as strong covalent, ionic, hydrogen bonds or weak dipole-dipole bonds, etc. it will be more likely to obtain miscible blends [29].

Although most of the polymer blends are immiscible in nature due to repulsive interactions of the constituents, miscible blends also exist i.e. Poly(styrene acrylonitrile)/poly(methyl methacrylate), poly(phenylene ether)/poly(styrene) [26].

### 1.2.1. Blending Techniques

There are many different ways to prepare polymer blends including dry mixing, solution casting, melt mixing, latex blending and preparation of interpenetrating polymer networks (IPNs), etc [28], [30], [31]. In this section, some of these methods are summarized.

- In *dry (powder) blending*, two powder polymers having different particle sizes are mixed mechanically. As blending carried out, fine sized particles adhere to the surface of large-sized grained particles and due to the collisions of the particles, electrical charge is generated. Newly created sample does not revert to any of the former components. However, since mixing efficiency is low, this technique is not employed widely. Ribbon blenders and paddle mixers are the common machines used in dry blending [30].
- *Solution casting* technique is a common way to prepare polymer blends (and composites) on a laboratory scale. First, components are dissolved in a suitable solvent and stirred, constantly. Then, evaporation of the solvent yields a uniform optically pure polymer film. Agitation time is critical for this method and should be optimized to obtain the desired system effectively. Homogeneous thickness distribution of films, being an easy, rapid and energy saving method and being useful for temperature sensitive materials are some of the significant advantages of solution blending [32].
- *Melt mixing* technique is a direct method in which polymer constituents are blended in the molten state. This technique is compatible with common industrial processes like injection molding and so it is more functional and economic for commercial uses. It also eliminates the solvent usage and; therefore, titled as an environmental friendly process. Melt mixing is the most widespread approach for the preparation of polymer blends (and polymer



composites) due to successful generation of good dispersion and easy temperature control. Equipment of melt mixing technique can be divided into two as batch mixers i.e. two roll mill, Banbury mixer and continuous mixers i.e. single or twin-screw extruders. Continuous mixers are more favored than the classic batch mixers due to its significant advantages like offering high shear stress, high product quality, uniformity and consistency [28].

- *Latex blending* is a common technique used to prepare elastomer blends. In this method, polymers in the form of microspheres are dispersed in aqueous rubber latex medium. Both natural and synthetic rubbers can be used as latices. With this method, good dispersion can be achieved since small polymer particles in latex are dispersed very well due to surfactants [31], [33].

### **1.2.2. PLA Based Blends**

The most common polymer used in poly(lactic acid) blends is poly(ethylene glycol). In addition PLA blends involving poly( $\epsilon$ -caprolactone), starch and poly(methyl methacrylate) also appeared in the literature.

Poly(ethylene glycol), (PEG), which is synthesized from ethylene glycol or ethylene oxide, is a thermoplastic polyether with ether group in the backbone chain and has a glass transition temperature between  $-40\text{ }^{\circ}\text{C}$  to  $-70\text{ }^{\circ}\text{C}$ . PEG is also known as Poly(ethylene oxide), (PEO) and main difference between them is the molecular weight. While molecular weight of PEG is between 400 to 40000 g/mol, PEO refers to higher molecular weights [34]. PEG due to its miscibility, biocompatibility, biodegradability, and food contactable application, is almost the most suitable

material which has been used as an impact modifier for PLA [35]. Its chemical structure is given in Figure 2.

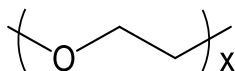


**Figure 2:** Chemical structure of poly(ethylene glycol), PEG.

It has been determined that both the molecular weight and the amount of PEG have significant effects on the properties of PLA/PEG blends [24], [25], [36]–[39]. A limit of miscibility and brittleness characteristics depending upon the plasticizer content and the molecular weight were detected [6], [36], [37], [40], [41]. The plasticizing efficiency was increased with decreasing molecular weight of PEG [24], [39]. Sheth et al. found that PLA/PEG blends varied from completely miscible to partially miscible, depending upon the PEG concentration [38]. Kim and coworkers showed that in the presence of 40% high molecular weight PEG percentage of elongation at break is improved significantly [39].

PEG, being a plasticizer, shows plasticization effect, gives rise to increase in PLA chain mobility and this segmental motion allows the rearrangement of the chains. PEG by disturbing the intermolecular forces, decreases the glass transition temperature of PLA [24], [25], [37]–[39], [42]. Increasing the amount of PEG up to a certain point leads to decrease in  $T_g$  and improvement in crystallization [37]. Ahmed and coworkers determined that the incorporation of PEG as a plasticizer reduces  $T_g$  and  $T_m$  of neat PLA significantly, as expected [25]. In a recent research, Stoehr and

coworkers examined the effect of PEG amount and recorded that PEG content affects  $T_g$  and cold crystallization temperature,  $T_{cc}$  [42].

Poly( $\epsilon$ -caprolactone), (PCL), is also a polyester which is derived from its monomer  $\epsilon$ -caprolactone by ring opening polymerization technique. PCL, which is generally employed to toughen the PLA, shows not only low  $T_g$  at around  $-60\text{ }^\circ\text{C}$  but also low  $T_m$  at around  $60\text{ }^\circ\text{C}$ . PCL is known as an easily processable biodegradable and biocompatible polyester with high elongation at rupture. Since PCL is a biocompatible polymer, it is also used in packaging, tissue engineering and drug-delivery systems as PLA [34]. In the literature, PCL/PLA blends were reported as immiscible due to the lack of interactions between the polymer phases [43]–[46]. López-Rodríguez N. et al. searched solution-casting PCL/PLA blends in the ratio of 80:20, 60:40, 40:60 and 20:80. They claimed that both differential scanning electron microscopy (DSC) and dynamic mechanical analyses (DMA) experiments revealed two different  $T_g$  which is an indication of phase separation for each composition. Phase boundary studies was also supported by scanning electron microscopy (SEM) images [43]. On the other hand, Yeh J. et al. prepared PCL/PLA blends by melt mixing technique but obtained similar results that is characterized by DSC, DMA and SEM analyses. The group also investigated the mechanical properties of blends and concluded that addition of PCL improves the ductility of PLA even though the system is immiscible [44].

Since PLA is a green polymer, its blends and composites with other biodegradable polymers becomes popular in response to sustainable studies. Starch is one of these prominent biodegradable polymers, which is mainly used as filler instead of polymer matrix. PLA/starch blend systems are investigated in different research groups where it has been reported that addition of starch decreases the tensile, flexural and impact strengths and elongation at breaks; in contrast, increases the moisture uptake compared to neat PLA [47]–[49]. In 2015, Yang et al. worked on native starch and chemically modified starch/PLA blends and investigated the effect of type of grafting

on mechanical properties of blends. Maleic anhydride grafted starch and epoxidized cardanol grafted starch is prepared by chemical modification of native starch and then blended with PLA. It has been concluded by the group that blending PLA with epoxidized cardanol grafted starch results in superior mechanical properties than other blend systems [47]. On the other hand, Yu and coworkers prepared several PLA/starch blends with and without the compatibilizer by melt mixing method. They used methylenediphenyl diisocyanate, MDI, as compatibilizer and searched the effect of mixing order of constituents. They claimed that presence of MDI enhances the tensile strength, modulus, toughness and also crystallization of blends. In addition, when MDI was incorporated to the PLA matrix before the addition of starch, its compatibilizing effect became more pronounced resulting in the increase in mechanical properties more effectively. In contrast, if MDI was first introduced with starch before blending with PLA, its compatibilizing effect decreased due to the chemical reactions of isocyanate groups in MDI [49].

On the other hand, poly(methyl methacrylate) (PMMA) which is an amorphous, synthetic and widely preferred material in many different industrial applications, is a non-biodegradable polymer. Even though PMMA is a hard, rigid and brittle material, it is transparent and exhibits good tensile and flexural strengths; therefore, its miscibility with PLA searched in several studies. [34], [50]–[52]. Eguiburu et al. investigated the miscibility between PMMA and both amorphous and crystalline PLA. The group prepared PLA/PMMA blends via solution casting technique and characterization studies revealed that the blends were miscible according to  $T_g$  criteria. They also concluded that if a thermal treatment was applied to the blends, phase separation was observed after the cooling process and single but enlarged glass transition, which indicates partial miscibility, were recorded [50]. In another research, Shirahase et al. prepared melt blended PLA/PMMA blend using a two-roll mill and studied the hydrolytic degradation behavior of these blends. They claimed that according to DSC and DMA analyses blends were miscible and degradation rate

was mainly affected by PMMA content. When PMMA content was below 30 wt%, hydrolytic degradation was favored in alkaline solution [51]. Differently, in a recent research, Anakabe and coworkers melt blended PLA with PMMA via twin-screw extruder at different processing conditions and obtained immiscible blends in the light of characterization studies. According to group, high molecular weight of PMMA and processing parameters; mixing temperature and screw speed, affected the miscibility of the blends [52].

### **1.3.Polymer Composites**

Composites are comprised of “continuous” matrix phase and “dispersed” reinforcing phase, which is surrounded by a matrix. The motivation behind obtaining a multi-phase material is to create new properties while protecting the main characteristics of the original components. Composites are divided into three main categories as metal, ceramic and polymer composites according to the matrix types. Among all of them, polymer composites have a significant place due to wide range applications i.e. automobiles, aircraft, spacecraft, packaging, etc. as a result of their outstanding mechanical, thermal and chemical properties [53], [54]. Polymer composites can be prepared by various methods including mainly melt blending and solution casting that are similar methods used in preparation of polymer blends, template synthesis (also known as sol-gel technology), and in-situ polymerization techniques, etc. For many industrial applications, melt blending is more preferred than other methods [32].

In polymer matrix composites, (PMCs), reinforcing materials are much stronger than the polymer matrix, which makes reinforcements the load-bearing components. In order to obtain an effective load transfer between matrix and reinforcements,

polymer the matrix should show good adhesion towards the reinforcements. When composite materials are subjected to mechanical or thermal load, load transfer from the matrix to the reinforcement takes place [53]. Therefore, the choice of reinforcing material is curial to obtain desirable properties. Among various fillers, nano-sized reinforcements are the most effective ones due to their high surface areas and aspect ratios. Addition of nano scale sized reinforcing phase, even at low loading levels, results in high interface to volume ratio, which governs the properties of composites.

Among many different nano-sized reinforcements including nanotubes, nanowires, nanographite, nanosilica, nanotitania, nanofibers etc., nanoclays are almost the most widely used additives since they are inexpensive, eco-friendly and eligible for many applications [55].

### **1.3.1. Nanoclays**

Clays, layered aluminium silicates, belong to a wide group of minerals and are naturally occurring materials. The crystal structure of nanoclay consists of layers that are composed of octahedral and tetrahedral sheets and these sheets can be in form different arrangements. In general, clays are divided into four major groups as; *kaolinite*, *smectite*, *illite* and *chlorite* groups. Kaolinites have one octahedral and one tetrahedral sheet, 1:1 layer type. Kaolinite and nacrite minerals are two known members of kaolinite group. Both smectite and illite groups are in the form of 2:1 layer in which one octahedral sheet is sandwiched between two tetrahedral sheets. Even though the arrangement of the layers are similar, their general chemical compositions are different from each other. Common members of smectite clays can be listed as; montmorillonite, talc, pyrophyllite and saponite. And, illite minerals take their group name from the most known member of them, illite. Finally, chlorites

have 2:1:1 type and in this layer structure, there is one octahedral sheet adjacent to a 2:1 layer. The members of this type of clay, i.e. amesite and cookeite, have their individual chemical structures so chlorites, unlike other clay groups, do not obey to a general chemical formula. Therefore, sometimes they are not classified as one of the clay types. Among all of the layered silicates mentioned above, montmorillonite is the most commonly employed one in academic and industrial applications [56], [57].

One silicate layer of clay has a thickness around 1 nm and stacking of layers are organized by Van der Waals forces. The distance between the two layers is named as “interlayer spacing” or “gallery” and in the galleries, there are small cations like  $\text{Li}^+$ ,  $\text{Na}^+$ , etc. It is known that clays are highly hydrophilic materials and so miscible with hydrophilic polymers. Since they are incompatible with most of the polymers because of their nature, surface treatments are applied to make them organophilic. For this purpose, ion-exchange reactions are conducted since small cations can easily be replaced with more voluminous organic modifiers such as alkyl ammonium or phosphonium cations. And, the modified nanoclays are sometimes called as organoclays [57]–[59]. The modification through ion-exchange reactions also enables the polymer chains to place in between the silicate layers by increasing the interlayer spacing. In Figure 3, schematic representation of several gap sizes and different orientations of modifiers are given. Depending on the characteristics of organic modifier i.e. chain length and cation exchange capacity; (a) monolayer, (b) bilayer or (c), (d) inclined paraffin structures can be obtained [59].

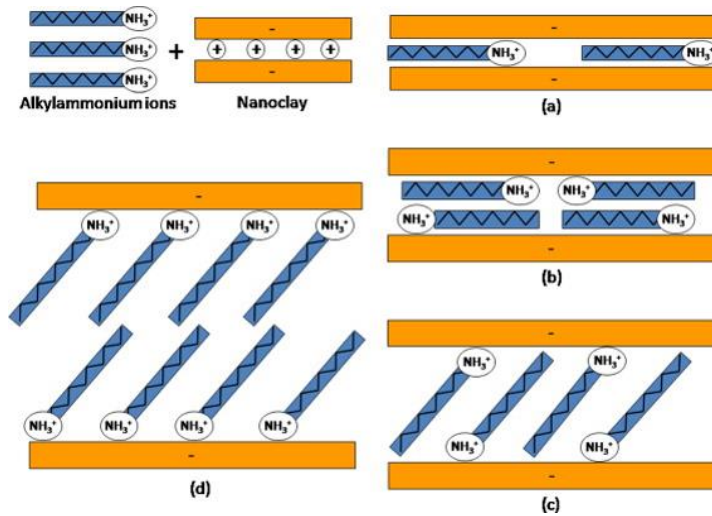


**Figure 3:** Schematic of ion-exchange reactions including (a) monolayer, (b) bilayer or (c), (d) inclined paraffin structures.

### 1.3.2. Nanoclay-Polymer Interaction

Polymer/clay composites can be divided into three main microstructures: unintercalated (or microcomposite), intercalated and exfoliated according to the dispersion states of reinforcements as represented in Figure 4 [32]. If the affinity between nanoclay and polymer is weak, clay layers cannot be separated from each other and unintercalated microcomposite structures are obtained. In contrast, if an efficient interaction between clay and polymer is achieved, two types of nanocomposite structures; intercalated and exfoliated, can be obtained. In intercalated nanocomposites, the distance between layers increases and polymer chains lay down between the layers but clay layers are still stacked and not separated completely from each other. Finally, in exfoliated nanocomposite structures, polymer chains surround the fully separated and well-dispersed silicate layers. In this type,



polymer-clay interaction is maximized due to well separation and distribution of layers through polymer matrix. Exfoliated layers can be in order or non-ordered and spread all around the polymer matrix. In Figure 4, a typical non-ordered exfoliation of layers is presented. Most of the polymer nanocomposites are reported as intercalated or a mixture of intercalated and exfoliated structures because complete separation of layers successfully is difficult to obtain [57], [60].

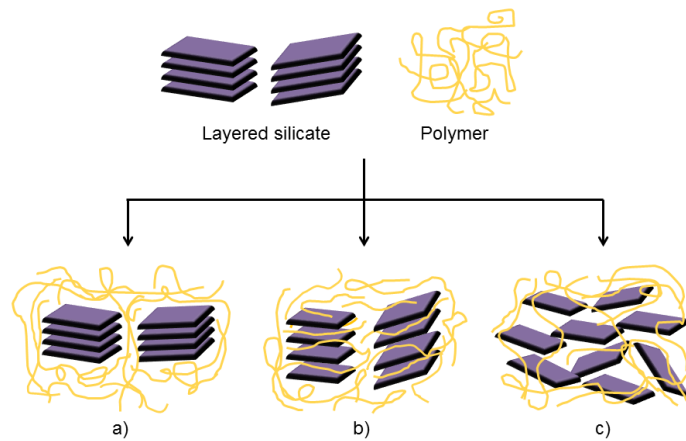


**Figure 4:** Types of composite structures: a) microcomposite b) intercalated nanocomposites c) exfoliated nanocomposites.

### 1.3.3. Structural Characterization of Composites

Two complementary and most commonly used techniques to characterize the morphology of nanocomposites are X-Ray Diffraction (XRD) and Transmission Electron Microscopy (TEM) methods [58], [61]–[64]. In case of XRD method, the

distance between the silicate layers can be determined according to Bragg's law. Since intercalation of polymer into clay layers increases the gallery, the diffraction peak of the clay shifts to lower angles, indicating larger d-spacing. And, for the exfoliated structures, disappearance of the characteristic peak of clay is recorded due to either disorganized separation of layers or expansion of galleries over 8 nm for ordered exfoliated structures [61], [65], [66]. On the other hand, TEM, which is a 2D qualitative analysis method, allows direct visualization of morphology of the composites. Since silicate layers are observed darker in a conventional bright-field TEM images, separation levels of a limited area can be monitored [63], [67].

Apart from these classical methods, Solid-State Nuclear Magnetic Resonance (NMR) [68]–[71], Small-Angle and Ultra-Small-Angle Neutron Scattering (SANS and USANS), Small-Angle X-ray Scattering (SAXS), Fourier Transform Infrared Spectroscopy (FTIR), etc. techniques are also used by some research groups for the characterization studies [57], [68], [72]–[74]. Shortly, in solid-state NMR, the longitudinal relaxations of proton (and carbon) is correlated with clay dispersion and then degree of separation of the platelets is quantified [68]. FTIR is preferred for detection of the differences in the bonding of a mixture and nanocomposite to predict the dispersion of clay platelets [62]. As mentioned, among all, the only direct method to monitor the degree of exfoliation of layers is TEM. Therefore, in a recent research, a quantitative 3D visualization method, electron tomography (ET) is suggested to explain the morphology by overcoming the limitations of TEM [72]. According to the group, this method provides information about dimensions and orientations as well as the distribution and dispersion of platelets. However, accuracy of topographic image strongly depends on adjustment of the tilt angle. Therefore, in order to obtain a correct and reliable methodology, many optimization studies are needed which is one of the important limitations of this technique [72].

#### 1.3.4. Nanoclay Based Composites

The importance and benefits of designing different nanoclay-based composite systems are reviewed in the many different literature studies [61], [71], [75]–[84]. On the other hand, since enhancement of the properties of polymers strongly depends on different variables such as mixing methods, processing conditions, amount of nanoclay incorporated, presence of other additives, chemical modifications of clays, etc., it is critical to study and optimize some of these parameters.

Junior et al. reported better dispersion and exfoliation of nanoclay in polystyrene (PS) matrix at higher screw speed (600 rpm) than the one observed at slower mixing speed (450 rpm) during melt mixing with a twin-screw extruder [85].

Tan et al. studied on rubber/nanoclay nanocomposites and finally, claimed that combination of latex compounding and melt mixing methods to prepare the nanocomposite yields to better dispersion. In this study, aqueous clay was mixed with natural rubber latex, stirred continuously and dried first and then, melt mixed with a two-roll mill [86]. On the other hand, Gu Z. and coworkers prepared rubber nanocomposites via solution casting. In this study, nanoclay was first pre-dispersed in an oil phase and then mixed with rubber solution. According to the group, continuous stirring for a limited time and evaporation of the solvent finally resulted in formation of intercalated nanocomposite [87].

In another research, effects of type of the organic modifier in nanoclays on polymer-clay interaction was searched. Labidi et al. melt mixed PCL and three different organically modified nanoclays in an extruder at the same processing conditions. Finally, TEM images revealed the mixture of exfoliated and intercalated structure for only one nanoclay, commercially named as Cloisite 30B. Other two clays, Nanofils5 and Nanofils2, could only form intercalated structures [88].

Cloisite 30B was also employed in another research. Unnikrishnan et al. blended C30B with PMMA and a grafting agent using a two-roller mixer. They claimed that grafting agent increased the interfacial interaction between nanoclay and PMMA and as a result, intercalation is successfully obtained [89].

Lastly, Shen Z. and coworkers prepared PEO/organically modified nanoclay nanocomposites using melt mixing and solution casting methods in order to compare the effect of mixing methods. According to XRD results, as the amount of PEO increased, the interlayer spacing remained the same for the samples prepared with melt mixing; in contrast, higher interlayer spacing was recorded for the ones prepared with solution casting technique [90].

#### **1.3.4.1. Composites of PLA with Nanoclays**

As mentioned before, incorporation of montmorillonites into PLA matrix is almost the most preferred way to eliminate deficient properties of PLA. For this purpose, Pochan and Krikorian investigated the effect of organic modifiers derived from Cloisite 30B, Cloisite 25A and Cloisite 15A on PLA. TEM and XRD studies revealed that Cloisite 30B has the highest performance among them, leading to a significant incorporation of PLA chains into layered silicates. This behavior was associated with the interaction between diols present in the organic modifier with C=O bonds present in PLA backbone [91].

Similarly, Liu et al. also investigated the effect of chemical modification of montmorillonites (MMT). Differently, they applied surface treatments themselves to modify the small cations of sodium montmorillonite (Na-MMT) through ion-exchange and adsorption methods. The group claimed that these multiple organically

modified montmorillonite yielded enhanced storage modulus, thermal stability and fire resistance compared to pure PLA [92]. The examples of enhanced properties of PLA including thermal, mechanical, viscoelastic, dielectric and gas barrier properties due to the addition of montmorillonite has been reported for many different researchers [93]–[98].

On the other hand, hybrid nanocomposite systems are also among the main research topics of nanocomposite studies due to the fact that synergistically enhanced properties can be created for some cases. For instance, in recent studies, montmorillonite/nanocellulose reinforced hybrid PLA composites has been reported as improved in terms of gas and water barrier properties, tensile strength, ductility, and thermomechanical properties [99]–[103]. Also, in one of our previous group works, Hatice et al. studied on the thermal degradation characteristics of PLA/aluminium diethylphosphinate, (AlPi), composites including organically modified montmorillonite, Cloisite 30B, (C30B) as reinforcing material [104]. It was revealed that silicate layers capsule the degrading molecules and this results in the enhancement of reactions between PLA, phosphinates and organic modifier of C30B at low temperatures.

Furthermore, nanoclays might be employed in immiscible blends as compatibilization agents. For example, nanoclays including different organic modifiers were added to PLA/PCL blends, which are immiscible as a result of their nature as mentioned in earlier sections. Many authors confirmed the compatibilization effect of montmorillonites on PCL/PLA blends in consideration of size reduction in the phase-separated droplets [105]–[109].

#### **1.3.4.2. Composites of PLA-PEG Blends with Nanoclays**

Even though the use of montmorillonite in PEG plasticized PLA composites has not been studied widely, some examples were appeared in the literature. Rodriguez-Llamazares et al. prepared melt mixed comparative composites of the plasticized PLA involving different amounts of PEG with C30B as filler. They claimed that PEG chains co-intercalate into the silicate layers leading to better intercalation of PLA through layers and better interaction between modifier of C30B and PLA molecules [110].

In addition, Paul and coworkers have investigated thermal and morphological properties of plasticized PLA/montmorillonite composites prepared by melt blending. They pointed out that incorporation of nanoclay increases the thermal stability of plasticized PLA when the clay load level is 3 wt% [97].

Gumus et al. claimed that clays are ineffective in crystallization since the organic modifier in nanoclay interact with matrix and prevent the chain folding which is necessary for crystallization. The group also concluded that phase separation between PLA and PEG took places within one year and as a result glass transition temperature of plasticized PLA and plasticized PLA composite increased due to physical aging phenomena [111].

### **1.4.Polymer Fibers**

Polymer fibers are commonly known as structures whose diameter is much smaller than its length and most of them are semi-crystalline. They are mainly produced by

spinning techniques and some of the common techniques can be summarized as follows.

In *melt spinning*, first a polymer is melted by heating in the extrusion and molten polymer forced to flow through die known as spinneret. Finally, cooling process solidifies the molten polymer. Since spinnerets have numerous small holes, final product is in form of filament. This is the most preferred method for production of polymer fibers that will not degrade at temperatures of desired viscosity. If the decomposition temperature of the polymer is lower than its melting temperature, then the polymer is dissolved in a suitable solvent and this solution is pumped through spinneret. If the solidification of liquefied polymer is provided by evaporation of the solvent by inert gases or air, then this method is named as *dry spinning*. On the other hand, if spinneret is placed in a chemical bath and the solidification is achieved via a solvent that precipitates the fiber, then the process called as *wet spinning* [112], [113]. Filaments can be stretched during spinning methods to change their sizes and orientations.

#### **1.4.1. Electrospinning**

In recent years, another method, *electrospinning*, becomes popular to generate ultra-thin, high strength fibers due to the ability to control fiber morphology, diameter, alignment and ease of use [114], [115]. Some of these properties cannot be controlled by conventional manufacturing methods mentioned above. Electrospinning allows the production of advanced structured fibers such as core-shell, porous, branched, multi-walled, necklace-like or hollow fibers that expand its scope of application areas [116], [117]. Today, electrospinning is mainly employed in medical

applications like drug delivery and cancer treatment studies as well as energy storage, sensors, catalysis or filtration applications [117]–[119].

Electrospinning, or sometimes entitled as “electrostatic spinning”, is a simple drawing process based on high electrostatic forces to produce fibers. In other words, in electrospinning, thin fibers form due to the uniaxial stretching via application of an external field [114], [115].

For an electrospinning setup, a voltage source, a capillary that filled with polymer solution, and a grounded metal collector that serves as counter-electrode, are the essential parts. Polymer solution is delivered to the tip of capillary, which is typically a metal syringe, with a specific pumping rate and forms a droplet. The needle of the syringe behaves as an electrode upon applied electrostatic field, and electrically charges the polymer solution. This electrical charge causes an instability at the surface of the droplet and creates a cone shape, known as “Taylor cone”. Finally, a jet of the polymer is ejected from Taylor cone towards the collector when the electrical charge reached is sufficient.

In Figure 5, SEM image of a typical electrospun fiber and sketch of the general structure of fibers are given. It is known that fibers show hierarchical structure including fibrils, lamellae and tie chains. During the process, polymer chains become folded and folded chains form stack of “lamellae” structures. As the electrospinning proceeds, the lamellae layers are organized due to the elongational and shear forces in order to form “fibrils”. In a fibril, there are also amorphous phases between the stack of lamellae layers, called as “tie chains”.



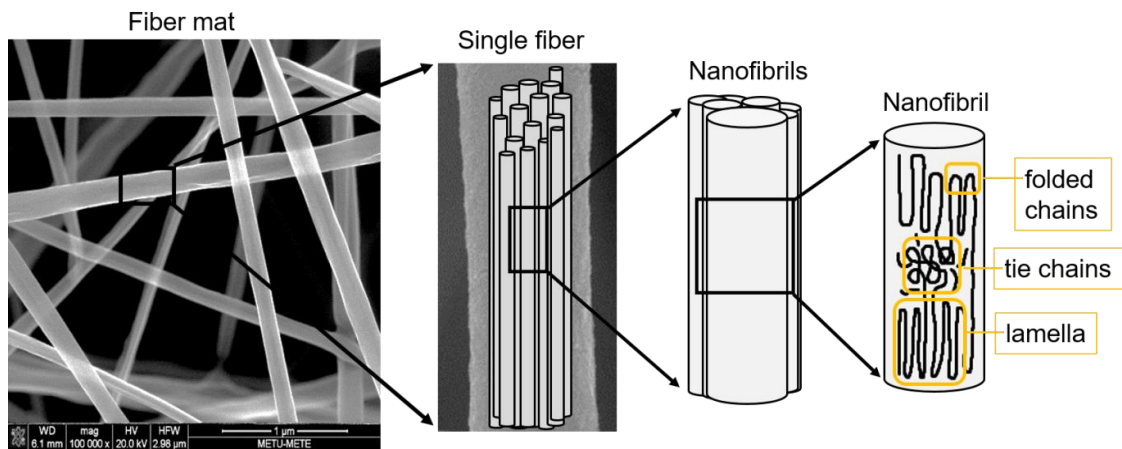


**Figure 5:** Structure of electrospun fibers.

### 1.4.2. Electrospun Fibers

Although electrospinning is a very practical method, fiber formation depends on many crucial criteria such as concentration of the polymer solution, molecular weight of the polymer, viscosity, solvent system, amount of applied voltage, distance between the collector and the tip of the syringe and ambient properties, etc. Therefore, to obtain bundle-free uniform shaped thin fibers, these parameters should be optimized.

Heikkila et al. studied the effects of the parameters including molecular weight of the polymer, viscosity and concentration of the solution, amount of the applied voltage, the distance between the collector and the nozzle on the fiber characteristics of polyamide-6 like diameter size and distribution. According to their results, polymer grade affected both surface tension and conductivity of the solution and so fiber distribution; yet, no change in fiber diameter was recorded when molecular weight of the polymer was altered. Besides, although thin but beaded fibers were mainly

created in case of low concentration and viscosity, applied voltage had also small effect on fiber bead formation. Since the distance between the tip of nozzle and the collector has an impact on the electric field, evaporation of the solvent and the deposition time, variations in fiber diameter were observed when distance was increased. Therefore, the group proposed to use a spinning voltage in the middle range to obtain small fibers [120].

In contrast, Deitzel et al. claimed that bead formation is strongly dependent to applied voltage for PEO/water electrospun fibers varying in the concentrations of 4-10 wt%. An increase in fiber diameter with increasing solution concentration and bimodal size distribution of fibers at higher concentrations (more than 7 wt% PEO/water) were observed [121].

As mentioned before, the design of more detailed structures is not complicated through the application of electrospinning technique. Morphological studies on complex core-shell structures revealed that feeding rates, blending ratios and molecular weights of components strongly affect the uniformity and thicknesses of the core and shell layers [116], [119], [122]. Besides the usage of miscible polymer blends, electrospinning method was also employed to generate fibers of immiscible blends. Zhang et al. investigated the internal fiber structure of PEO/chitosan immiscible blends upon the changes in the component fraction. Electrospinning of PEO/Chitosan blends by a single-nozzle setup created the core-shell structure (PEO as core, Chitosan as shell) up to a certain fraction ratio. As the amount of chitosan increased, microphase-separated fibers (PEO as discrete phase, Chitosan as continuous phase) was fabricated [122]. Due to the controllability of layer thicknesses and the use of biocompatible polymers, applications of core-shell fibers were thought to be a good potential for biomedical studies [119].

Another example to the employment of immiscible polymer blends in an electrospinning system can be found in Li and coworkers' study [117]. They span poly(styrene) and poly(vinyl pyrrolidone)/titania nanoparticle solution as core and

shell substances, respectively, to form fibers via a two capillary setup. In this research, hollow shaped nanofibers having a polymer composite as the shell structure were fabricated and then poly(styrene) core phase was removed by a calcination process to form highly porous nanotubes.

#### **1.4.2.1. PLA Fibers**

The production of PLA fiber by melt spinning, dry spinning, dry-jet wet spinning, wet spinning have been discussed in several studies [123]–[133]. The effects of solution properties such as boiling point, viscosity, conductivity and surface tension on morphology and fiber diameter, and the effects of melt mixing processing conditions on crystallinity and mechanical properties were discussed in detail. It has been determined that these properties are the key parameters to optimize the fiber characteristics [130]–[132].

Apart from the conventional production methods, in the last decade, fabrication of PLA fibers via electrospinning has become very popular. In 2014, Casasola et al. focused on different solvent systems in order to clarify its effects on fiber morphology, diameter, spinnability and rheological properties. According to their results, among all of the solvent systems including acetone (Ac), tetrahydrofuran (THF), dichloromethane (DCM), dimethylformamide (DMF) and binary solvent systems of Ac/DMF, Ac/THF, Ac/DCM, the finest bead-free fibers were obtained by Ac/DMF system. Then, the group continued their work by changing the solvent ratio of Ac/DMF in the proportions of 0/100, 20/80, 40/60, 60/40, 80/20, 100/0 (v/v) to investigate this system in detail. 40% by volume DMF resulted in defect-free nanofibers with smallest diameter and highest conductivity [134].

Yang et al. fabricated a mixture of nano and micro sized poly(L-lactic acid) (PLLA) fibrous scaffolds via electrospinning and compared with standard PLLA scaffolds. Based on the *in vitro*, cell morphology and neurite growth evaluations, PLLA fibrous could be employed in neural tissue engineering applications [135]. In another research, Li and coworkers developed an ecofriendly membrane via electrospinning of PLA and applied annealing processes to the fibers to improve its mechanical properties. Apart from the successful increment in mechanical strength and Young's modulus, filtration tests revealed that annealed membrane also represents microfiltration property [136].

Limited number of literature studies mainly published in recent years on fabrication and characterization of PLA-PEG blend electrospun fibers has been published [137]–[143]. Toncheva et al. electrospun both physically blended and chemically grafted PLA/PEG, loaded with an antibacterial drug. According to their results, physically blended PLA/PEG fiber represented more effective antibacterial property [140]. Since PLA is known as a hydrophobic polymer and in contrast, PEG is a hydrophilic polymer, Xu et al. aimed to create a fiber mat, which can release both hydrophobic and hydrophilic drugs [139]. In 2014, Buttaro et al. added PEG into PLA phase to generate biodegradable and hydrophilic yet water insoluble electrospun fibers, which is a desirable property for moisture wicking fabrics [138].

In addition, electrospinning of PLA composites containing different types of nano reinforcements has been studied [144]–[152]. Au et al. span the poly(lactic acid)/chitosan blend and composites involving silver nanoparticles in order to increase the antibacterial property of electrospun fibers. It has been determined that Ag nanoparticles homogeneously distributed at the surfaces of fibers and the addition of nanoparticles increased the spinnability of the blend. Finally, it was concluded that the fiber diameter is mainly influenced by the amount of chitosan incorporated [147]. In a very recent study, Liu et al. examined electrospun fibers of PLA/graphene oxide-silver nanoparticle hybrid nanocomposite in terms of the antibacterial, mechanical

and thermal properties. They aimed to minimize the attachments of bacteria in order to enhance the application area of PLA fibrous mats in biomedical uses. Their results indicated that fibrous mats of hybrid nanocomposites possess superior antibacterial resistance against *Escherichia coli* (*E. coli*) and/or *Staphylococcus aureus* (*S. aureus*) depending on Ag nanoparticle content. Also, addition of graphene oxide-Ag nanoparticle reinforcing materials increased the elastic modulus, tensile modulus and tensile strength as well as the thermal stability compared to PLA [148]. On the other hand, electrospun fibers of graphene/PLA composites, which are not enriched with Ag nanoparticles presented improved storage modulus, loss modulus, hydrophilicity and decreased fiber diameter [144], [149].

Further examples on electrospinning studies of PLA composites can be increased with the ones containing carbon nanotubes, CNTs, as reinforcing materials. PLA/CNT composite fibers were studied in terms of solvent effects, solution concentrations and CNT loading levels [150], [153]. It has been determined that the loading levels of nanotubes influence the fiber morphology. As the amount of CNT incorporated increased, entangled bundles was recorded [150]. Uniform dispersion of PLA electrospun mats involving multi-walled carbon nanotubes, MWCNT, with hydroxyapatite was observed [154]. The electrical conductivity studies of PLA electrospun nanofibers involving MWCNT was analyzed by Shao et al. [155].

As mentioned before, various types of nano-sized additives in which diamond nanoparticles can be classified as one of the uncommon examples, has been embedded in PLA fibers and characterized. In a few studies, poly(lactide) and nano-diamond were combined to fabricate electrospun fibers and characterization studies revealed a significant increase in thermal stability, mechanical properties, bioactivity, wettability and cell adhesion upon incorporation of nanodiamond at very low concentrations, typically 0.1 to 1 wt% [146], [151].

Some research groups have studied on preparation and characterization of nanoclay-incorporated PLA fibers [156]–[161]. Dual-sized porous fiber structures, from a few

nanometers to a few hundred micrometers, were fabricated by the use of electrospinning and salt leaching methods. The cold compression molding was applied to entangle the dual porosity fibers to create 3D scaffolds [156]. Alongi et al. investigated the effect of montmorillonite on thermal stability and air permeability of electrospun PLA fibers. It was observed that presence of C30B increases thermal stability of fiber with respect to  $T_{max}$  and  $T_{onset5\%}$  measurements in TGA measurement. Furthermore, incorporation of clays drastically decreased the air permeability of PLA up to 90% [158]. In other study, polylactide was mixed with layered double hydroxides, which is another yet less studied type of montmorillonite, to create composites, and composite fibers were successfully fabricated through a single-nozzle electrospinning setup. Decrement of melting point of PLA has been recorded as the montmorillonite content was increased [159].

### **1.5.Aim of Work**

This thesis work can be divided into two major subgroups as; the characterization studies of various poly(lactic acid) based systems and the correlation studies between Direct Pyrolysis Mass Spectrometry (DP-MS) and X-Ray Diffractometer (XRD) to characterize morphology of the polymer/clay systems.

In the first part, morphological, mechanical and thermal characterization studies on various poly(lactic acid) based systems have been investigated systematically via Transmission Electron Microscope (TEM), Scanning Electron Microscope (SEM), X-Ray Diffractometer (XRD), Differential Thermal Analysis (DTA), and Direct Pyrolysis Mass Spectrometry (DP-MS) techniques. Poly(ethylene glycol) in several proportions has been mixed with poly(lactic acid) via both solution casting and melt mixing methods and then characterization studies have been conducted. Furthermore,

PEG plasticized PLA/nanoclay composites, involving methyl, tallow, bis-2-hydroxyethyl, ammonium modified montmorillonite, Cloisite 30B (C30B), was selected as the reinforcing material and melt mixed via a twin-screw extruder. In addition, PLA nanocomposite fibers involving various quaternary ammonium salt modified natural montmorillonites, and PEG plasticized PLA/C30B composite fibers were fabricated successfully and characterized. Thermal characteristics such as thermal stability, melting temperature, char yield, crystallinity, thermal degradation mechanisms and possible chemical interactions were studied.

In the second part of this work, Direct Pyrolysis Mass Spectrometry has been applied to investigate the characteristics of polymer/nanoclay composites. For this purpose, various quaternary ammonium salt modified natural montmorillonites were incorporated into poly(lactic acid), poly(methyl methacrylate) and polyethylene matrices and analyzed via XRD and DP-MS techniques. The temperatures at which the organic modifier lost determined via DP-MS were correlated with inter-layer spacings calculated from XRD analyses. Furthermore, the interactions between the organic modifier and the matrix polymer were investigated





## CHAPTER 2

### 2. EXPERIMENTAL

#### 2.1. Materials

Poly(lactide), PLA, (number average molecular weight,  $M_n \sim 190000$ ), and Poly(ethylene glycol), PEG, ( $M_n \sim 8000$ ), were purchased from Cargill Dow. Poly(methyl methacrylate), PMMA, ( $M_n \sim 105000$ ) with the trade name SUMIPEX® Clear 011 was obtained from Sumitomo Chemical Co., Ltd. Low density polyethylene, LDPE, with a commercial name, Petilen F2-12, was supplied from Petkim Petrochemical Holding.

Several nanoclays involving methyl tallow bis-2-hydroxyethyl ammonium modified montmorillonite, Cloisite 30B, (C30B), dimethyl dihydrogenated tallow quaternary ammonium modified montmorillonites, Cloisite 15A, (C15A) and Cloisite 20A, (C20A), dimethyl, hydrogenated tallow, 2-ethylhexyl quaternary ammonium modified montmorillonite, Cloisite 25A, (C25A), methyl, dihydrogenated tallow quaternary ammonium modified montmorillonite, Cloisite 93A, (C93A) were provided by Southern Clay Products Inc. Also, dihydrogenated tallow dimethyl ammonium salt consisting mainly  $C_{18}$  and  $C_{16}$  hydrocarbons as tallow was purchased from Sigma Aldrich with a trademark Arquad® 2HT-75. Characteristic properties of the organically modified nanoclays were given in Table 1.

**Table 1:** Properties of montmorillonites.

Commercial names	Interlayer spacing, $d_{001}$ (nm)	Modifier concentration, meq/ 100g clay	Chemical structure of organic modifier
Cloisite 15A	3.15	125	$\begin{array}{c} \text{CH}_3 \\   \\ \text{H}_3\text{C}-\text{N}^+-\text{HT} \\   \\ \text{HT} \end{array}$
Cloisite 20A	2.42, 1.21	95	$\begin{array}{c} \text{CH}_3 \\   \\ \text{H}_3\text{C}-\text{N}^+-\text{HT} \\   \\ \text{HT} \end{array}$
Cloisite 25A	1.86	95	$\begin{array}{c} \text{CH}_3 \\   \\ \text{CH}_3-\text{N}^+-\text{CH}_2\text{CH}(\text{CH}_2\text{CH}_2\text{CH}_2\text{CH}_2\text{CH}_3) \\   \\ \text{HT} \end{array}$
Cloisite 30B	1.85	90	$\begin{array}{c} \text{CH}_2\text{CH}_2\text{OH} \\   \\ \text{H}_3\text{C}-\text{N}^+-\text{T} \\   \\ \text{CH}_2\text{CH}_2\text{OH} \end{array}$
Cloisite 93A	2.36	90	$\begin{array}{c} \text{H} \\   \\ \text{H}_3\text{C}-\text{N}^+-\text{HT} \\   \\ \text{HT} \end{array}$

Chloroform,  $\text{CHCl}_3$ , with a trade name EMSURE, ISO, (99 %), was purchased from Merck Millipore. Other solvents, dichloromethane, DCM, (99 %), and dimethylformamide, DMF, (99 %) were obtained from Sigma Aldrich. All materials were used without further purification.

## **2.2.Preparation Methods**

All experimental details including preparation procedures and processing conditions were divided into two major subtitles as seen below.

### **2.2.1. Preparation of PLA Based Blends, Composites and Electrospun Fibers**

#### **2.2.1.1. Preparation of PLA-PEG Blends with 90/10, 85/15 and 80/20 Blend Ratios and Their Composites Involving Cloisite 30B**

PLA and C30B were dried at 60 °C and PEG at 45 °C overnight under reduced pressure prior to the mixing processes. The mixtures of PLA-PEG with appropriate blend ratios, 90/10, 85/15 and 80/20 (wt/wt) and their composites with 3 wt% C30B were melt-compounded using a DSM Xplore twin screw micro compounder at 190 °C, with a screw speed 100 rpm for 8 min.

Before melt compounding, in order to achieve homogeneous mixtures, all components of the blends and the composites were mixed in chloroform at room temperature and solutions were stirred continuously for 1 hour with a 50/60 Hz frequency using a WiseStir MSH-20A magnetic stirrer. Then, prepared solutions were first dried at room temperature overnight and further vacuum dried at 50 °C for two days to evaporate chloroform completely prior to the melt-compounding process.

Finally, melt mixed samples were shaped to the dog-bone structure, shown in Figure 6, with dimensions 50.0, 7.6, 2.0 mm length, width and thickness, respectively by Daga Injection Molding Instrument at a barrel temperature of 190-195 °C and mold temperature of 40 °C. Samples were forced to mold cavities at 8 bar.

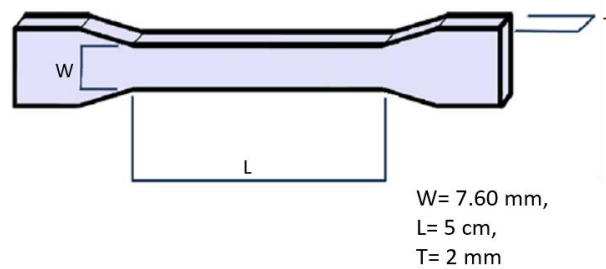


**Figure 6:** Representation of dog-bone specimen

Also, in order to compare the effects of blending methods, PLA-PEG 80/20 (wt/wt) blends were prepared by solution mixing method using the magnetic stirrer (1000 rph) for 1 hr, 12 hr and 24 hrs in chloroform and dried at 60 °C overnight in a vacuum oven to evaporate the solvent.

### 2.2.1.2. Preparation of Electrospun Fibers

For the fabrication of fibers, solutions were spun in an enclosed chamber at around 25 °C and 20% relative humidity with 1 ml syringes with metallic needle of 0.6 mm inner diameter. The syringe was placed horizontally on a New Era Pump Systems, Inc NE 300. The metal collector was covered with aluminum foil and then positive and negative electrodes of voltage supply were clamped to the metal needle and the collector, respectively. To visualize the electrospinning setup, a symbolic design is given in Figure 7.

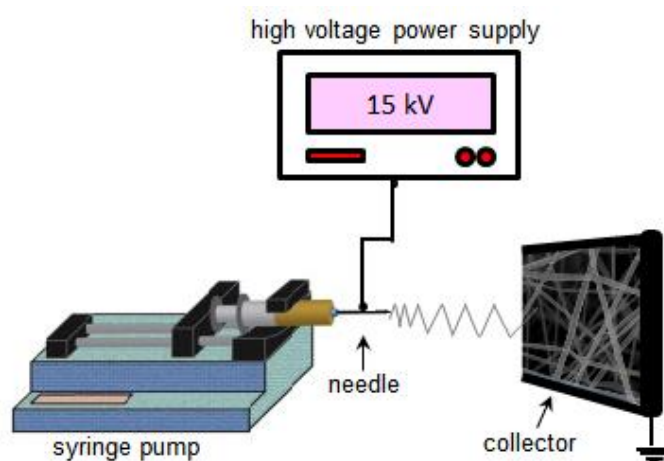


**Figure 7:** Electrospinning setup used for generation of fibers.

After several attempts,  $\text{CHCl}_3/\text{DMF}$  mixture was chosen as the most suitable solvent system and beaded and/or bead-free fibers were obtained. To create fibers, first

solvent concentrations have been chosen in the range of 100:0, 50:50, 60:40, 70:30, 80:20 and 90:10 (v/v) (CHCl<sub>3</sub>:DMF) while holding the PLA concentration constant and then, PLA concentration has been varied from 3% to 20% (w/v) keeping the solvent system constant. The electrospinning was conducted under 0.5 ml/h flow rate of the polymer solution, 12.5 kV the applied voltage and 10 cm tip to the collector distance.

#### **2.2.1.2.1. Preparation of Electrospun Fibers of PLA Composites Involving Cloisite 15A, Cloisite 20A and Cloisite 30B**

For the fabrication of PLA composites fibers, composites of PLA with Cloisite 15A, Cloisite 20A, and Cloisite 30B was employed. These composites were produced during my master's studies and, shortly, PLA and 1, 3 and 5 wt% montmorillonite was melt mixed in a twin screw extruder at 190 °C and 100 rpm for 8 min [162]. In line with the optimization studies of neat PLA fiber, 15% (w/v) PLA in 90:10 (v/v) CHCl<sub>3</sub>: DMF solvent system were selected for generation of PLA composite fibers. The electrospinning parameters were selected as 0.5 mL/h for the flow rate of the polymer solution, 12.5 kV for the applied voltage and 10 cm for the tip-to-collector distance, as the most favorable results were obtained for these parameters.

#### **2.2.1.2.2. Preparation of Electrospun Fibers of PLA-PEG Blends and Fibers of Blend Composites Involving Cloisite 30B**

In this part, fibers of PLA-PEG blends with blend ratios 90/10, 85/15 and 80/20 (wt/wt) and fibers of blend composites involving 3 wt% Cloisite 30B were described (*see section 2.2.1.1. for preparation procedures of blends and composites*). Fibers of 15 wt% melt mixed samples were dissolved in 90:10 (v/v) CHCl<sub>3</sub>: DMF solvent system. The selected parameters were 0.5 ml/h solution flow rate, 16 kV for the applied voltage and 13 cm tip to the collector distance.

#### **2.2.2. Preparation of PLA, PMMA and PE Composites Involving Several Organoclays for Morphological Characterization Studies of Polymer/Clay Composite Systems via DP-MS**

Polymers (PLA, PMMA and PE) and montmorillonites (C15A, C20A, C25A, C30B, C93A) were dried in vacuum oven overnight at 60 °C before use. All melt-compounded samples were prepared with DSM Xplore twin-screw micro compounder at constant screw speed; yet, using different processing conditions. PMMA composites were solution mixed at room temperatures in CHCl<sub>3</sub> by WiseStir MSH-20A stirrer at 1000 rph. In Table 2, mixing methods and the process conditions used for the preparation of composites are collected. Except PLA-C20A and PLA-C30B, all composites involved 5 wt% organoclays. PLA-C20A and PLA-C30B contained 3 wt% organically modified montmorillonite.

**Table 2:** Mixing methods and process parameters of composites involving 3-5 wt% organoclay.

<b>Polymer</b>	<b>Mixing method</b>	<b>Nanoclay</b>	<b>Mixing Parameters</b>
<b>PLA</b>	Melt compounding	C15A C20A* C25A C93A C30B*	Processing temperature: 190 °C, Screw speed: 100 rpm, Mixing time: 8 min
<b>PMMA</b>	Solution casting	C15A C25A C93A C30B	Mixing rate: 1000 rph Mixing time: 1 hr for C15A & C30B, 24 hrs for C25A & C93A
<b>PE</b>	Melt compounding	C15A C25A C93A C30B	Processing temperature: 185 °C, Screw speed: 100 rpm, Mixing time: 3 min

\*for starred ones 3 wt% organically modified montmorillonite was incorporated.



## **2.3.Characterization Techniques**

### **2.3.1. X-ray Diffractometer (XRD)**

XRD analyses of the clay-containing polymer samples and pure clays were performed on Rigaku X-ray diffractometer (Model, Miniflex) with a radiation source of  $\text{CuK}_\alpha$  (30 kV, 15 mA,  $\lambda = 1.54051 \text{ \AA}$ ) at room temperature.  $2\theta$  ranges were set in between  $0^\circ$  to  $10^\circ$  where the characteristic peaks of nanoclays were observed. Also, 1 degree/minute was selected as scan speed. Bragg's law was used to calculate the interlayer spacings from the XRD patterns determined.

### **2.3.2. Transmission Electron Microscope (TEM)**

TEM images of composites were monitored with a FEI Tecnai G2 Spirit BioTwin CTEM. Two types of sampling methods were used depending on the physical structures of samples i.e. bulk or solution forms. For the bulk forms, ultra-thin slices (approximately, 100 nm thickness) of dog-bone shaped specimens were cut by ultramicrotomy process. For the solution forms, very dilute solutions of composites was transferred to the carbon coated copper TEM-grids (3 mm diameter and 400 mesh) with a micro syringe and then, solvent,  $\text{CHCl}_3$ , evaporated at room temperature overnight. Finally, after samplings, TEM analyses were carried out.

### **2.3.3. Scanning Electron Microscope (SEM)**

Scanning electron microscope was used to examine the morphology of fiber mats. SEM images were obtained by using a FEI Nova NanoSEM 430 JSM 6400 Electron Microscope (JEOL). All the samples were coated with 5 nm Au/Pd (PECS-682) prior to the SEM imaging.

### **2.3.4. Molecular Masses and Polydispersity**

Number average ( $M_n$ ) and weight average ( $M_w$ ) molecular masses, and polydispersities were determined by gel permeation chromatography (GPC). GPC with the trade name Shimadzu LC-20AD and with refractive index detector, RID 20A was used. The instrument had a PSS SDV analytical linear M model column and  $\text{CHCl}_3$  was used as the eluent (4 mg PLA or PLA-PEG/2 mL  $\text{CHCl}_3$ ). Calibration studies was made with Polystyrene standards.

### **2.3.5. Mechanical Analyses**

For the mechanical analyses of PLA-PEG blends and composites, Lloyd LR 30K universal tensile testing machine was used. The measurement of mechanical properties including tensile strength, Young's modulus and percentage strain at break were performed according to ASTM D638 standards.

For each sample, 4 dog-bone shaped specimens were tested to ensure the reliability. The results were given by taking the average of these 4 measurements. The specimens were tested with 5 cm/min crosshead speed and 5 kN of cell load at room temperature. Before mechanic tests, specimens were held in vacuum oven at 50°C overnight to remove any possible moisture.

### **2.3.6. Thermal Analyses**

#### **2.3.6.1. Simultaneous Thermal Analyses (STA)**

STA is a simultaneous technique that combines the features of thermogravimetry (TG) and differential analysis (DTA or DSC). For TG and DTA measurements, a Perkin Elmer Simultaneous Thermal Analyzer 6000 instrument was used. STA 6000 measures the changes in weight of a sample and change in temperature between the sample and the reference simultaneously as a function of temperature and/or time [163]. STA analyses were performed at a constant flow rate of 20 mL/min under inert nitrogen atmosphere. Pressure of gas regulator outlet was set to 2.6 bar for each experiment. Also, in order to prevent the influence of sample size difference on thermal properties, 6.5 mg of samples were used in every analyses. The samples were heated from 25 °C to 550 °C with a heating rate of 10 °C/min.

### 2.3.6.2. Direct Pyrolysis Mass Spectrometer (DP-MS)

In this section, besides the experimental and instrumental details, basic working principles and important technical information are also given since DP-MS is not a widely known technique.

Basically, pyrolysis is known as thermal degradation of materials by cleavage at their weakest point in an inert atmosphere and/or vacuum. When pyrolysis technique is coupled with a mass spectrometer, it is possible to separate and identify degradation products. Therefore, DP-MS is generally employed to analyze the thermal characteristics including thermal stability, degradation mechanisms and pyrolysis products [164].

In DP-MS, first a polymer is heated under high vacuum and as a result it is separated into its fragments. Then, these fragments are ionized with an ionization source. Finally, the ionized fragments are separated according to their  $m/z$  ratios through a analyzer which creates a total ion current, TIC, curve. TIC curve is the variation of total ion yield as a function of temperature or time.

It is important to point out that during ionization, generation of secondary reactions are almost totally eliminated since pyrolysis products are rapidly removed from the hot zone due to high vacuum inside mass spectrometer. However, pyrolysis fragments further dissociate in the ionization process. In addition, generally, a very complex mass spectrum is generated as various fragments having different combinations of C, H, N or O atoms may have the same  $m/z$  values. Therefore, to characterize the thermal decomposition of a sample and predict the degradation mechanisms correctly, besides the TIC curve and the mass spectra, single ion evolution profiles (pyrograms) of selected ions should be examined. According to the trends in the single ion evolution profiles, products can be grouped and so the degradation mechanisms can be presented.

For pyrolysis analyses, two different mass spectrometers; HP Agilent 5973 mass spectrometer, coupled to a JHP SIS direct insertion probe system and Waters Micromass Quattro Micro GC Mass Spectrometer coupled to a direct insertion probe, were used. For DP-MS analyses, 100 mg of melt-compounded blends and/or composites were dissolved in 2 mL  $\text{CHCl}_3$ . On the other hand, solution casted composites or blends were directly prepared by preserving this concentration. For each test, the same amount of sample was analyzed, except fibers since dissolving in a solvent destroys their structures.

During the pyrolysis experiments using HP Agilent 5973 Mass Spectrometer, ions are generated by electron impact source selecting 70 eV as ionization energy. Pyrolysis mass spectra were recorded at 2 scans/s mass scan rate. 2  $\mu\text{L}$  of 0.01 mg sample containing solution were poured into in the flared glass vials with a micropipette and then the solvent was evaporated in a vacuum oven. Samples were heated up to 450 °C from 30 °C with a 10 °C/min heating rate.

On the other hand, Waters Micromass Quattro Micro GC Mass Spectrometer allows to heating up to 650 °C. Therefore, during the pyrolysis experiments via this system, temperature was increased to 650 °C from 50 °C at a heating rate of 10 °C/min. About 0.01 mg samples were scanned in quartz vials with 1 scan/s mass scanning rate. Ions were again generated by electron impact source using 70 eV as ionization energy.

Before the analyses of the samples, background analyses of empty vials were performed to check presence of any impurity. In addition, analyses were repeated for several times to ensure reproducibility.



## **CHAPTER 3**

### **3. RESULTS AND DISCUSSIONS**

#### **3.1. PLA Based Blends, Composites and Fibers**

In this part of this work, characteristics of poly(lactic acid)-poly(ethylene glycol), PLA-PEG, blends and their organoclay composites were investigated [165], [166]. For this purpose, DSC, TGA, DP-MS and tensile strength analyses of all samples and in addition morphological analyses of organoclay composites were performed. Furthermore, morphological and thermal characterizations of electrospun fibers of PLA, PLA-PEG blends and corresponding composites were discussed in detail [161], [167].

### **3.1.1. PLA-PEG Blends And Composites Involving Cloisite 30B**

#### **3.1.1.1. Poly(lactic acid)-poly(ethylene glycol), PLA-PEG Blends**

Thermal and mechanical characteristics of poly(lactic acid)-poly(ethylene glycol), PLA-PEG blends involving 10, 15 and 20 wt% PEG prepared by melt blending were investigated [165].

##### **3.1.1.1.1. Thermal Analyses**

Thermal characteristics of PLA-PEG blends were studied by applying DSC, TGA and DP-MS analyses.

##### **3.1.1.1.1.1. Differential Thermal and Thermogravimetry Analyses**

In Figure 8, DTA curves of neat PLA, neat PEG, melt mixed PLA-PEG blends with 10, 15 and 20 wt% PEG ratios were given. The endothermic melting peak of PLA at around 172 °C was shifted to 166, 167 and 166 °C with the addition of 10, 15 and 20 wt% PEG into PLA respectively, mainly due to the plasticizing effect of PEG [168]. The presence of single melting point was associated with the generation of compatible blend systems. Upon addition of 10, 15 and 20 wt% PEG, the cold



crystallization temperature ( $T_{cc}$ ) of PLA appeared at 86.2, 77.3 and 88.4 °C respectively. The glass transition temperature ( $T_g$ ) of PLA decreased drastically to 52.3 °C from 73.4 °C for PLA90-PEG10 blend and attributed to the increase in the segmental motion due to the plasticizing effect of PEG as expected in accordance with the literature results [6], [7], [25]. Also, as the amount of PEG was increased from 10 wt% to 15 and 20 wt%, the  $T_g$  was not observed in DTA analysis since it was shifted to lower temperatures below the temperature range of the instrument as the amount of PEG increased.

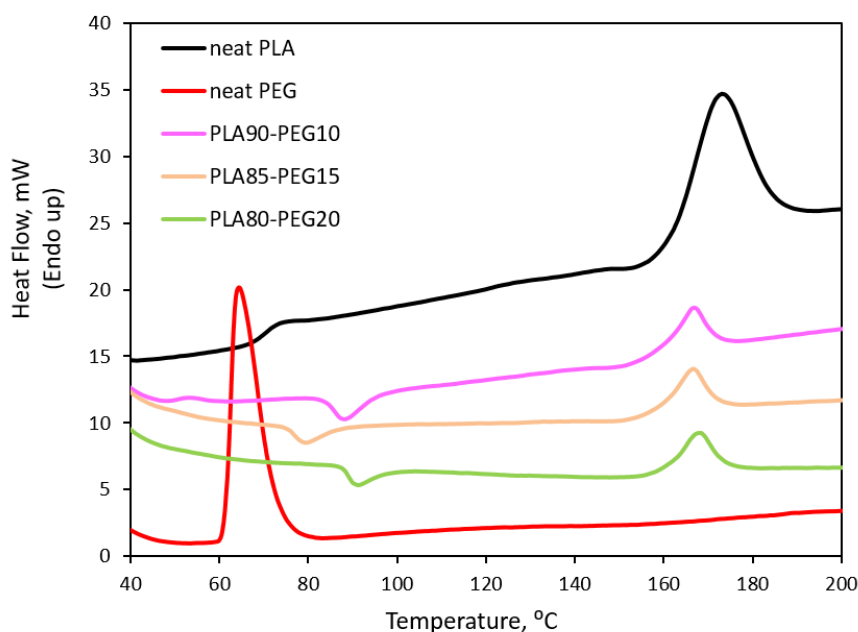


**Figure 8:** DTA curves of neat PLA, neat PEG, PLA-PEG blends with 10 wt%, 15wt% and 20 wt% PEG.

In Figure 9, TGA curves and differential thermal gravimetry (DTG) curves of PLA-PEG blends are depicted and the relevant data, the temperatures at which 5% ( $T_{5\%}$ ) and 10% ( $T_{10\%}$ ) and maximum ( $T_{max}$ ) weight losses recorded for neat PLA, neat PEG, PLA-PEG blends with 10 wt%, 15 wt% and 20 wt% PEG are summarized in Table 3.

Thermal stability of PEG was noticeably higher than that of PLA. Neat PLA and neat PEG started to decompose at 329.1 and 338.4 °C, respectively. Decrease in the thermal stability of PLA and PEG was detected for the blends compared to the pure polymers. The thermal decomposition of PLA was shifted to lower temperatures in the presence of PEG. As the amount of PEG increased, the decrease in the thermal stability of PLA became more significant for the blends. For the blends involving 15 and 20 wt % PEG, thermal degradation took place in two steps; the first step was associated with degradation of PLA and the second step becoming more pronounced with the increase in PEG content was attributed to degradation of PEG.

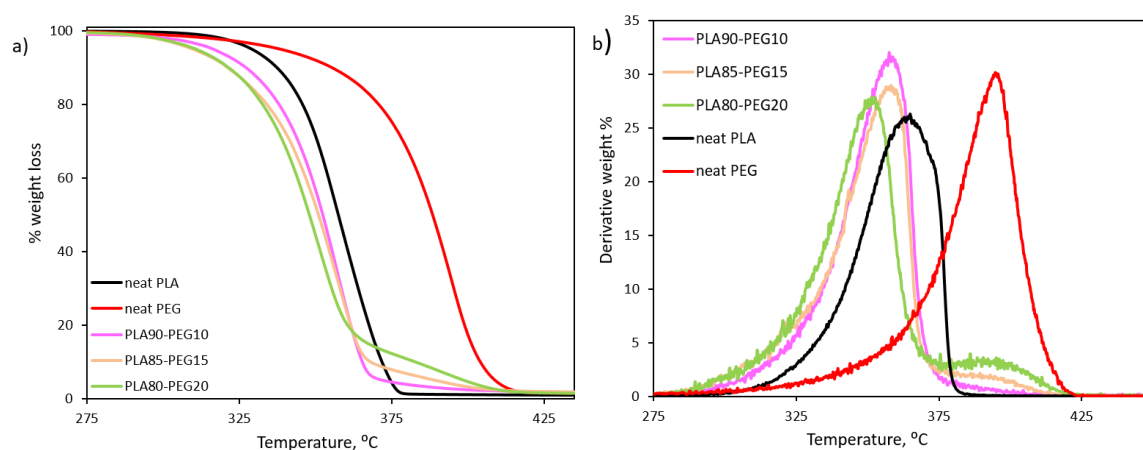


**Figure 9:** a) TGA b) DTG curves of neat PLA, neat PEG, PLA-PEG blends with 10 wt%, 15wt% and 20 wt% PEG.

**Table 3:** TGA data of neat PLA, neat PEG, PLA-PEG blends with 10 wt%, 15wt% and 20 wt% PEG.

	<b>T<sub>5%</sub></b>	<b>T<sub>10%</sub></b>	<b>T<sub>max1</sub></b>	<b>T<sub>max2</sub></b>	<b>%char yield</b>
<b>neat PLA</b>	329.1	336.9	366.9	-	0.8
<b>neat PEG</b>	338.4	354.9	-	395.3	1.0
<b>PLA90-PEG10</b>	315.8	326.9	358.3	-	0.8
<b>PLA85-PEG15</b>	308.8	320.8	358.6	394.3	1.2
<b>PLA80-PEG20</b>	310.5	320.6	351.0	397.7	0.9

#### 3.1.1.1.1.2. Direct Pyrolysis Mass Spectrometry Analyses

The total ion current, TIC, curves which is the variation of total ion yield as a function of temperature, of neat PLA, neat PEG and PLA-PEG blends, prepared by melt mixing, and their mass spectra recorded at peak maxima were given in Figure 10

As observed in TGA analyses, the thermal stability of neat PEG was significantly higher than that of neat PLA. The TIC curves of the blends showed two peaks, an intense one associated with the decomposition of PLA and a weak one at higher temperatures attributed to the degradation of PEG. In general, the evolution of thermal degradation products of PLA was detected almost in the same temperature region as the neat PLA. On the other hand, the high temperature peak associated with the decomposition of PEG was shifted to low temperature regions with the increase in the amount of PEG incorporated.

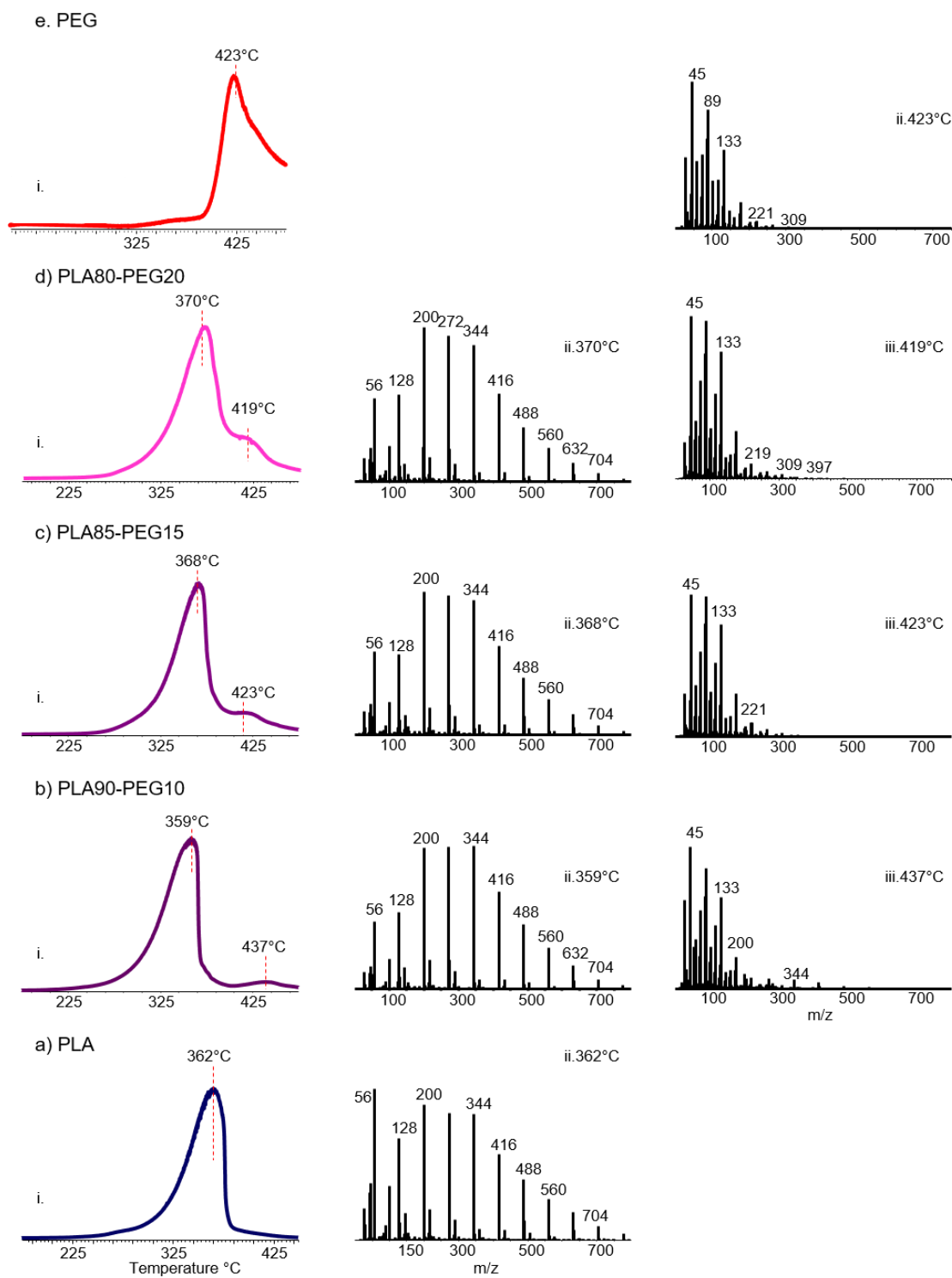


**Figure 10:** Total ion current curves and recorded mass spectrum of neat PLA, neat PEG and PLA-PEG blends at the recorded peak maxima.

In order to analyze the degradation behaviors and products and also predict the products of possible reactions, single ion pyrograms which represents the degradation behavior of each ion should be examined [169], [170]. In Figure 11, single ion pyrograms of characteristic degradation products of PLA, PEG and PLA-PEG blend with 10 wt% PEG, PLA90-PEG10, are depicted.

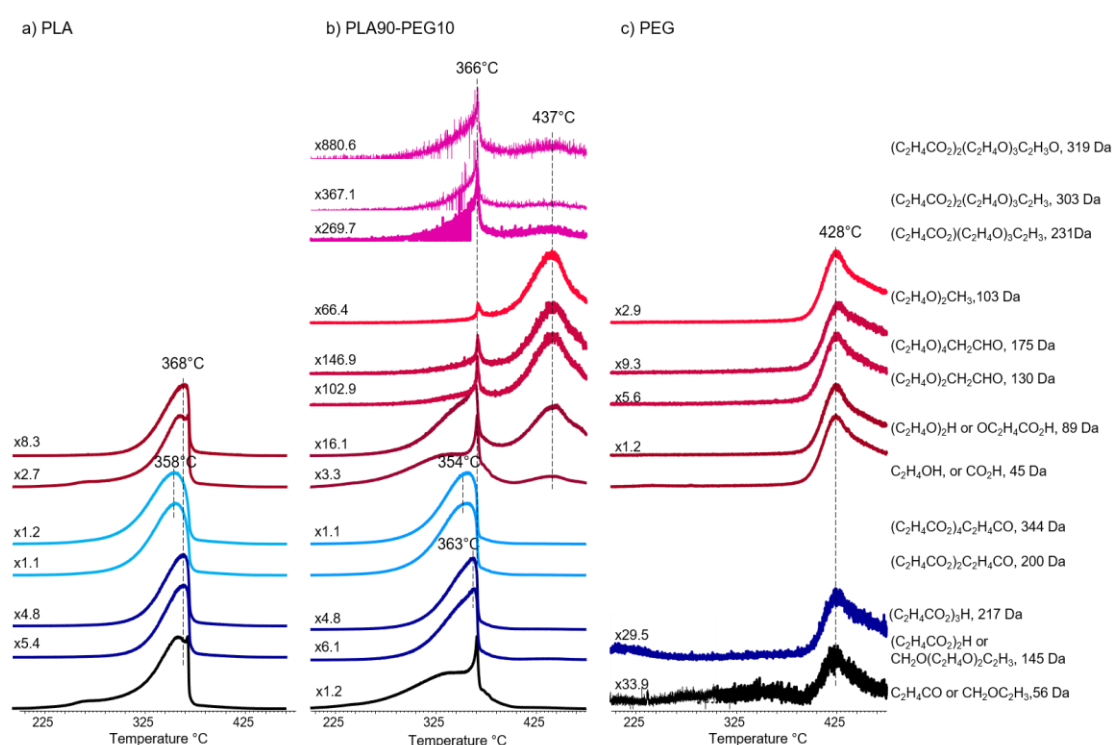


**Figure 11:** Single ion evolution profiles of some selected products recorded during the pyrolysis of a) neat PLA, b) PLA-PEG blend with 10 wt% PEG, PLA90-PEG10 and c) neat PEG.

Thermal degradation of PLA is mainly dominated by random bond cleavages and trans-esterification reactions. Fragments of trans-esterification reactions with general formula  $(C_2H_4CO_2)_x C_2H_4CO$  ( $m/z=72x-88$  for  $x=2$  to  $12$ ), i.e.  $(C_2H_4CO_2)_2 C_2H_4CO$  (200 Da) and  $(C_2H_4CO_2)_4 C_2H_4CO$  (344 Da) are generated by elimination of the neutral molecules like  $CO_2$  and acetaldehyde during ionization of the cyclic oligomers. In addition, low mass fragments are produced by random chain homolysis reactions i.e.  $(C_2H_4CO)$  (56 Da) [6], [37]–[39], [41]. A second and much less pronounced series of peaks with  $m/z=72x+73$  for  $x=2$  to  $12$  are associated with fragments produced by cis-elimination reactions with general formula  $(C_2H_4CO_2)_x H$  i.e.  $(C_2H_4CO_2)_3 H$  (217 Da).

It is known that thermal degradation of PEG mainly occurs via random chain cleavages of C-O and C-C bonds followed by H transfer reactions [24], [25], [42]. Several end groups such as;

- ✓ methyl,  $(C_2H_4O)_x CH_3$  ( $m/z=44x+15$  for  $x=2$  to  $12$ ) i.e.  $(C_2H_4O)_2 CH_3$  (103 Da),
- ✓ ethyl,  $(C_2H_4O)_x C_2H_5$  ( $m/z=44x+29$  for  $x=2$  to  $12$ ) i.e.  $(C_2H_4O)_3 C_2H_5$  (161 Da),
- ✓ hydroxyl, ( $m/z=44x+17$  for  $x=2$  to  $12$ ) i.e.  $(C_2H_4O)_2 OH$  (105 Da)
- ✓ aldehyde  $(C_2H_4O)_x C_2H_3O$  ( $m/z=44x+43$  for  $x=0$  to  $17$ ) i.e.  $(C_2H_4O)_2 C_2H_3O$  ( $m/z= 130$  Da) and  $(C_2H_4O)_4 C_2H_3O$  ( $m/z= 175$  Da)
- ✓ unsaturated groups,  $(C_2H_4O)_x C_2H_3$  ( $m/z=44x+27$  for  $x=0$  to  $17$ ) i.e.  $(C_2H_4O)_3 C_2H_3$  ( $m/z= 159$  Da)

are generated. As a consequence of further dissociation during ionization, peaks due to low mass fragments are more intense. Among these, the most abundant product is  $C_2H_4OH$  fragment ( $m/z=45$  Da) and the yields of the products involving hydroxyl end groups are more intense.

On the other hand, unfortunately, some of the thermal degradation products of PLA and PEG have the same  $m/z$  values due to the similarities in their repeating units i.e.  $CO_2H$  from PLA and  $C_2H_4OH$  from PEG have  $m/z$  value 45 Da and  $OC_2H_4CO_2H$  from PLA and

$(\text{C}_2\text{H}_4\text{O})_2\text{H}$  from PEG have  $m/z$  value 89 Da. However, as thermal degradations of PLA and PEG occur at two distinct temperature regions, the trends in single ion evolution profiles have significant importance to analyze their thermal degradation behaviors.

As seen in Figure 11, the products generated by cis-elimination reactions and those produced by trans-esterification reactions showed almost identical trends during the pyrolysis of neat PLA and PLA90-PEG10 blend. In contrast, noticeable changes in the evolution profiles of low mass products such as  $\text{CO}_2\text{H}$  (45 Da) and  $\text{C}_2\text{H}_4\text{CO}$  (56 Da) were detected. According to the relative intensities, degradation products diagnostic to PEG were less abundant in the pyrolysis mass spectra of the blend, as expected. In addition, a sharp peak at around 366 °C appeared in the single ion pyrograms of PLA90-PEG10 blend. One possibility was the contribution of PLA based products with the same  $m/z$  values. However, the evolution profiles of fragments which were only attributed to products of PEG; such as  $m/z=$  130 Da, 175 Da and 103 Da also showed two peaks, a sharp one with a maximum at around 366°C and a broad peak with a maximum at around 442°C. Also, elimination of new products that were not recorded during the pyrolysis of the neat PLA and PEG was also noticed upon inspection of pyrolysis mass spectra. These relatively weak products (i.e. fragments with  $m/z$  values 231, 303 and 319 Da) showed a single peak at around 366°C. The single ion evolution profiles of these products are also included in the figure for comparison.

In Figure 12, the pyrolysis data for PLA-PEG blends involving 10, 15 and 20 wt % PEG were given. The most abundant products were due to the thermal degradation of PLA chains via trans-esterification reactions. However, the relative yields of low mass products and the products generated by cis-elimination reactions were decreased as the amount of PEG in the blend was increased. Increase in the relative yields of PEG based products was detected as expected. In addition, as observed for PLA90-PEG10 blend, the relative yields of the products showing a single sharp peak in their evolution profiles were also increased noticeably.

The trends in the single ion evolution profiles revealed that the evolution of major thermal degradation products of PLA generated by trans-esterification and cis-elimination reactions were shifted slightly to high temperature regions from 354°C to 370°C and from 363°C to 375°C as the amount of PEG in the blend was increased. A shift to high temperature regions was also recorded for the sharp peak appeared at around 366°C in the same order. In contrast, the peak at around 437°C associated with degradation of PEG was shifted to low temperatures with the increase in PEG amount in the blend.

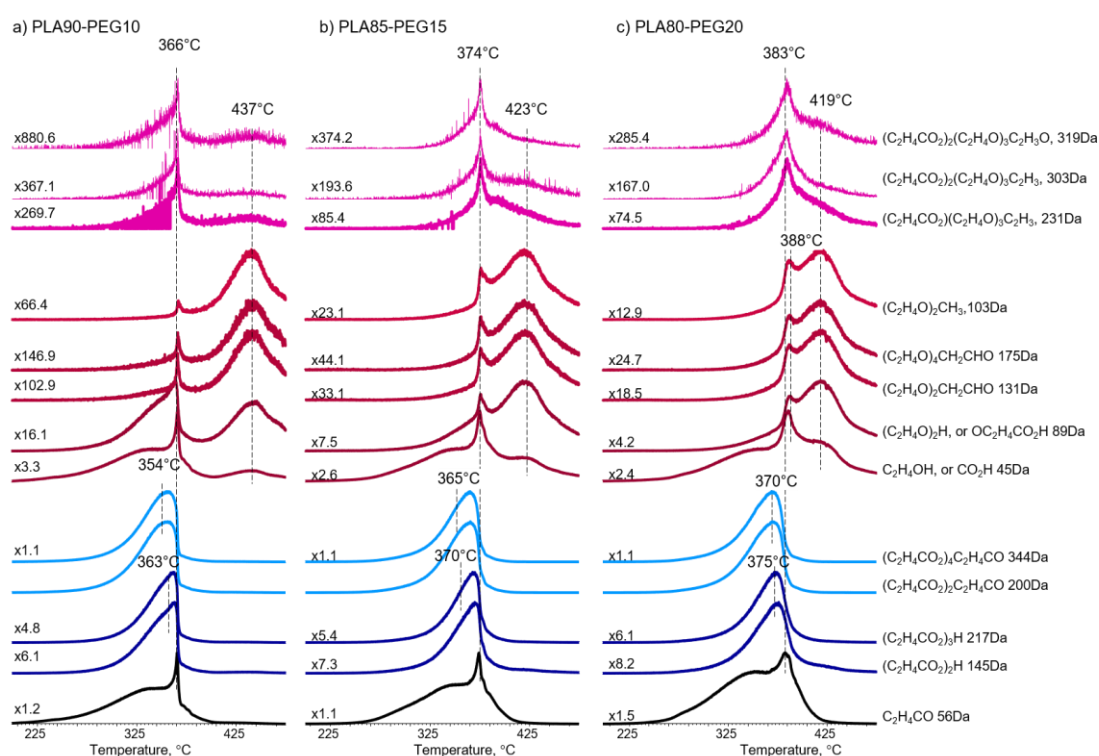
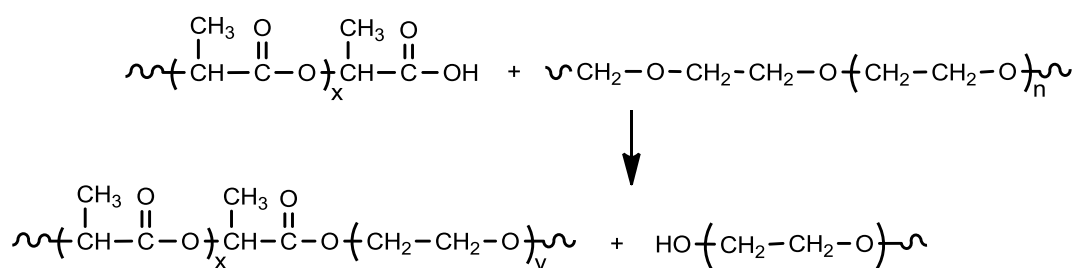


**Figure 12:** Single ion evolution profiles of some selected products recorded during the pyrolysis of a) PLA90-PEG10, b) PLA85-PEG15, c) PLA80-PEG20 blends.



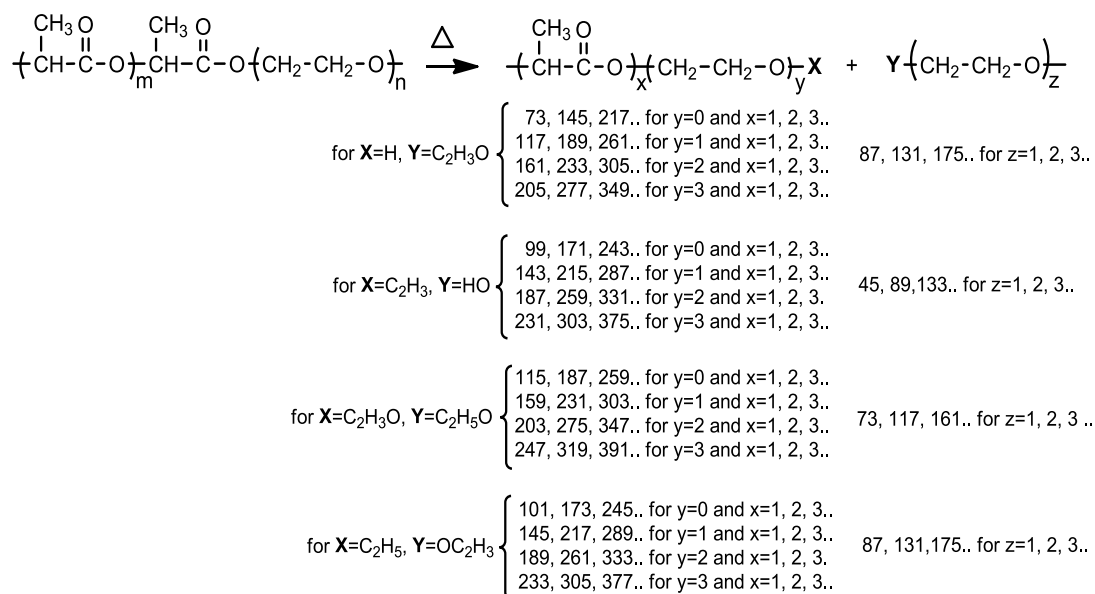
Therefore, it is clear that thermal degradation behaviors were changed upon incorporation of PEG into PLA matrix. It may be proposed that during the mixing process via melt blending at 190 °C or during the pyrolysis of the blends in mass spectrometer, the PLA chains or fragments involving COOH end groups, lead to the cleavage of the ether groups of PEG as shown in Scheme I. Consequently, lower mass chains of PEG bearing OH end groups and PLA chains linked to ethylene oxide units should be generated.

**Scheme I:** Acid decomposition of ether linkages.



On the other hand, thermal degradation of PLA chains with ethylene oxide units may generate products involving both repeating units. Hence, it may be thought that the decomposition of these chains yields products with general formula  $(\text{C}_2\text{H}_4\text{CO}_2)_x(\text{C}_2\text{H}_4\text{O})_y\text{H}$ ,  $(\text{C}_2\text{H}_4\text{CO}_2)_x(\text{C}_2\text{H}_4\text{O})_y\text{C}_2\text{H}_3$ ,  $(\text{C}_2\text{H}_4\text{CO}_2)_x(\text{C}_2\text{H}_4\text{O})_y\text{C}_2\text{H}_3\text{O}$  and  $(\text{C}_2\text{H}_4\text{CO}_2)_x(\text{C}_2\text{H}_4\text{O})_y\text{C}_2\text{H}_4\text{H}$ ,  $(\text{C}_2\text{H}_4\text{CO}_2)_x(\text{C}_2\text{H}_4\text{O})_y\text{CH}_3$  by the cleavage of ether linkages followed by H-transfer reactions. The proposed degradation mechanism for these fragments was given in Scheme II.

**Scheme II:** Possible thermal degradation products of PLA chains involving ethylene oxide units as the end groups.



As discussed before, some of the pyrolysis products of PLA, PEG or both have the same m/z values with some of these products. However, products with m/z values 231, 303 and 319 Da which were not detected during the pyrolysis of neat PLA and neat PEG, can directly be associated with chemical formula  $(\text{C}_2\text{H}_4\text{CO}_2)(\text{C}_2\text{H}_4\text{O})_3\text{C}_2\text{H}_3$ ,  $(\text{C}_2\text{H}_4\text{CO}_2)_2(\text{C}_2\text{H}_4\text{O})_3\text{C}_2\text{H}_3$ , and  $(\text{C}_2\text{H}_4\text{CO}_2)_2(\text{C}_2\text{H}_4\text{O})_3\text{C}_2\text{H}_3\text{O}$ , respectively. The significant increase in the relative abundances of these fragments with the increase in the amount of PEG incorporated can be regarded as a direct evidence for the proposed chemical interactions between PLA and PEG.

The pyrolysis experiments were carried under the high vacuum conditions and thus, secondary reactions were almost totally avoided. However, in order to clarify whether the pyrolysis or mixing process was effective in acid-ether reactions, PLA-

PEG 80/20 (wt/wt) blends were also prepared by solution mixing with 1, 12 and 24 h mixing times and analyzed by pyrolysis mass spectrometry. Single ion evolution profiles of selected thermal degradation products detected during the pyrolysis of the PLA80-PEG20 blends prepared by melt mixing and solution mixing, are given in Figure 13. The characteristic products associated with the degradation of PLA chains involving ethylene oxide units as the end groups (i.e. 231 Da and 303 Da) were also detected during the pyrolysis of the blends prepared by solution mixing.

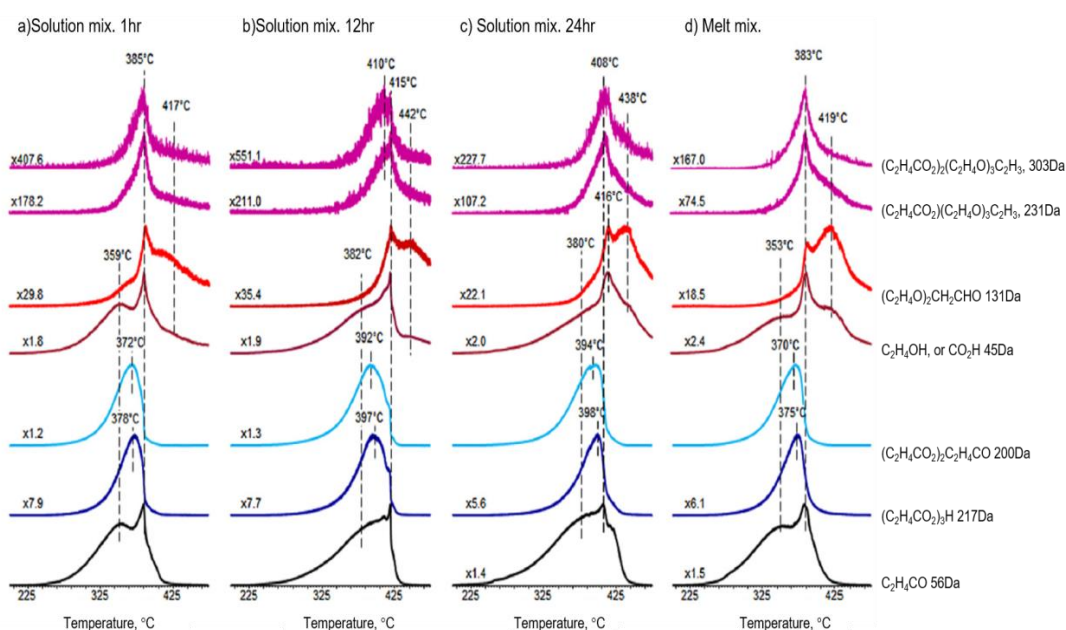


**Figure 13:** Single ion evolution profiles of selected products recorded during the pyrolysis of solution mixed PLA80-PEG20 blends having a) 1 h, b) 12 h, and c) 24 h mixing time and the pyrolysis of d) melt mixed PLA80-PEG20 blend.

As the mixing time increased to 24 h, the relative yields of these products were also increased supporting the idea that the acid-ether reactions mainly took place during the mixing processes. The increase in the thermal stability of the blends prepared by solution mixing for 12 h and 24 h may be associated with the generation of a crosslinked structure increasing the thermal stability of both PLA and PEG chains.

#### **3.1.1.1.2. Mechanical Properties**

Tensile tests were performed for four dog-bone shaped materials and the averages of these measurements were calculated and given in Table 4. Since there was no extensometer in tensile tester used, the results are given as comparison. Typically, the neat PLA is very brittle and rigid. Therefore, it has high tensile strength and Young's modulus values; yet very low % elongation at break. Since PLA is a rigid polymer, PEG is used as a plasticizer to improve its ductility. As the amount of PEG incorporated into PLA matrix was increased, the tensile strength and elastic modulus (Young's modulus) drastically were decreased compared to virgin PLA, which can be associated with the plasticizing effect of PEG. PLA80-PEG20 blend presented a decrease in tensile strength to the tune of 75.0% and elastic modulus to 72.0% respectively, compared with the neat PLA. In addition, the %elongation at break was increased noticeably only for the blend containing 20 wt% PEG indicating that PEG transformed the brittle fracture of PLA to the ductile fracture. For PLA90-PEG10 and PLA85-PEG15 blends, no significant change in %elongation within the experimental errors compared to virgin PLA was detected. For blends, the %elongation values did not present an increasing trend with increasing amount of PEG.

**Table 4:** Tensile test results of neat PLA, PLA-PEG blends with 10 wt%, 15wt% and 20 wt% PEG.

	<b>Tensile Strength (MPa)</b>	<b>% Elongation at Break (%)</b>	<b>Apparent Young's Modulus (MPa)</b>
<b>neat PLA</b>	64.5 ± 1.3	11 ± 0.5	1180 ± 30
<b>PLA90-PEG10</b>	48.9 ± 0.7	12.1 ± 2.1	905 ± 30
<b>PLA85-PEG15</b>	31.5 ± 2.5	8.1 ± 0.8	650 ± 40
<b>PLA80-PEG20</b>	16.1 ± 1.6	43.1 ± 10.4	330 ± 30

### 3.1.1.2. PLA-PEG Composites Involving Cloisite 30B

Morphological, thermal and mechanical characteristics of poly(lactic acid)-poly(ethylene glycol), PLA-PEG, blends involving 10, 15 and 20 wt % PEG and organically modified montmorillonite, Cloisite 30B prepared by melt blending were investigated [166].

#### 3.1.1.2.1. Morphological Analyses

For morphological characterizations of PLA-PEG blend composites, two complementary methods, X-ray diffraction, XRD, analyses and transmission electron microscope, TEM, images were used. XRD patterns and TEM images were analyzed together to investigate inter-layer spacing of clay layers and the dispersion states of clay layers.

In Figure 14, X-ray diffractogram of C30B and composites of PLA-PEG blends with several PEG ratios are given. X-ray patterns were used to determine the dispersion states of the C30B in the PLA-PEG blend composites. The diffractogram of C30B has a distinct maximum at around  $2\Theta=5.0^\circ$  corresponding to an inter-reticular distance of  $d_{001}=1.8$  nm according to Bragg's law. The characteristic peak of C30B was almost totally disappeared for all the composites of PLA-PEG blends.

Since the disappearance of the peak in the XRD diffractogram can be interpreted either as the well separation of the clay layers from each other or formation of tactoid structures, for a better understanding of the morphology of composites, TEM analyses were also conducted. TEM images were taken from a representative region of the composites involving 3 wt% C30B in 90/10, 85/15 and 80/20 wt % PLA-PEG blends are presented in Figure 15.

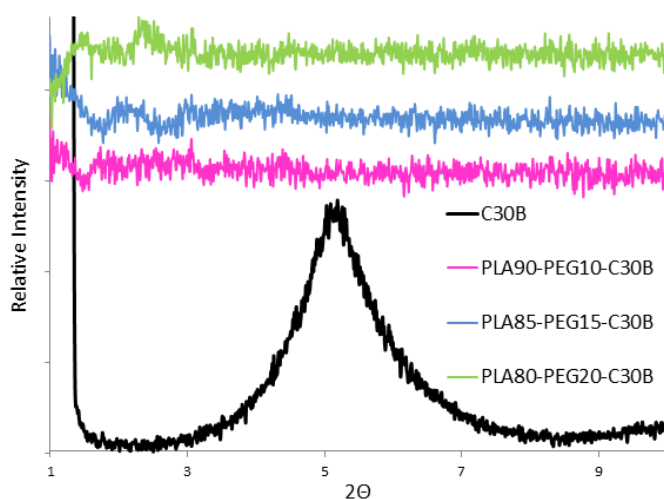


**Figure 14:** XRD diffractogram of C30B and PLA-PEG blend composites involving C30B.

It is known that mainly dispersion and localization of nano-fillers are needed for morphology refinement and stabilization in blend systems. And, this is generally achieved by the localization of particles at the blend interface. In Figure 16, high-magnification TEM images showed the existence of intercalated and exfoliated clay layers dispersed in the polymer matrix. It can be observed from TEM images that clay platelets tended to localize at the droplet interface of PEG and the size of the droplets decreased as the amount of PEG in the blend was increased. This may be associated with the interaction between OH groups of the organic modifier of the C30B with those of PEG at the interface. In addition, it may be thought that the more flexible PEG may penetrate more efficiently into the clay layers.

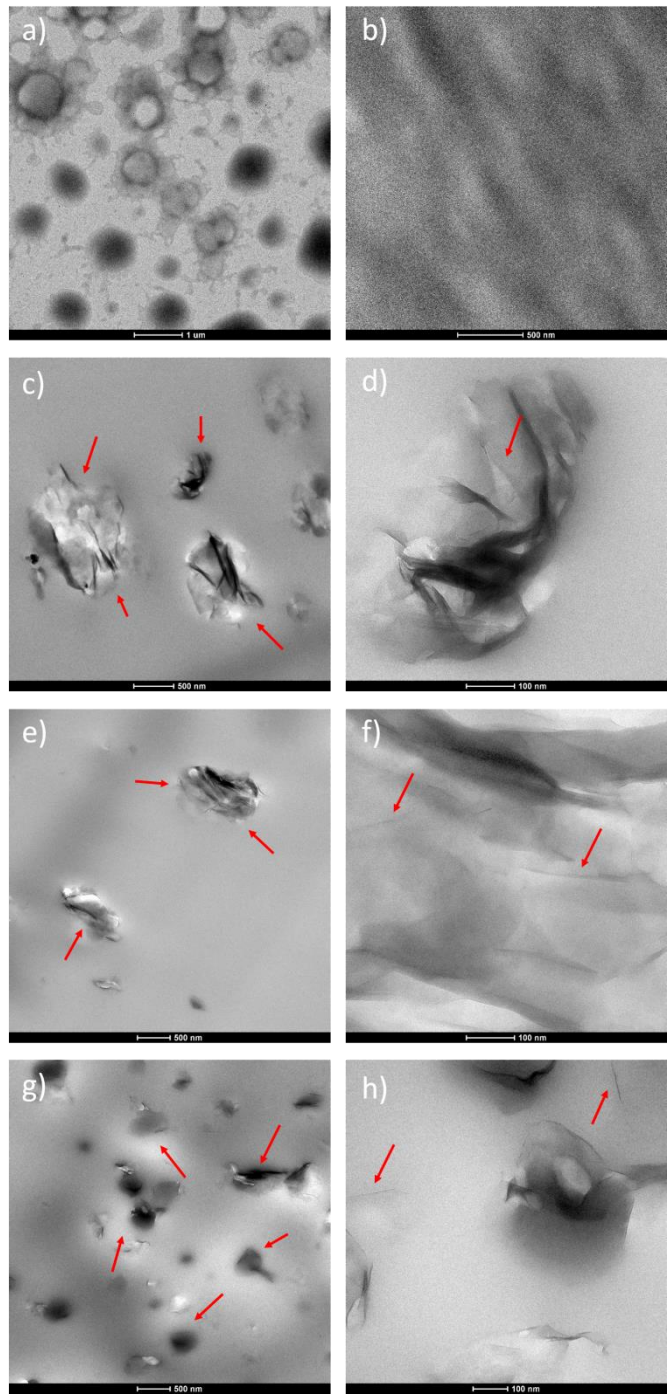


**Figure 15:** TEM images of a) neat PEG, b) neat PLA, and PLA-PEG blend composites with c,d) 10 wt%, e,f) 15 wt%, g,h) 20 wt% PEG amounts at low (bar scale= 500 nm) and high (bar scale= 100 nm) magnifications.



### **3.1.1.2.2. Thermal Analyses**

#### **3.1.1.2.2.1. Differential Thermal and Thermogravimetry Analyses**

In Figure 16, DTA thermograms of neat PLA, neat PEG, PLA-PEG composites with 10, 15 and 20 wt% PEG ratios and their comparison with corresponding blends were given.

As mentioned before, the endothermic melting peak of PLA at around 172 °C was decreased with the addition of 10, 15 and 20 wt% PEG mainly due to the plasticizing effect of PEG [168]. Upon incorporation of Cloisite 30B into the PLA-PEG blends, almost no change in the melting temperatures was observed. Similar to the blends, single melting point was thought to be an indication for the generation of compatible blend system after the addition of Cloisite 30B.

For composites, glass transition temperature ( $T_g$ ) could only observed for PLA-PEG composites with 10 wt% PEG (Figure 16). The glass transition temperature ( $T_g$ ) of PLA which was observed at 73.4 °C drastically decreased to 54.2 °C upon incorporation of C30B into PLA90-PEG10 blend. This significant decrease in  $T_g$  value was again attributed to the increase in the segmental motion due to the plasticizing effect of PEG. The slightly higher  $T_g$  value for PLA-PEG composite involving 10wt% PEG, PLA90-PEG10-C30B, compared to the corresponding blend, PLA90-PEG10, may be associated with stiffening action of organoclay particles toward plasticized PLA matrix.

According to first heating cycles, the cold crystallization temperature ( $T_{cc}$ ) of PLA appeared at 86.2, 77.3 and 88.4 °C with the addition of 10, 15 and 20 wt% PEG, respectively and upon incorporation of 3 wt % C30B increased slightly to 89.6, 79.0

and 89.5 °C compared to the corresponding blends, respectively. This increase can be associated with the nanofiller-induced nucleation effect of the nanoclays. This stiffening action of organoclay particles toward plasticized PLA matrix may also be due to the inability of PEG chains to interact with PLA as they were already interacting with the C30B. A similar behavior was observed by Pluta et al. [171].

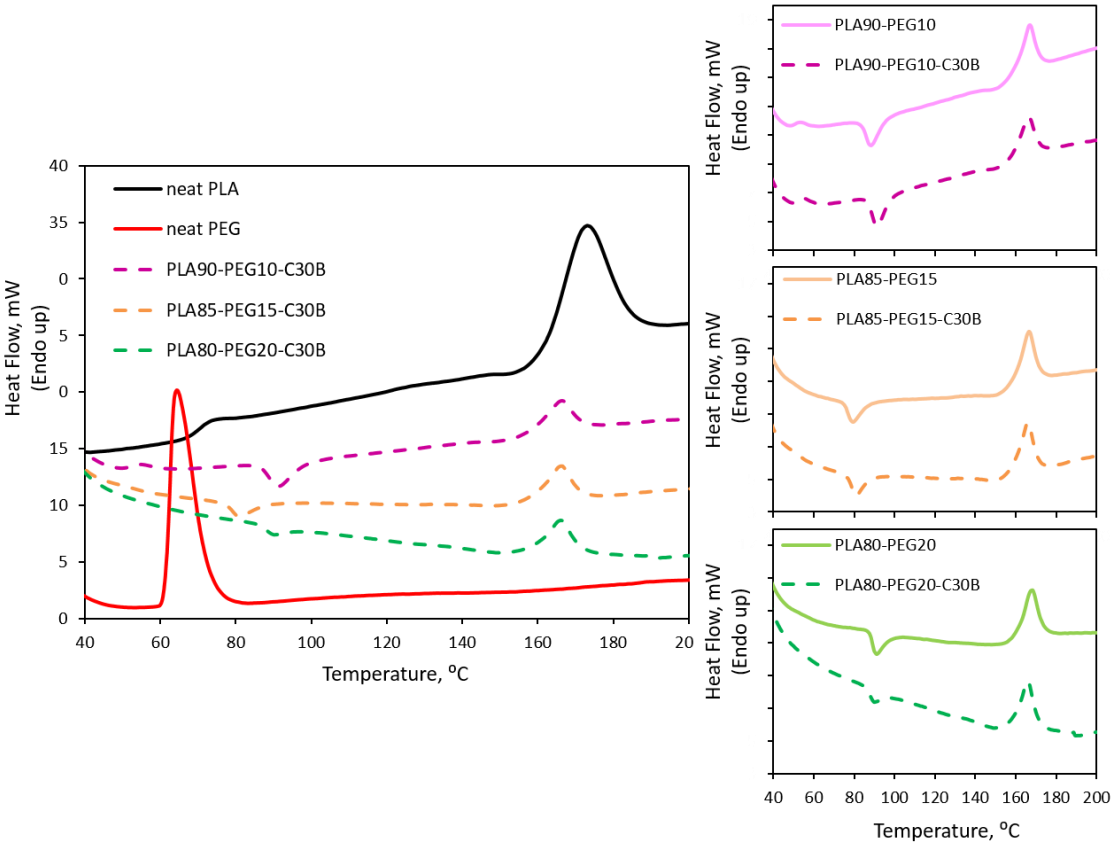


**Figure 16:** DTA curves of neat PLA, neat PEG, PLA-PEG blends with 10 wt%, 15wt% and 20 wt% PEG and their composites involving C30B.

On the other hand, to investigate the effects of clays on crystallinity of blends more detail, the thermal history of polymers were also removed by a temperature program and percent crystallinity values, X%, were calculated from 2<sup>nd</sup> heating and slow cooling ramps. Polymers were heated from 30 °C to 230 °C with 20 °C/min rate (1<sup>st</sup> heating), cooled from 230 °C to 30 °C with 5 °C/min cooling rate (slow cooling) and then reheated to 230 °C with 10 °C/min (2<sup>nd</sup> heating). In Table 5, the results of enthalpy of fusion,  $\Delta H_m$ , enthalpy of crystallization,  $\Delta H_c$ , and percent crystallinity of PLA-PEG blends and composites recorded during the second heating and slow cooling cycles were given. Also, the percent crystallinity values was normalized for those having C30B. For all the samples, the degree of crystallinity was increased after the incorporation of C30B into blends due to the nucleation effect of organoclay. In Figure 17, heating and cooling curve of PLA80-PEG20 blend was given as an example. In the first heating cycle, the cold crystallization was appeared as a result of rapid cooling of polymers during preparation via extrusion. On the other hand, the cold crystallization was not observed at the second heating curve as expected since amorphous regions were crystallized (melt crystallization) upon exposure to slow cooling temperature.

**Table 5:** DTA results of PLA-PEG blends and composites involving C30B detected during the second heating cycles

	$\Delta H_m(\text{J/g})$	$\Delta H_c(\text{J/g})$	X%	Normalized X%
<b>neat PLA</b>	15.9	-	17.2	17.2
<b>PLA90-PEG10</b>	28.5	6.9	38.0	38.0
<b>PLA90-PEG10-C30B</b>	27.9	13.4	44.4	45.8
<b>PLA85-PEG15</b>	28.4	18.1	50.0	50.0
<b>PLA85-PEG15-C30B</b>	28.4	21.1	53.2	54.8
<b>PLA80-PEG20</b>	24.9	21.2	49.5	49.5
<b>PLA80-PEG20-C30B</b>	29.3	18.6	51.5	53.1

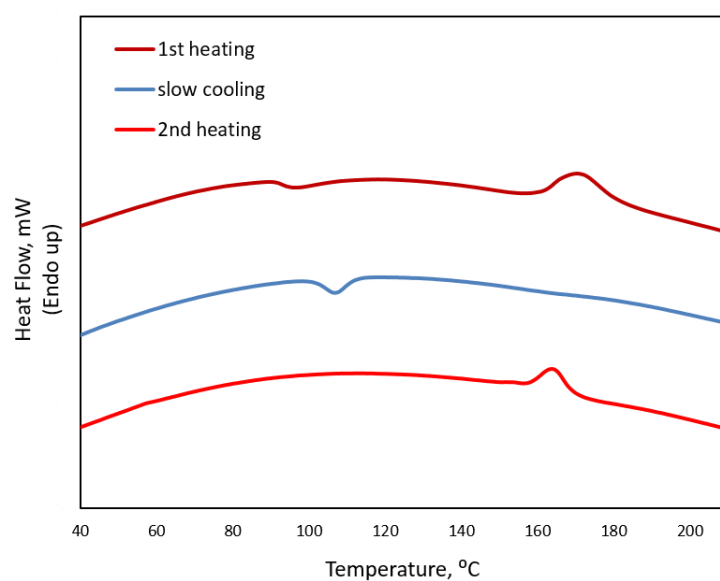


**Figure 17:** DTA curves of PLA80-PEG20 blend recorded during first heating, slow cooling and second heating cycles

In Figure 18, TGA and DTG curves of PLA-PEG blends and their composites are depicted and the relevant data are summarized in Table 6. Decrease in the thermal stability of PLA and PEG was detected for the blends and composites compared to neat PLA and PEG. The thermal decomposition of PLA was shifted to lower temperatures in the presence of PEG. Upon incorporation of Cloisite 30B, an increase in the char yield was detected as expected, yet, no systematic effect on thermal stabilities was detected. Also, according to DTG curves, in the presence of C30B, thermal decomposition of PLA-PEG occurred in a single-step.

**Table 6:** TGA data of neat PLA, neat PEG, PLA-PEG blends and their composites involving C30B.

	<b>T<sub>5%</sub></b>	<b>T<sub>10%</sub></b>	<b>T<sub>max1</sub></b>	<b>T<sub>max2</sub></b>	<b>%char yield</b>
<b>neat PLA</b>	329.1	336.9	366.9	-	0.8
<b>neat PEG</b>	338.4	354.9	-	395.3	1.0
<b>PLA90-PEG10</b>	315.8	326.9	358.3	-	0.8
<b>PLA90-PEG10-C30B</b>	305.5	317.9	354.2	-	2.1
<b>PLA85-PEG15</b>	308.8	320.8	358.6	394.3	1.2
<b>PLA85-PEG15-C30B</b>	308.7	323.4	359.0	-	2.6
<b>PLA80-PEG20</b>	310.5	320.6	351.0	397.7	0.9
<b>PLA80-PEG20-C30B</b>	305.9	320.2	353.5	-	3.1

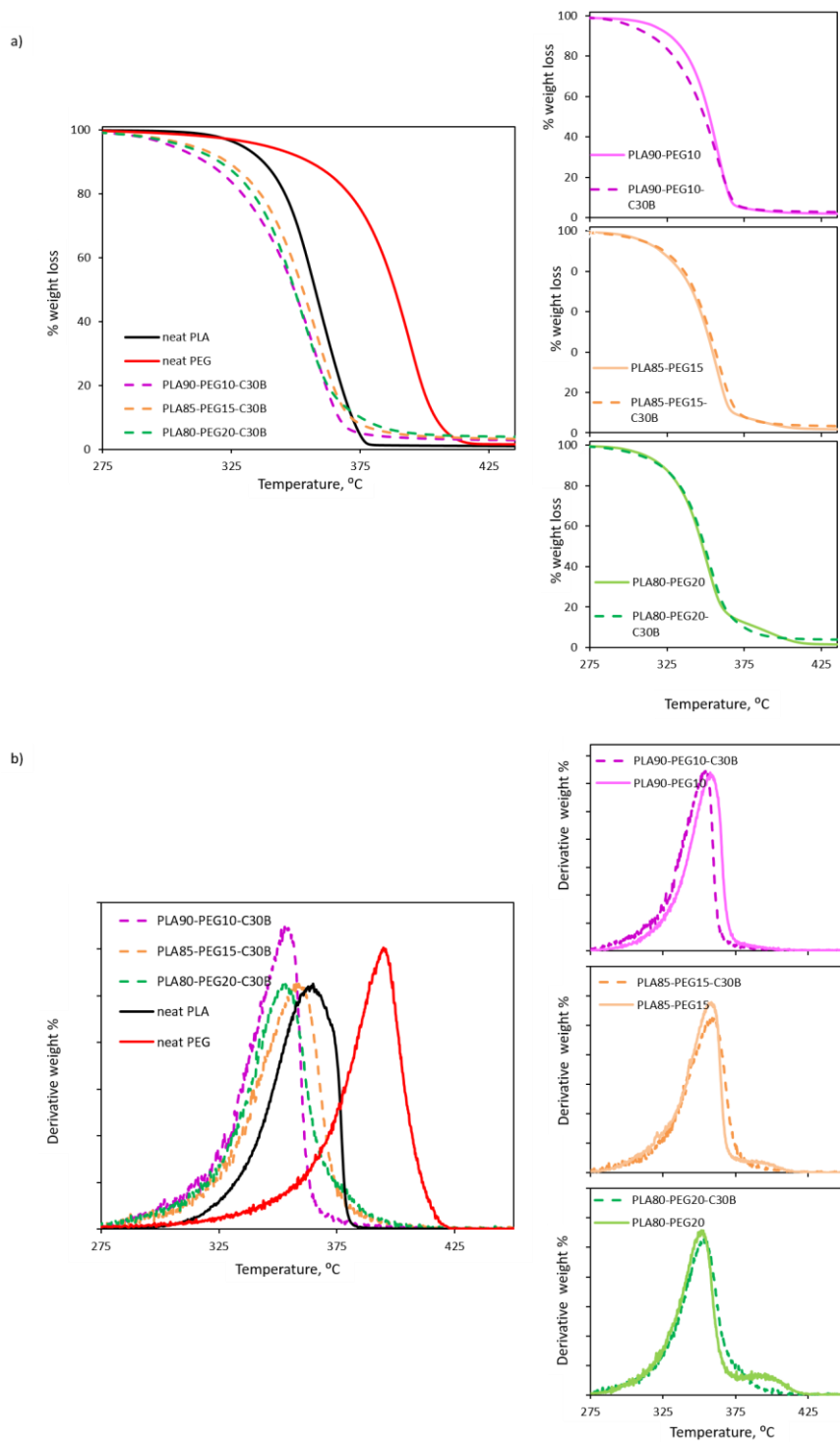


**Figure 18:** a) TGA and b) DTG curves of neat PLA, neat PEG, PLA-PEG blends and their composites.

### 3.1.1.2.2.1. Direct Pyrolysis Mass Spectrometry Analyses

The TIC curves and the mass spectra recorded at their peak maxima and low temperature shoulder of PLA-PEG composites and neat polymers were given in Figure 19. The TIC curves of the composites showed a broad peak with a low temperature shoulder. As the amount of PEG incorporated into composite increased both the shoulder and the peak maximum was shifted to high temperatures, but the shift was more pronounced for the shoulder. The most intense peak in pyrolysis spectra recorded at the shoulder and peak maxima was due to  $C_2H_4CO$  and/or  $C_3H_4O$  fragment, ( $m/z=56$  Da) for all the composites the contrary to the results obtained for PLA-PEG blends. In addition, after incorporation of C30B, the relative abundances of the low mass fragment ions were increased.

In Figure 20, single ion pyrograms of the degradation products of PLA, PEG, PLA-PEG blend with 10 wt% PEG and its composite were depicted. In the presence of C30B, the gap between the thermal degradation regions of PLA and PEG were decreased due to the increase in thermal stability of PLA and the decrease in thermal stability of PEG chains. The loss of low mass fragments, i.e. 45 and 56 Da, was recorded at relatively low temperatures at around 350 °C. On the other hand, the products generated by cis-elimination and trans-esterification reactions were recorded at significantly higher temperatures compared to the corresponding ones recorded during the pyrolysis of the pure PLA and PLA-PEG blends.

Moreover, the products due to the decompositions of units generated by the reactions between PLA and PEG (i.e. 231 Da, 303 Da and 319 Da) became more dominant and observed in the temperature region where PEG decomposition took place after the incorporation of C30B. In addition, thermal stability of these fragments increased significantly to 402 °C where PEG decomposition took place, with the incorporation of C30B compared to the corresponding blend, PLA90-PEG10.

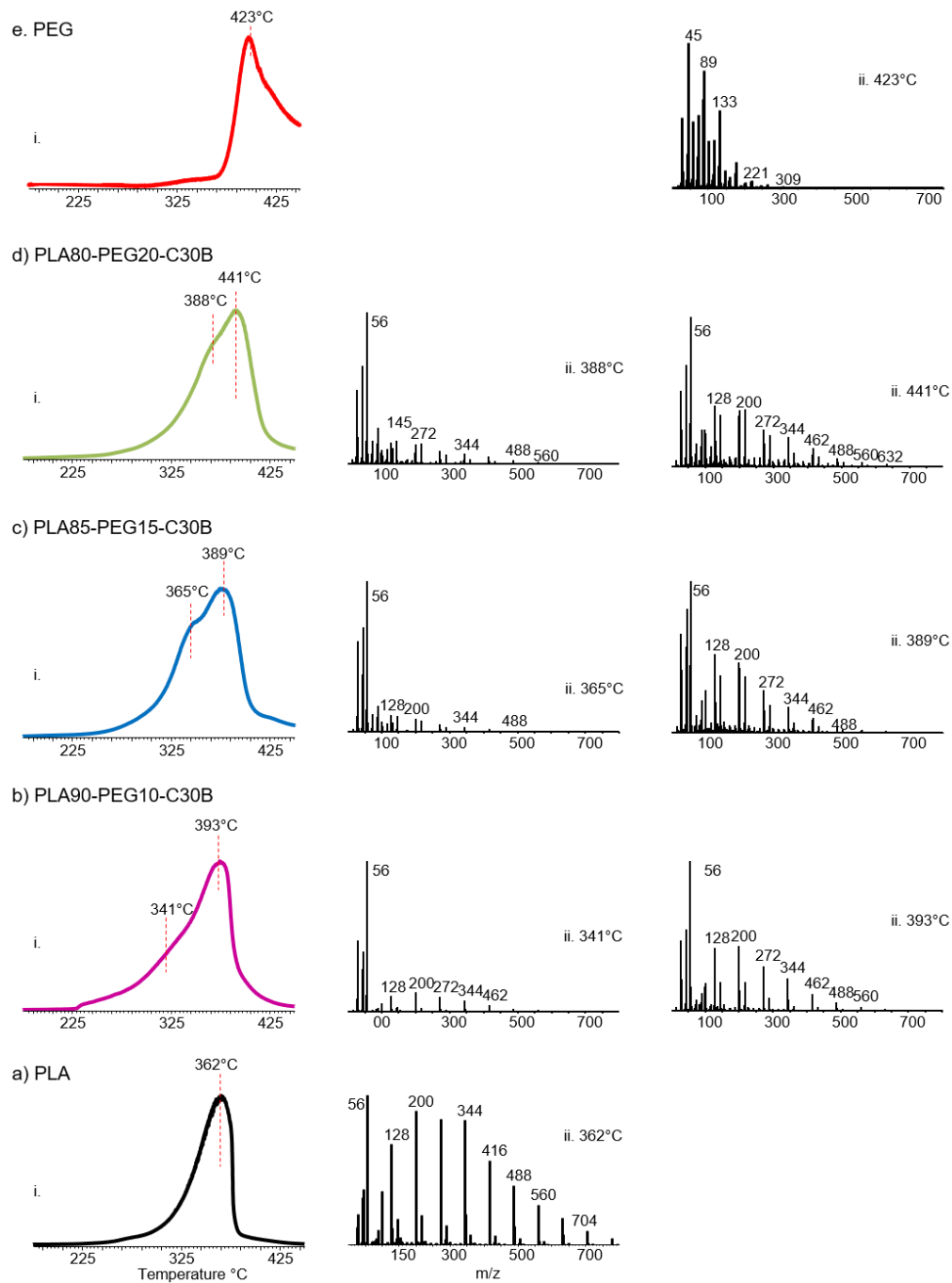


**Figure 19:** i. TIC curves and ii. the mass spectrum recorded at the peak maxima and low temperature shoulder of neat PLA, neat PEG, PLA-PEG blend composites involving C30B.



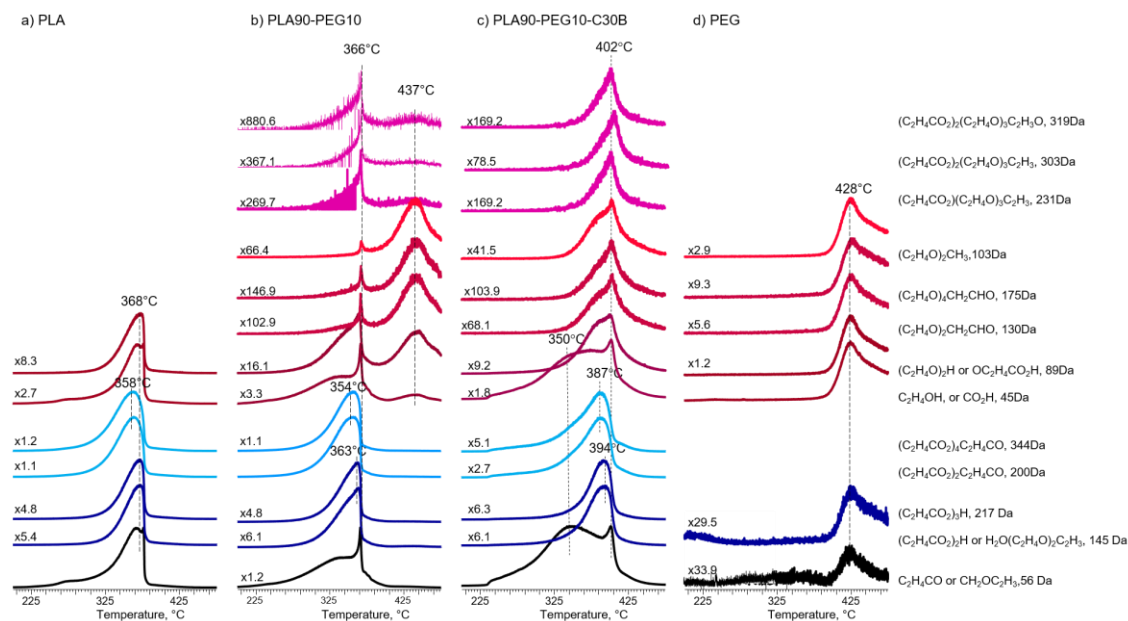


**Figure 20:** Single ion evolution profiles of a) neat PLA, b) 10 wt% PEG plasticized PLA, PLA90-PEG10, c) its composite involving C30B, PLA90-PEG10-C30B and d) neat PEG.

In Figure 21, single ion pyrograms of selected ions of PLA-PEG-C30B blend composites having 10, 15, and 20 wt % PEG are given. In addition to the characteristic products of PLA, PEG and the units generated by interaction of PLA and PEG chains, the single ion evolution profile of the main degradation product of the organic modifier of C30B associated with  $C_{18}H_{37}(CH_3)NHCH_2$ , and/or  $C_{19}H_{38}NO$  fragment,  $m/z = 296$  Da, is depicted. The relative yields of the products due to the degradation of PEG chains and the fragments generated by interaction of PLA and PEG chains were increased as the amount of PEG in the composite was increased. The increase was more pronounced for the products related to interactions between PLA and PEG. As the amount of PEG incorporated increased, the loss of organic modifier was shifted to significantly higher temperatures and the relative abundance of this fragment was also increased.

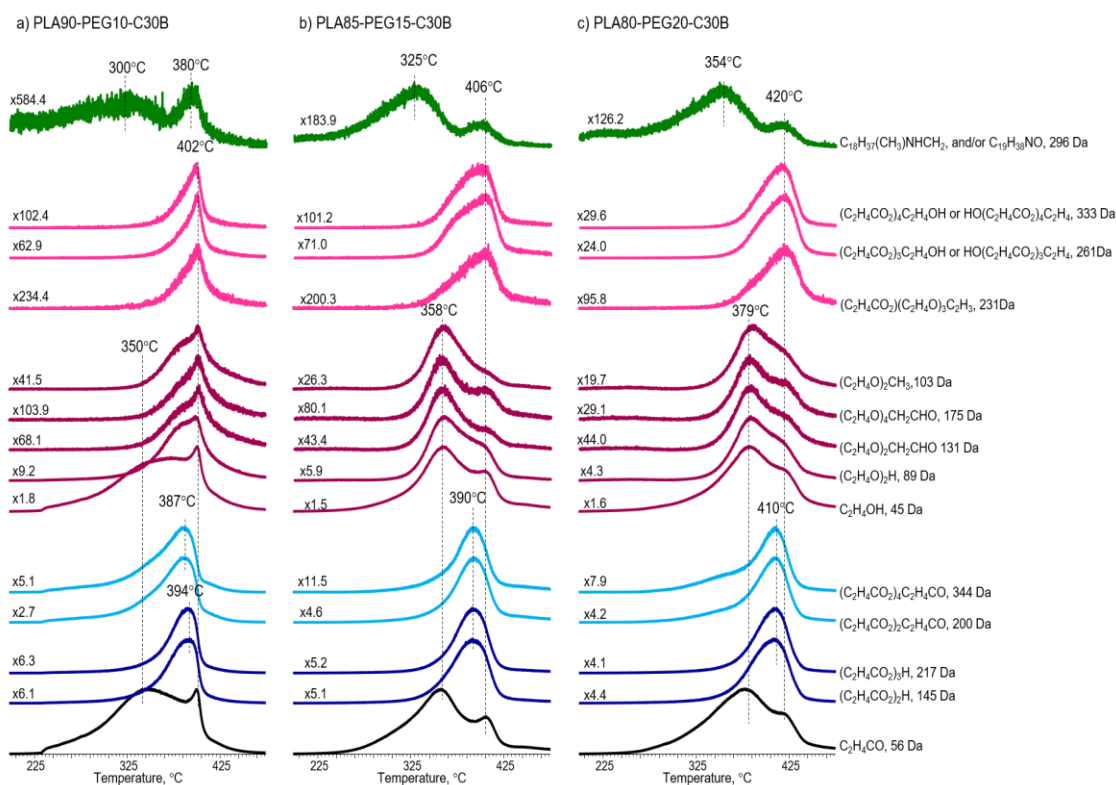
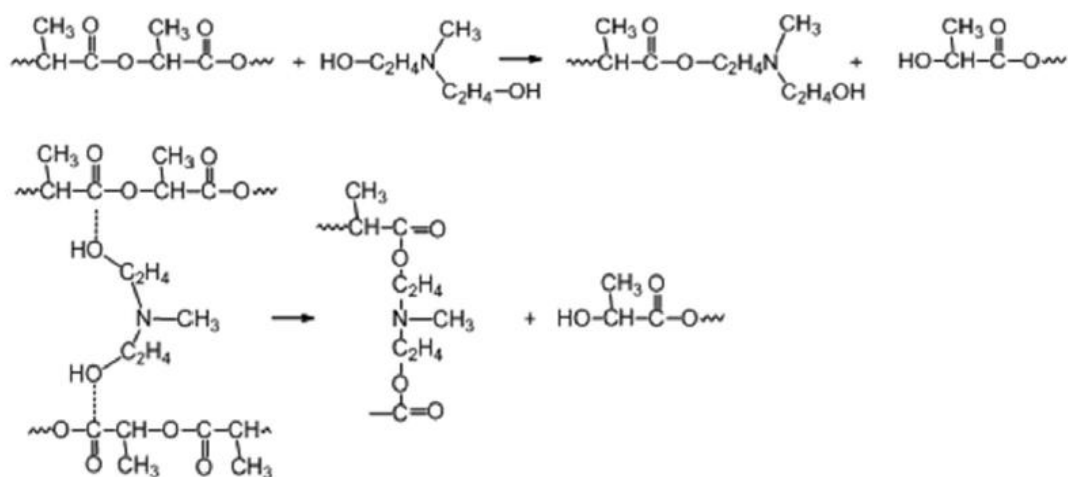


**Figure 21:** Single ion evolution pyrograms of selected ion of PLA-PEG-C30B blend composites having a) 10, b) 15, c) 20 wt% PEG content, respectively.

In a recent study, we proposed an interaction between the organic modifier of C30B and PLA chains as shown below in Scheme III, leading to significant increase in the relative yields of  $(C_2H_4CO_2)_xOH$  fragment ions, and decrease in the relative yields of the products associated with trans-esterification reactions [162]. However, in the presence of PEG, no evidence was detected for such an interaction between PLA and the organic modifier. Even though there was a decrease in the relative yields of the products associated with trans-esterification reactions, those of the products generated by cis-elimination reactions were almost constant. In addition, the yield of the product with m/z value 296 Da was significantly higher than the corresponding value detected for PLA-C30B composite although all the

composites involved the same amount of C30B [162]. Thus, it may be thought that in the presence of PEG the interactions between PLA and organic modifier of C30B were inhibited and the degradation of PEG took place more readily yielding mainly low mass fragments, as the clay platelets tended to localize at the droplet interfaces of PEG as depicted by TEM images. As a consequence, the interaction of these low mass PEG based fragments with PLA chains as shown in Scheme I may be expected to be enhanced. It may be proposed that the low mass fragments may diffuse into PLA more efficiently. The increase in the yield of the products generated by interactions between PLA and PEG, and significant increase in thermal stability of PLA even compared to PLA-C30B composite, supported this proposal.

**Scheme III:** Trans-esterification reactions between the organic modifier of C30B and PLA.



### 3.1.1.2.3. Mechanical Properties

Tensile test results of neat PLA, PLA-PEG blends and their composites involving C30B were collected in Table 7. In the mechanical analyses, upon incorporation of C30B into blends, an increase in the tensile strength and elastic modulus compared to their corresponding blends were detected. This result can be associated with the reinforcing effect of Cloisite 30B. Yet, the tensile strength of plasticized PLA composite was still low when compared to virgin PLA. Also, an interesting result for % elongation of PLA-PEG composite with 20 wt % PEG was recorded. The composite showed a drastic increase in % elongation. However, the increase in the standard deviations of % elongation was also noticeable for PLA80-PEG20 blend and PLA80-PEG20-C30B composite which might be due to the miscibility and homogeneity problems of bulk blends. In contrast to our result, Mohapatra et al. said that %elongation decreases upon incorporation of variable wt% nanoclay into PLA/PEG blends [6]. The unexpected behavior we observed may be associated with the more effective interactions of PLA and PEG chains in the presence of nanoclay.

**Table 7:** Tensile test results of neat PLA, PLA-PEG blends and their composites involving C30B.

	<b>Tensile Strength (MPa)</b>	<b>% Elongation at Break (%)</b>	<b>Apparent Young's Modulus (MPa)</b>
<b>neat PLA</b>	64.5 ± 1.3	11 ± 0.5	1180 ± 30
<b>PLA90-PEG10</b>	48.9 ± 0.7	12.1 ± 2.1	905 ± 30
<b>PLA90-PEG10-C30B</b>	49.8 ± 0.7	9.8 ± 0.9	950 ± 30
<b>PLA85-PEG15</b>	31.5 ± 2.5	8.1 ± 0.8	650 ± 40
<b>PLA85-PEG15-C30B</b>	38.2 ± 2.2	12.0 ± 2.8	710 ± 30
<b>PLA80-PEG20</b>	16.1 ± 1.6	43.1 ± 10.4	330 ± 30
<b>PLA80-PEG20-C30B</b>	26.9 ± 1.9	255.1 ± 62.5	470 ± 30

#### 3.1.1.2.4. Molecular Masses and Dispersity

The average molecular masses and dispersity of neat PLA, PLA-PEG blends and composites involving C30B determined by GPC are listed in Table 8. A significant decrease in the average molecular masses upon addition of PEG into PLA was detected. The decrease became more pronounced as the amount of PEG in the blend was increased. Upon incorporation of C30B into PLA-PEG blends a slight increase especially in the weight average molecular masses compared to neat blends was detected. The increase in  $M_w$  values became more significant as the amount of PEG present in the composite was increased. These trends may be due to interaction of PLA and PEG chains generating new segments in the presence of C30B.

**Table 8:** Number averaged and weight averaged molecular weights and polydispersity indexes of neat PLA, PLA-PEG blends and composites involving C30B.

	<b>M<sub>n</sub>/Da</b>	<b>M<sub>w</sub>/Da</b>	<b>PDI</b>
<b>neat PLA</b>	152600	230200	1.51
<b>PLA90-PEG10</b>	96800	156000	1.60
<b>PLA90-PEG10-C30B</b>	100500	159600	1.58
<b>PLA85-PEG15</b>	75700	122000	1.60
<b>PLA85-PEG15-C30B</b>	87800	127500	1.45
<b>PLA80-PEG20</b>	71600	107600	1.50
<b>PLA80-PEG20-C30B</b>	71200	131500	1.85

### 3.1.2. Electrospun Fibers of PLA Based Systems

Electrospun fibers of PLA based systems, namely neat PLA, PLA involving C15A, C20A and C30B, PLA-PEG blends involving 10, 15 and 20 wt % PEG and PLA-PEG blends involving 10, 15 and 20 wt % PEG and C30B were prepared and characterized [161], [167].

### **3.1.2.1. Electrospun Fibers of PLA**

Electrospun fibers of PLA were prepared using  $\text{CHCl}_3/\text{DMF}$  solvent systems. Both composition of the solvent system and the concentration of PLA were optimized in order to obtain bead-free PLA fibers. The morphology of the fibers was characterized by SEM analyses. Then, thermal properties of bead-free PLA fibers were investigated via DP-MS. Also, electrical conductivities of solutions used to create PLA fibers was measured as  $2 \mu\text{S}/\text{cm}$  for all samples.

#### **3.1.2.1.1. Morphological Analyses**

SEM was employed to visualize the structure of electrospun fibers. In Figure 22, 23 and 24, SEM images of fibers of neat PLA including several concentrations and solvent compositions are given.

In Figure 22 and Figure 23, SEM images of 7 wt% and 10 wt% PLA fibers in  $\text{CHCl}_3/\text{DMF}$  solvent systems with volume ratios 70:30, 80:20 and 90:10 (v/v) at high and low magnifications are depicted respectively. As the volume ratio of DMF in the solvent was increased keeping the concentration of PLA constant, the number of beads on the fibers decreased, but fiber diameters became slightly thicker. Similarly, as the concentration of PLA was increased from 7 wt% to 10 wt% keeping the solvent system constant, the existence of beads and beaded fibers were reduced but again fibers became thicker, as expected. For obtaining thinner fibers 90:10 (v/v)  $\text{CHCl}_3/\text{DMF}$  solvent system was chosen as the most suitable solvent. As the concentration of PLA was increased to 15% (w/v) bead-free fibers having fiber diameter around 500 nm were obtained (Figure 24).

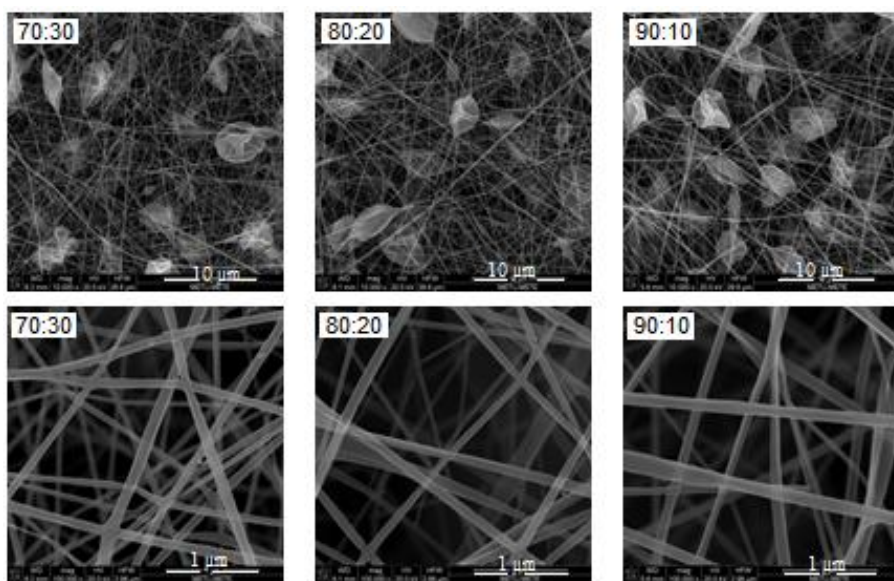


**Figure 22:** SEM images of 7 wt% PLA nanofibers at high and low magnifications in  $\text{CHCl}_3/\text{DMF}$  solvent systems with volume ratios 70:30, 80:20 and 90:10 (v/v).

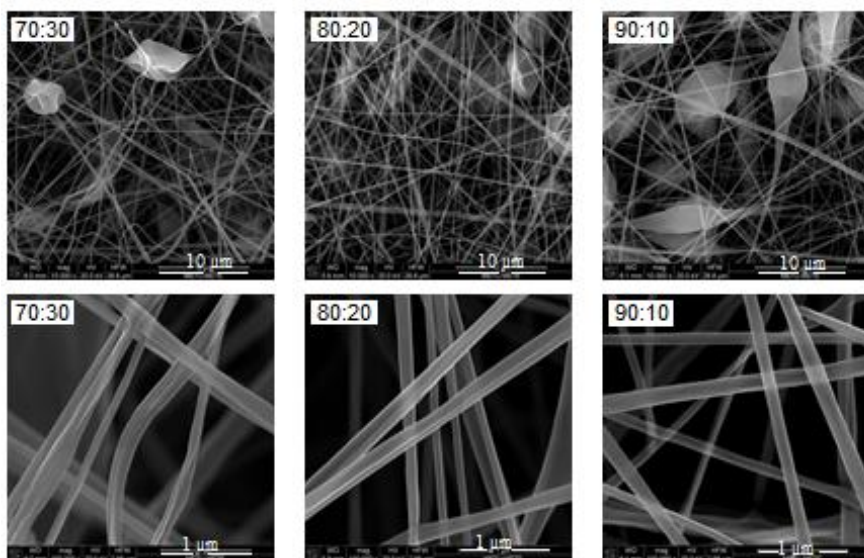


**Figure 23:** SEM images of 10 wt% PLA nanofibers at high and low magnifications in  $\text{CHCl}_3/\text{DMF}$  solvent systems with volume ratios 70:30, 80:20 and 90:10 (v/v).



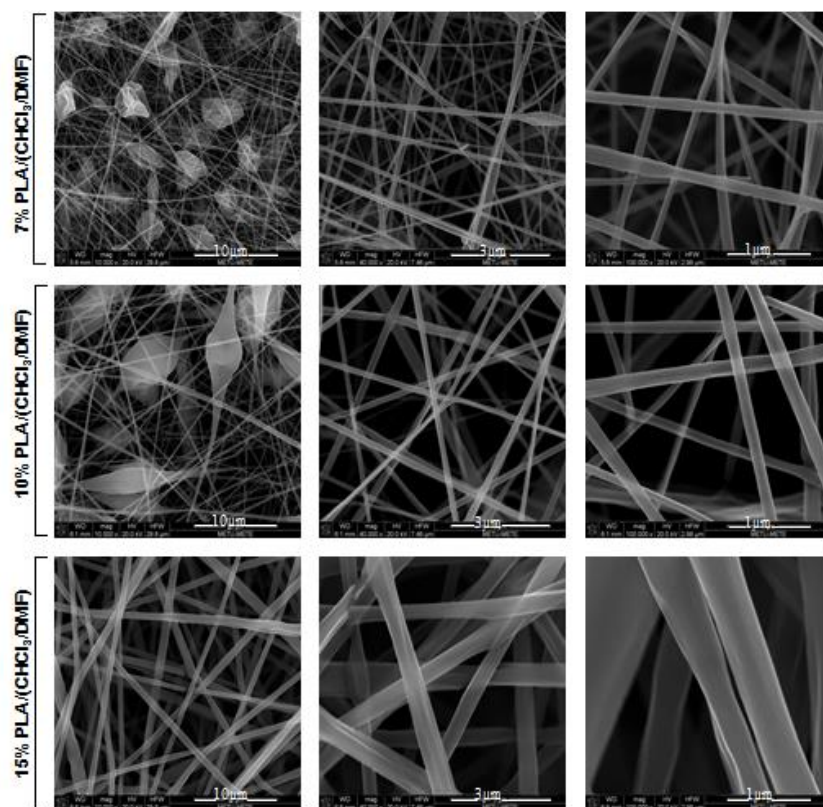


**Figure 24:** SEM images of 7 wt%, 10 wt% and 15 wt% PLA nanofibers in  $\text{CHCl}_3/\text{DMF}$  90:10 (v/v) solvent systems.

### 3.1.2.1.2. Thermal Analyses

The TIC curve and the pyrolysis mass spectrum at peak maximum, at around 350 °C and single ion evolution profiles of the characteristic degradation products recorded during the pyrolysis of 15% (w/v) PLA fiber prepared using  $\text{CHCl}_3/\text{DMF}$  90:10 solvent system are given in Figure 25. According to the single ion evolution profiles, Figure 25c, the relative intensities of the degradation products due to cis elimination reactions (i.e. 145 Da, 217 Da, etc.) were noticeably reduced compared to neat PLA. In contrast, the products generated by trans-esterification reactions (i.e. 128 Da, 200 Da, etc.) became slightly more

pronounced. The evolution profiles of these products were shifted to low temperatures and the shift was more significant for the fragments associated with trans-esterification reactions. On the other hand, the evolution of products generated by random chain scissions almost did not change. Thus, it may be thought that since the polymer chains were aligned upon nanofiber formation, the probability of intermolecular trans-esterification reactions was increased and energetically became more favorable.

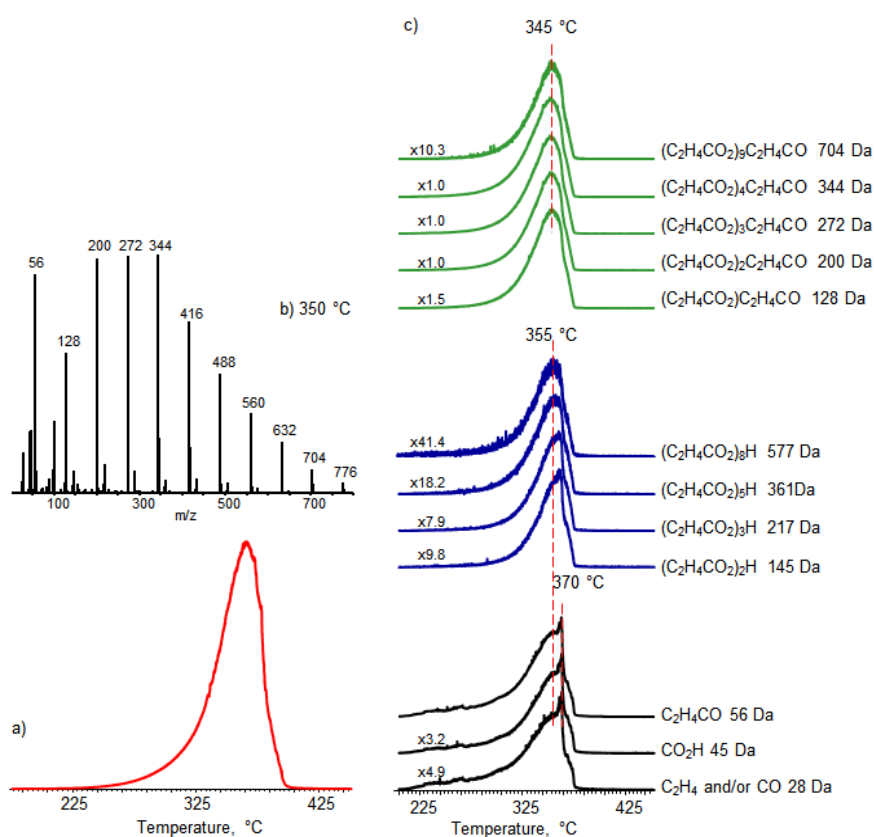


**Figure 25:** (a) Total ion current curve, (b) pyrolysis mass spectrum at 350 °C, and (c) single ion evolution profiles of some selected products recorded during the pyrolysis of 15% (w/v) PLA fiber  $CHCl_3/DMF$  90:10 solution system.

### **3.1.2.2. Electrospun Fibers of PLA Composites Involving Cloisite 15A, Cloisite 20A and Cloisite 30B**

As mentioned in the previous section, in order to spun bead-free and thinner PLA fibers, PLA concentration was optimized as 15% (w/v) in  $\text{CHCl}_3/\text{DMF}$  90:10 (v/v) solvent system. In the light of this information, these optimized values were selected for the generation of PLA composite electrospun fibers involving 1, 3 or 5 wt% organically modified montmorillonites, Cloisite 15A, 20A, or 30B. Morphologic analyses involved investigation of dispersion of clay layers via XRD and TEM analyses and characterization of structure of electrospun fibers by SEM analyses [161].

#### **3.1.2.2.1. Morphological Analyses**

X-ray diffractograms and TEM images of organically modified montmorillonite composites of PLA are given in Figure 26. The diffraction pattern of Cloisite 15A included three peaks at around  $2\Theta = 3.34, 5.18$  and  $7.72^\circ$  corresponding to inter-reticular distances of  $d_{001} = 2.64, 1.70$  and  $1.16$  nm, respectively. As it can be seen in Figure 26a, for, small budges located around  $2\Theta = 4^\circ$  and a weak peak located at around  $1.8^\circ$  which corresponds to interlayer spacing of  $d_{001} = 2.6$  nm were detected in the diffractogram of PLA/C15A composite. In the XRD pattern of PLA/C15A fiber, a weak and broad peak at around  $3.3^\circ$  indicating was detected. The XRD pattern of Cloisite 20A presented two characteristic peaks at around  $2\Theta = 3.9$  and  $7.4^\circ$  corresponding to inter-reticular distances of  $d_{001} = 2.21$  and  $1.19$  nm and after incorporation of C20A into PLA matrix, a broad peak was detected at around  $3.0^\circ$  indicating separation of clay layers to  $2.94$  nm. The XRD diffractograms of

PLA/20A fiber showed again very weak peak at around  $3.3^\circ$  corresponding to 2.67 nm. For Cloisite 30B, a sharp peak was located at  $2\Theta = 5.0^\circ$  corresponding to an inter-reticular distance of  $d_{001} = 1.8$  nm and for all samples of C30B, this sharp peak of C30B was almost totally disappeared.

The TEM images taken from representative regions of the PLA composites showed mainly good dispersion and intercalation of montmorillonites with some regions of tactoids, Figure 26b. For all composites, single unit layers of montmorillonites can be observed indicating the presence of exfoliated clay layers.

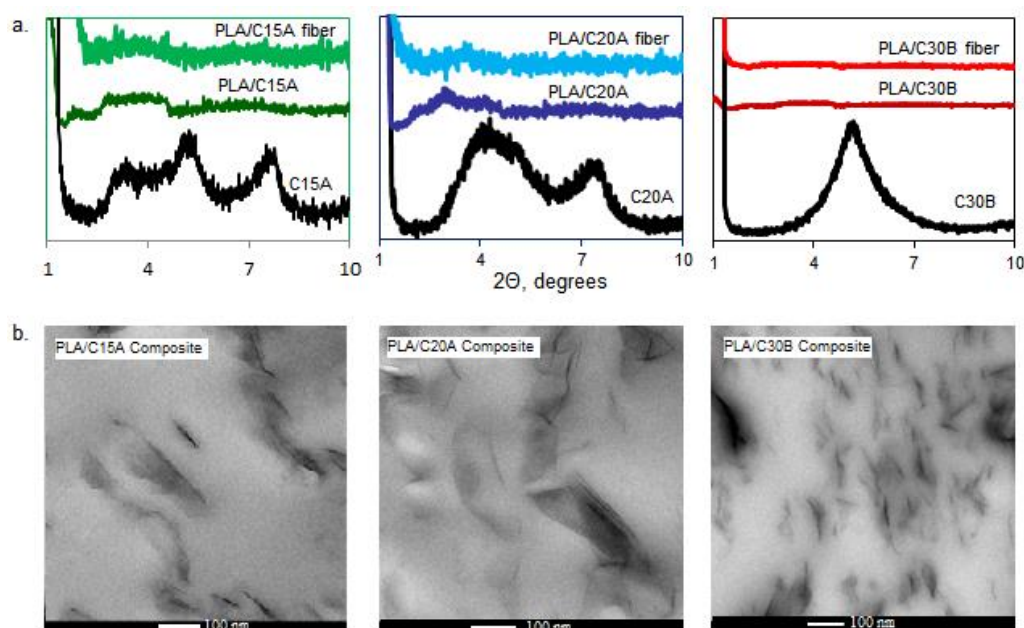


**Figure 26:** a. XRD diffractograms of C15A, C20A, C30B montmorillonites, PLA composites and composite fibers and b. TEM images of PLA composites involving 3wt% C15A, C20A and C30B.

SEM images of PLA composite fibers involving C15A, C20A and C30B montmorillonites are depicted in Figures 27, 28 and 29. In the presence of C15A, C20A and C30B, bead-free and fine fibers having diameters around approximately 200-400 nm were generated. Slightly narrower fibers were created compared to neat PLA fibers upon incorporation of organically modified montmorillonites. As the amount of clay incorporated was increased, the fiber diameter became slightly narrower. A similar result was observed for PLA/cellulose nanocrystal electrospun fibers by Shia and coworkers [172]. The quaternary ammonium salts present as an organic modifier in the montmorillonites increase the electrical conductivity, which creates finer fibers. Therefore, it is expected to have fibers with smaller diameters as the amount of organoclay is increased [172]. However, high magnification SEM images of PLA fibers involving 5 wt% organoclays revealed non-homogenous surface structures of fibers which may be correlated with the aggregation of clay layers as a result of high loading levels.

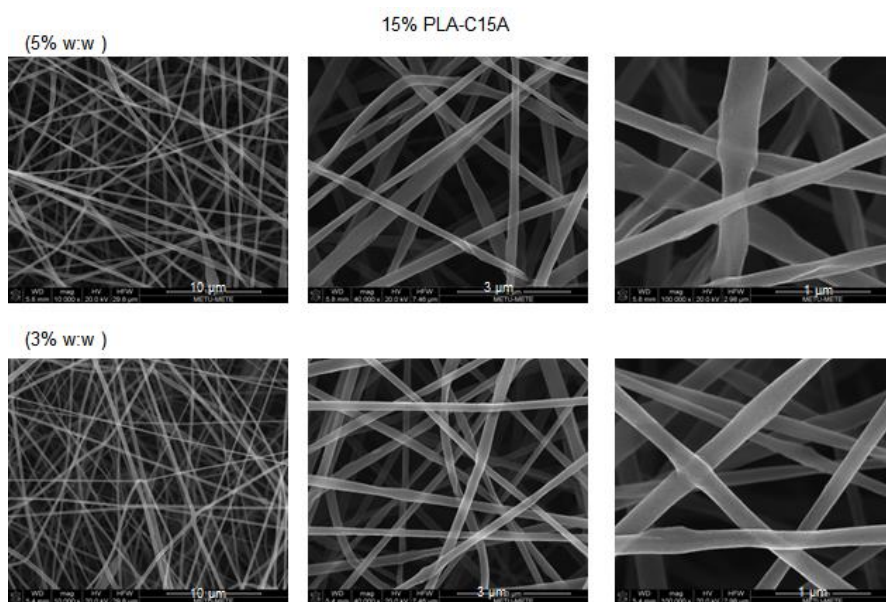


**Figure 27:** SEM images of 15% (w/v) PLA/nanoclay fibers involving 3 and 5wt% C15A.

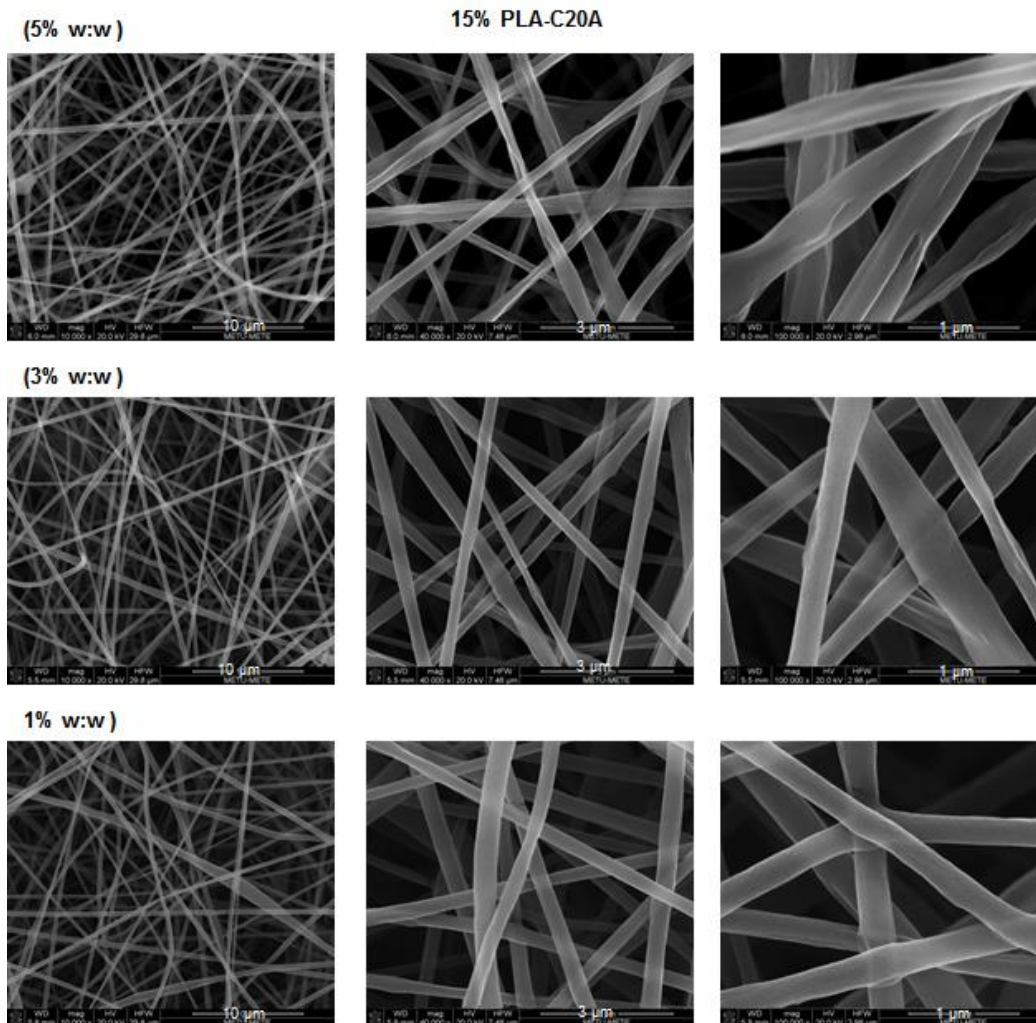


**Figure 28:** SEM images of 15% (w/v) PLA/nanoclay fibers involving 1, 3 and 5wt% C20A.

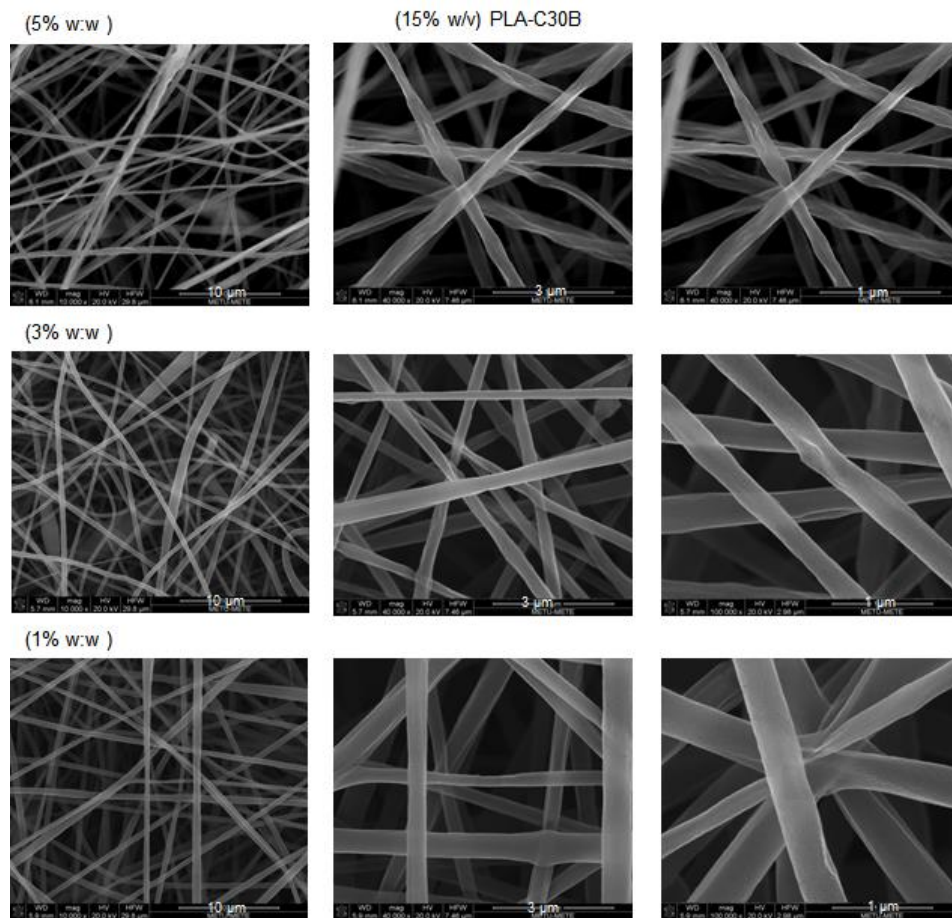


**Figure 29:** SEM images of 15% (w/v) PLA/nanoclay fibers involving 1, 3 and 5wt% C30B.

In Figure 30, SEM images of neat PLA fiber and PLA composite fibers involving 3 wt% C15A, C20A and C30B are shown together for comparison the effect of organoclay. It can be noted from the figure that among all composites the finest fibers were generated in the presence of C15A and the thickest in the presence of C30B. This behavior may be related with the amount of organic modifier present in the montmorillonite. The electrical conductivities of solutions used to prepare composite fibers was measured as 2  $\mu$ S/cm for all samples, yet the effect of counter

ion present in the organoclays was observed in the presence of electric field. Thus, the finest fibers obtained for the composites involving C15A was associated with slightly enhanced electrical conductivity during electrospinning process due to the greatest content of organic modifier present in the montmorillonite.

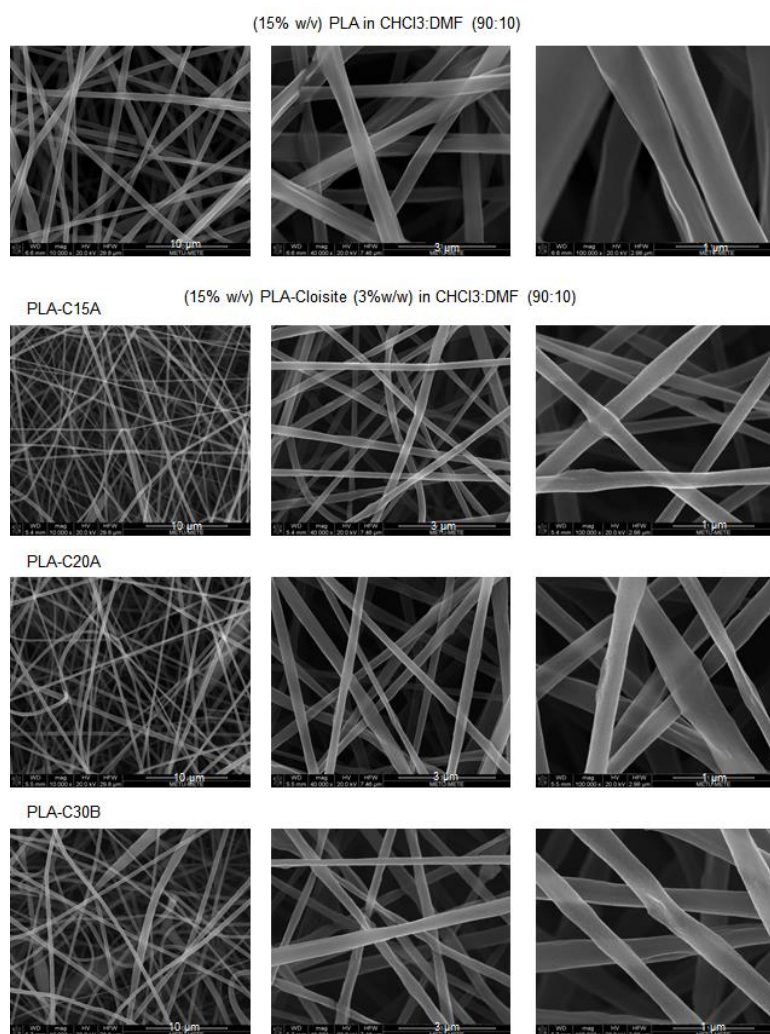


**Figure 30:** SEM images of 15% (w/v) PLA fiber and PLA composite fibers involving 3 wt% C15A, C20A or C30B (bar scales= 10 μm, 3 μm and 1 μm from left to right, respectively).



### **3.1.2.2.2. Thermal Analyses**

Thermal analyses of PLA composite fibers involved DTA, TGA and DP-MS analyses.

#### **3.1.2.2.2.1. Differential Thermal and Thermogravimetry Analyses**

Differential thermal analyses of PLA and PLA fibers revealed that the endothermic melting peak of PLA at around 172 °C, was decreased to 167.5, 169.2 and 168.8 °C for PLA composite fibers involving 3 wt% C15A, C20A or C30B, respectively. Corresponding DSC curve were given in Figure 31.

No cold crystallization temperature ( $T_{cc}$ ) was detected for neat PLA, but it showed up at 92°C after generation of fibers via electrospinning process, as expected. It was also observed that degree of crystallinity was decreased as fiber formation due to rapid evaporation of solvent during electrospinning process. For PLA composite fibers, the presence of  $T_{cc}$  were associated with the nanofiller-induced nucleating effects of clays. As it was clearly seen in the graph, the lowest and highest  $T_{cc}$  was recorded for PLA/C15A and PLA/C30B composite fibers, respectively.

The melting temperature of PLA was shifted to lower temperatures upon fiber formation, since heat absorption was more effective in case of fibers due to their high surface areas.

The glass transition temperature,  $T_g$ , of the electrospun fibers of PLA and/PLA composites was lower than that of the as-received PLA granules during the 1st heating cycle of DTA. A decrease in  $T_g$  values has also been reported in several studies [173]–[176]. Zong et al. attributed the decrease to the plasticization of fibers

during electrospinning process due to the solidification of fibers in air medium conditions [174].

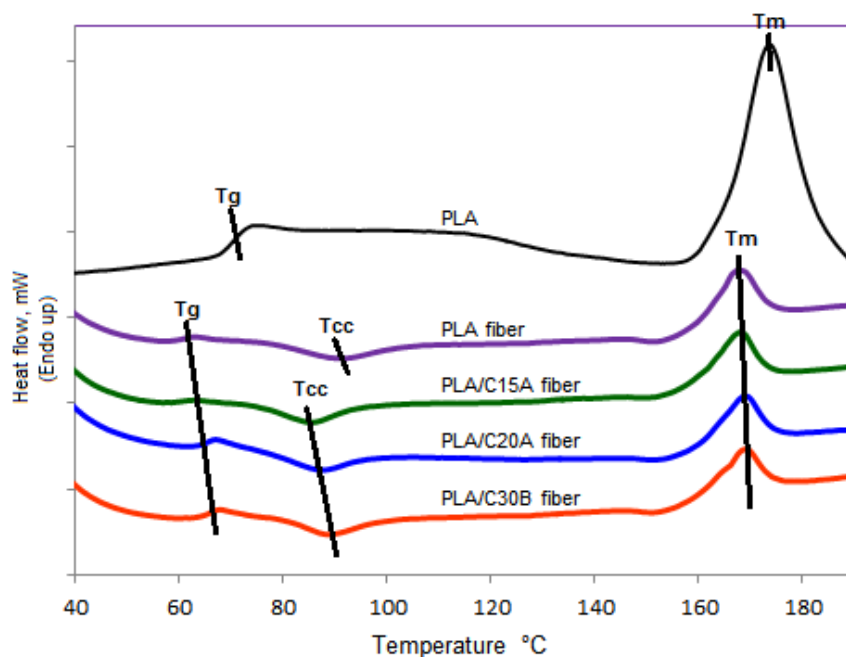


**Figure 31:** DTA curves of PLA, PLA fiber and composite fibers involving 3wt% C15A, C20A and C30B.

Both PLA/montmorillonite composites and their corresponding fibers had noticeably higher  $T_{max}$  values, the temperature at which maximum degradation occurs, than neat PLA. Even though the degradation of fibers started at slightly lower temperatures than their corresponding composites, there was almost no difference in between  $T_{max}$  values of the composites and the fibers (Figure 32). In Table 9, TGA data of neat

PLA, PLA composites involving C15A, C20A and C30B and their corresponding fibers are collected.

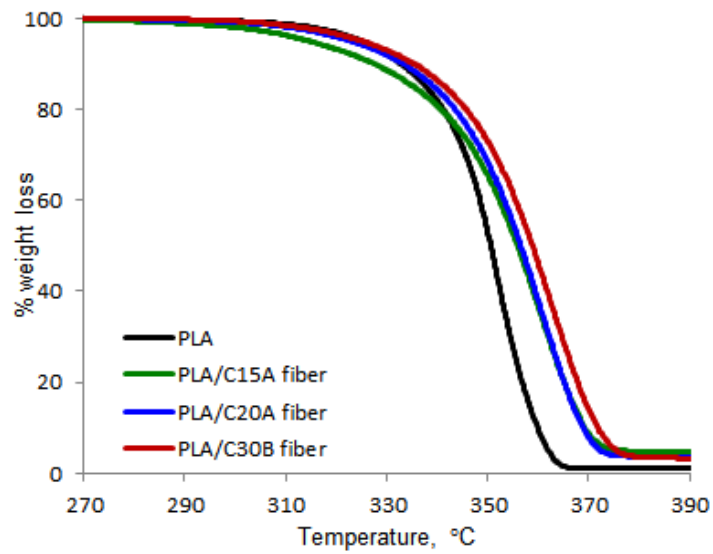


**Figure 32:** TGA curves of PLA and PLA composite fibers involving 3wt% C15A, C20A and C30B.

**Table 9:** TGA data of neat PLA, PLA composites involving C15A, C20A and C30B and their corresponding fibers.

	<b>T<sub>5%</sub></b>	<b>T<sub>10%</sub></b>	<b>T<sub>max</sub></b>	<b>%char yield</b>
<b>neat PLA</b>	324.4	332.2	355.1	0.37
<b>PLA/C15A</b>	318.2	331.3	360.9	1.16
<b>PLA/C15A fiber</b>	314.1	327.3	361.2	3.22
<b>PLA/C20A</b>	323.4	334.5	362.0	1.71
<b>PLA/C20A fiber</b>	322.5	333.2	361.8	2.43
<b>PLA/C30B</b>	328.3	328.3	363.3	2.05
<b>PLA/C30B fiber</b>	324.9	324.9	363.7	1.91

#### 3.1.2.2.2. Direct Pyrolysis Mass Spectrometry Analyses

DP-MS analyses indicated decrease in thermal stability of PLA upon fiber formation and increase upon incorporation of organically modified montmorillonites, Cloisite 15A, 20A and 30B into PLA matrix. During the pyrolysis of neat PLA, PLA fiber and PLA composites, identical products generated by trans-esterification and cis-elimination reactions were detected, yet, relative intensities showed noticeable differences.

In Figure 33, TIC curves and the mass spectra recorded at peak maxima of of 15% (w/v) PLA fiber and PLA composite fibers involving 3 wt% C15A, C20A or C30B in CHCl<sub>3</sub>/DMF 90:10 (v/v) solvent system are depicted. The maximum degradation temperatures of composite fibers were detected at 387, 398 and 410 °C indicating noticeable increase in thermal stability compared to PLA fiber (*mentioned in section*

3.1.2.1) and corresponding PLA composites. Previously, the maximum degradation temperatures of PLA composites involving 3wt% C15A, C20A and C30B were detected as 386, 378, 380, respectively [162]. The significant increase in the thermal stability of PLA composite fibers compared to their corresponding composites may be associated with the better delamination and intercalation of PLA chains into clay layers upon fiber formation.

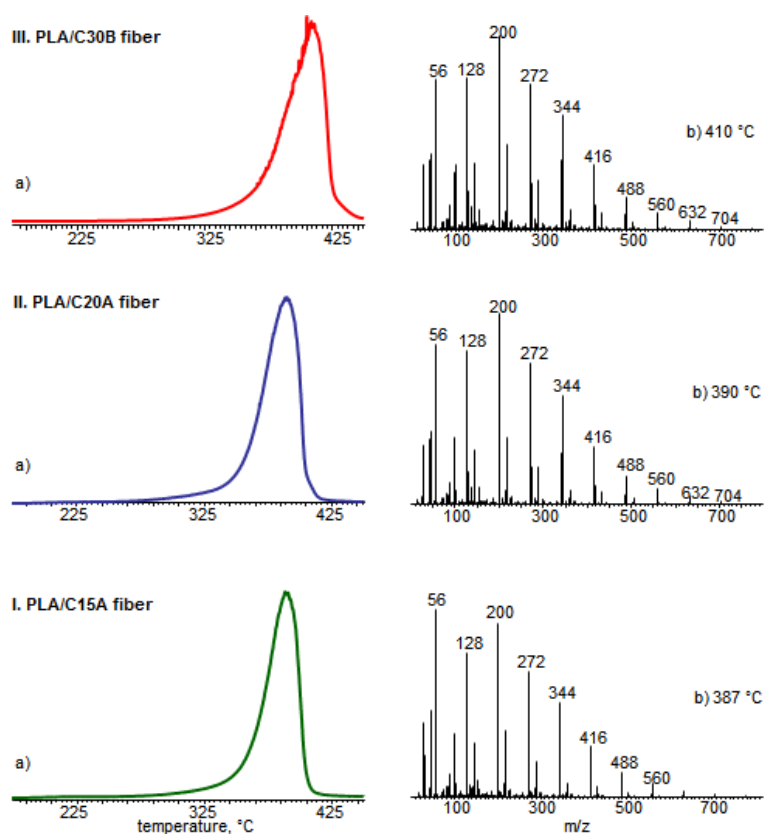


**Figure 33:** a) The TIC curves and b) the pyrolysis mass spectra recorded at peak maxima detected during the pyrolysis of 15% (w/v) PLA composite fibers involving 3 wt% I. C15A, II. C20A or III. C30B.

Single ion evolution profiles of some of the characteristic products of PLA and the most abundant product of the organic modifiers recorded during the pyrolysis of PLA composites were depicted in Figure 34. Contrary to the trends observed for PLA, its fiber and PLA composites, the evolution profiles of the products due to cis-elimination and trans-esterification reactions presented similar behavior for PLA composite fibers. In addition, the relative yields of high mass products generated by trans-esterification and cis-elimination reactions were significantly decreased. It may be thought that the presence of tactoids and intercalated structures restricts the intermolecular interactions of PLA chains in the PLA composite fibers.

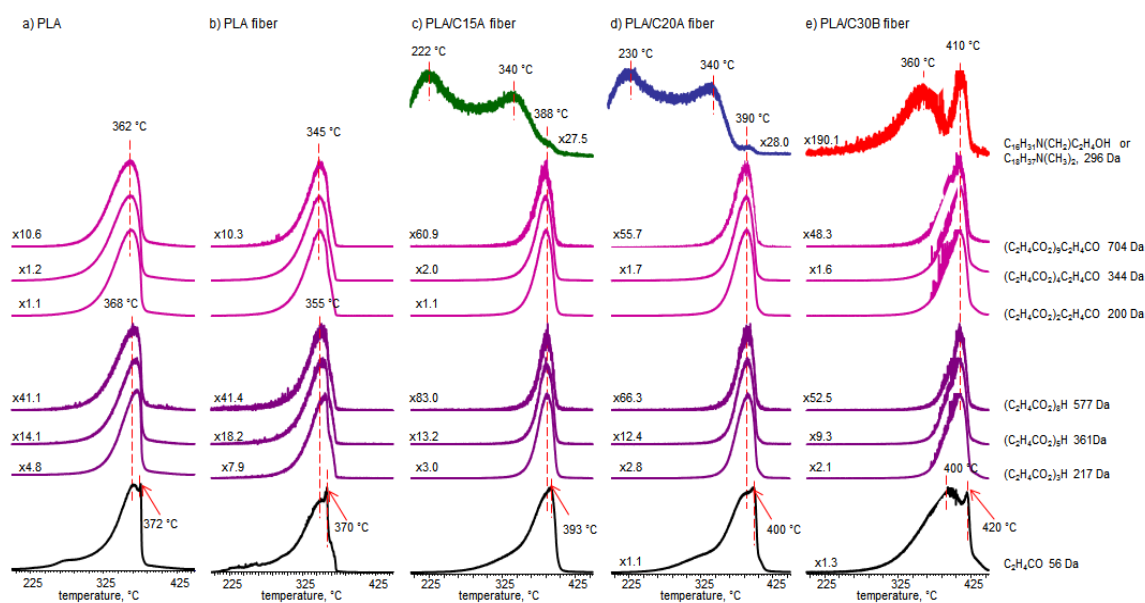


**Figure 34:** Single ion evolution profiles of selected products of a) PLA, b) PLA fiber and PLA composite fibers involving 3wt% c) C15A, d) C20A and e) C30B.

The organic modifiers of the organoclays degraded over a broad temperature range. Therefore, to better understand the effects of fiber formation on degradation behavior, single ion evolution profiles of the characteristic fragment with  $m/z = 296$  Da associated with  $C_{18}H_{37}(CH_3)NHCH_2^+$  for Cloisite 15A, C20A and attributed to  $C_{16}H_{31}N(CH_2)C_2H_4OH^+$  for C30B recorded during the pyrolysis of pure organoclays, PLA/organoclay composite or composite fibers are collected in Figure 35. The pyrolysis mass spectra of C15A, C20A and C30B were mainly dominated with characteristic peaks of amines and were almost similar. The base peak was at 296 Da and other intense peaks were detected at 268 and 56 Da. For C15A and C20A, these peaks were attributed to fragments  $C_{18}H_{37}(CH_3)NHCH_2^+$  (296 Da),  $C_{16}H_{33}(CH_3)NCH_2^+$  (268 Da) and  $C_3H_6N^+$  (56 Da), whereas for C30B, attributed to  $C_{16}H_{31}N(CH_2)C_2H_4OH^+$  (296 Da),  $C_{14}H_{27}N(CH_2)C_2H_4OH^+$  (268 Da) and  $C_3H_6N^+$  (56 Da). It was clear that upon incorporation of C15A and C20A into PLA matrix, loss of organic modifiers was shifted to low temperature regions which may be correlated with the separation of clay layers.

During the pyrolysis of PLA/C15A and PLA/C20A fibers, loss of significant amount of the organic modifier of C15A and C20A was detected at initial stages of pyrolysis, (Figure 35a and 35b). This low temperature loss of organic modifier may be associated with both separation of clay layers and the degradation of the organic modifier up to a certain extent during the electrospinning process. On the other hand, almost a negligible amount of organic modifier of C30B was lost at initial stages of pyrolysis for PLA/C30B fiber. In contrast to composites and composite fibers of PLA involving C15A and C20A, for PLA/C30B composite and composite fiber, thermal degradation of the characteristic products of the organic modifier of C30B was shifted to high temperature regions. It may be thought that due to the transesterification reactions between the ester groups of PLA and the hydroxide groups of the organic modifier of C30B, a crosslinked structure that decomposed at high temperatures was generated and the organic modifier was lost in the temperature

region where PLA decomposition took place. In addition, the highest thermal stability of PLA/C30B fiber can be associated with this crosslinking effect of the organic modifier of C30B (Figure 34e).

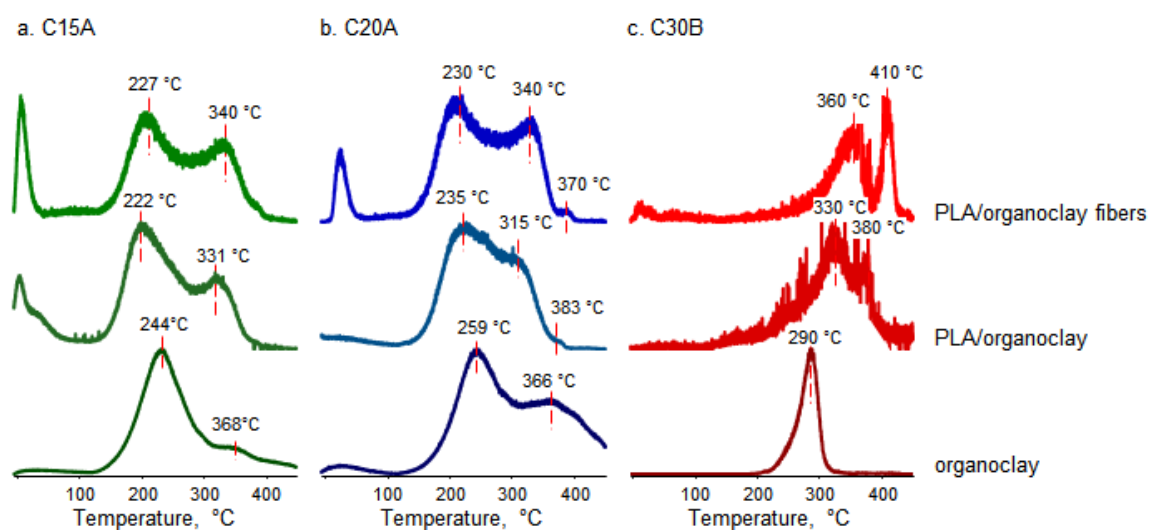


**Figure 35:** Single ion evolution profiles of characteristic fragment with  $m/z=296$  Da of a) C15A b) C20A c) C30B recorded during the pyrolysis of pure organoclay, PLA/organoclay composite or composite fibers.

### 3.1.2.3. Electrospun Fibers of PLA-PEG Blends

Electrospun fibers of PLA-PEG blends, involving 10, 15 and 20 wt % PEG, were prepared and characterized. The experimental parameters optimized for obtaining bead-free PLA were also applied for the generation of PLA-PEG fibers as 15% (w/v) PLA-PEG in  $\text{CHCl}_3/\text{DMF}$  90:10 (v/v) solvent system. The optimum voltage used to



generate fibers of neat PLA, 12.5 kV, was too low to initiate successful spinning of solution of PLA-PEG blends, a higher accelerating voltage, 16 kV, have been applied for spinning. Also, electrical conductivities of solutions used to prepare fibers was measured as 2  $\mu\text{S}/\text{cm}$  for all samples, yet the effect of counter ion present in the organoclay was observed in the presence of electric field.

#### **3.1.2.3.1. Morphological Analyses**

In Figure 36, SEM images of electrospun fibers of PLA and PLA-PEG blends involving 10, 15 and 20 wt % PEG depicted. SEM images revealed generations of bead-free and slightly thicker fibers compared to neat PLA fibers having diameters around 200 nm to 800 nm in the presence of PEG. However, no detectable change was observed as the amount of PEG increased from 10 to 20 wt%. It is known that higher voltages facilitate the formation of larger fiber diameters. Thus, the increase in the diameter of the fibers may be correlated with the increase in the applied voltage.

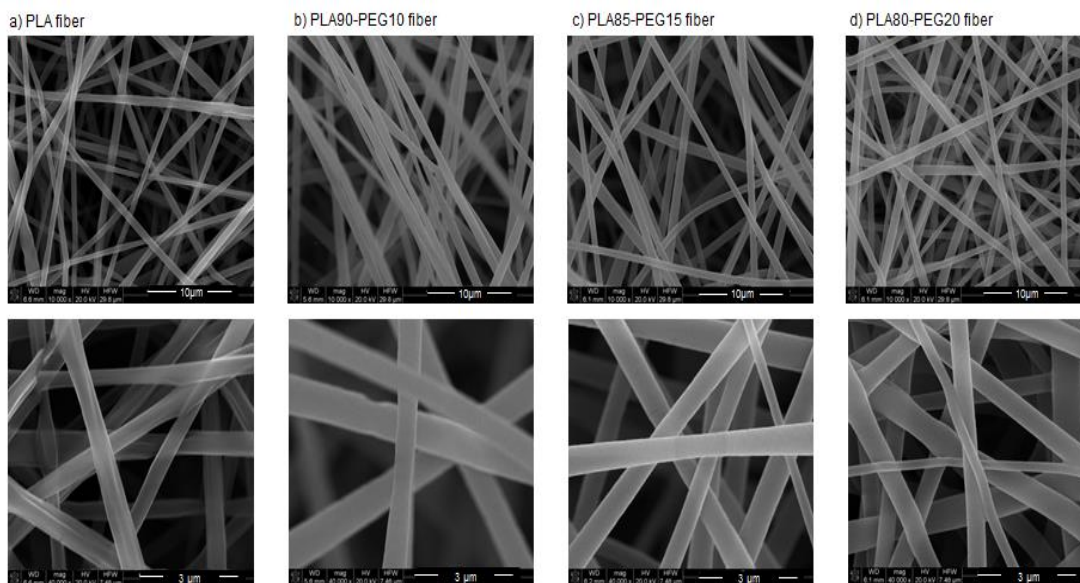


**Figure 36:** SEM images of electrospun fibers of a) PLA and PLA-PEG blends involving b) 10, c) 15 and d) 20 wt % PEG.

### 3.1.2.3.2. Thermal Analyses

DTA, TGA and DP-MS analyses were performed to investigate the thermal characteristics of electrospun fibers of PLA-PEG blends.

#### 3.1.2.3.2.1. Differential Thermal and Thermogravimetry Analyses

DTA curves of neat PLA, PLA-PEG blends and their corresponding electrospun fibers are given in Figure 37. The melting peak,  $T_m$ , of PLA at around 172.3 °C was

shifted to lower temperatures with the addition of PEG into PLA matrix for both blends and electrospun fibers due to the plasticizing effect of PEG. However, no systematic change of  $T_m$  was detected with increasing amount of PEG in the blend. In addition, the cold crystallization temperature,  $T_{cc}$ , of PLA-PEG blends were decreased upon fiber generation and the maximum shift in  $T_{cc}$  was detected for the sample involving 10 wt% PEG.  $T_{cc}$  of electrospun fibers of blends involving 10 wt%, 15 wt% and 20 wt% PEG was detected at 77.0, 68.9, and 87.4 °C, respectively. The lower  $T_{cc}$  values compared to neat PLA fiber can be thought as an indication of easier crystallization.

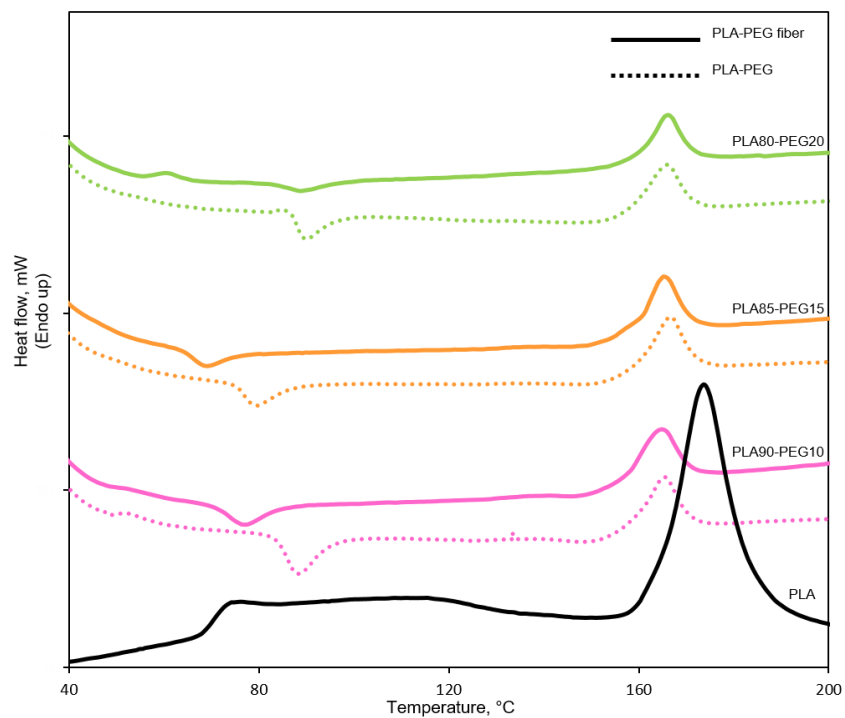


**Figure 37:** DTA curves of neat PLA, PLA-PEG blends and fibers of PLA-PEG.

The TGA curves of PLA-PEG fibers are shown in Figure 38 and the relevant data are listed in Table 10. In general, similar to the corresponding blends, thermal degradation of PLA-PEG fibers occurred in two steps, the first step being due to the degradation of PLA and the second due to the degradation of PEG. TGA analyses indicated a single step decomposition for PLA-PEG fiber involving 10 wt% PEG and two step degradation for PLA-PEG fibers involving 15 and 20% PEG similar to the corresponding blends. As the amount of PEG increased to 20 wt% the second step became more apparent.

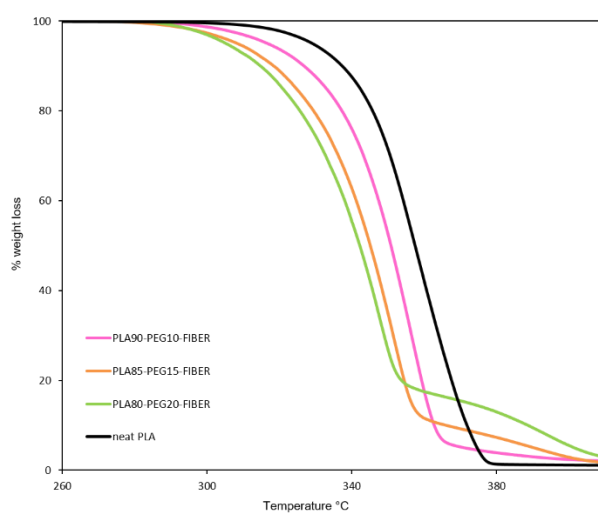


**Figure 38:** TGA curves of neat PLA and electrospun fibers of PLA-PEG blends.

**Table 10:** TGA data of neat PLA, neat PEG, and fibers of PLA and PLA-PEG blends.

	<b>T<sub>5%</sub></b>	<b>T<sub>10%</sub></b>	<b>T<sub>max1</sub></b>	<b>T<sub>max2</sub></b>	<b>%char yield</b>
<b>neat PLA</b>	329.1	337.0	366.9	-	0.8
<b>neat PEG</b>	338.4	354.9	-	395.3	1.0
<b>PLA-fiber</b>	322.6	33.4	362.6	-	0.4
<b>PLA90-PEG10</b>	315.8	326.9	358.3	-	0.8
<b>PLA90-PEG10-fiber</b>	316.5	326.6	357.8	-	0.7
<b>PLA85-PEG15</b>	308.8	320.8	358.6	394.3	1.2
<b>PLA85-PEG15-fiber</b>	308.0	318.1	352.5	394.5	0.3
<b>PLA80-PEG20</b>	310.5	320.6	351.0	397.7	0.9
<b>PLA80-PEG20-fiber</b>	304.7	314.3	348.3	396.6	1.3

#### **3.1.2.3.2.2. Direct Pyrolysis Mass Spectrometry Analyses**

In Figure 39, the total ion current, TIC, curves and the mass spectra recorded at the maxima of the peaks present in the TIC curves recorded during the pyrolysis of PLA-PEG fibers are depicted.

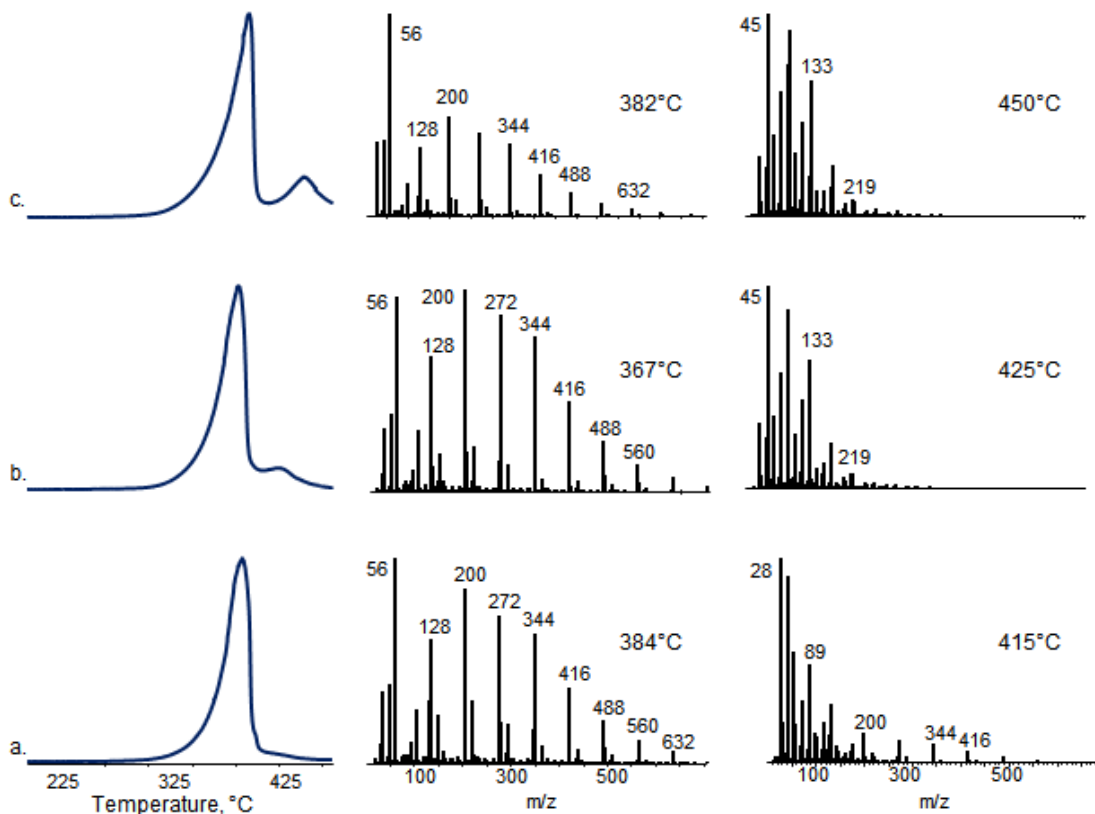


**Figure 39:** The TIC curves and the pyrolysis mass spectra recorded at peak maxima detected during the pyrolysis of 15% (w/v) PLA-PEG fibers involving a) 10 wt% b) 15 wt% c) 20 wt% PEG.

The fibers of PLA-PEG blend involving 15 wt% and 20 wt% PEG showed two peaks at distinct temperature regions and the relative intensity of the high temperature peak was increased as the amount of PEG in the blend was increased. The mass spectra recorded at the maxima of the low temperature peaks were mainly dominated by the products due to the thermal degradation of PLA, whereas, those recorded at the maxima of the weak high temperature peaks showed characteristic products of PEG.

As mentioned in previous sections in detail, as the amount of PEG involved in PLA-PEG blends was increased, the thermal stability of PLA chains increased while that of PEG chains decreased slightly due to the reactions between PLA and PEG. The thermal stability of the PLA chains during the pyrolysis of electrospun fibers of PLA-PEG blends increased noticeably compared to the corresponding blends.

In Figure 40, single ion evolution profiles of the characteristic degradation products of PLA i.e. 56 Da, 145 Da, 217 Da and 200 Da and those of the most abundant degradation products of PEG i.e. 45 Da and 89 Da recorded during the pyrolysis of PLA-PEG fibers involving 10, 15 and 20 wt% PEG are given. In addition, the evolution profiles of fragments with  $m/z$  values 231 Da, 261 Da and 333 Da attributed to the decomposition of units generated by the interactions between PLA and PEG chains are included.

It is important to point out that as the amount of PEG was increased in the blend, the relative yields of the products related to decomposition of the units generated by interactions between PLA and PEG decreased, in contrast to neat blends. The decomposition of these products was recorded in the same temperature regions for both blends and their corresponding fibers. Upon fiber formation, degradation of the PEG based products was shifted to significantly high temperatures, to the regions where neat PEG decomposed. Therefore, it may be thought that the interactions between the PLA and PEG chains were diminished upon fiber formation indicating phase separation between PLA and PEG.

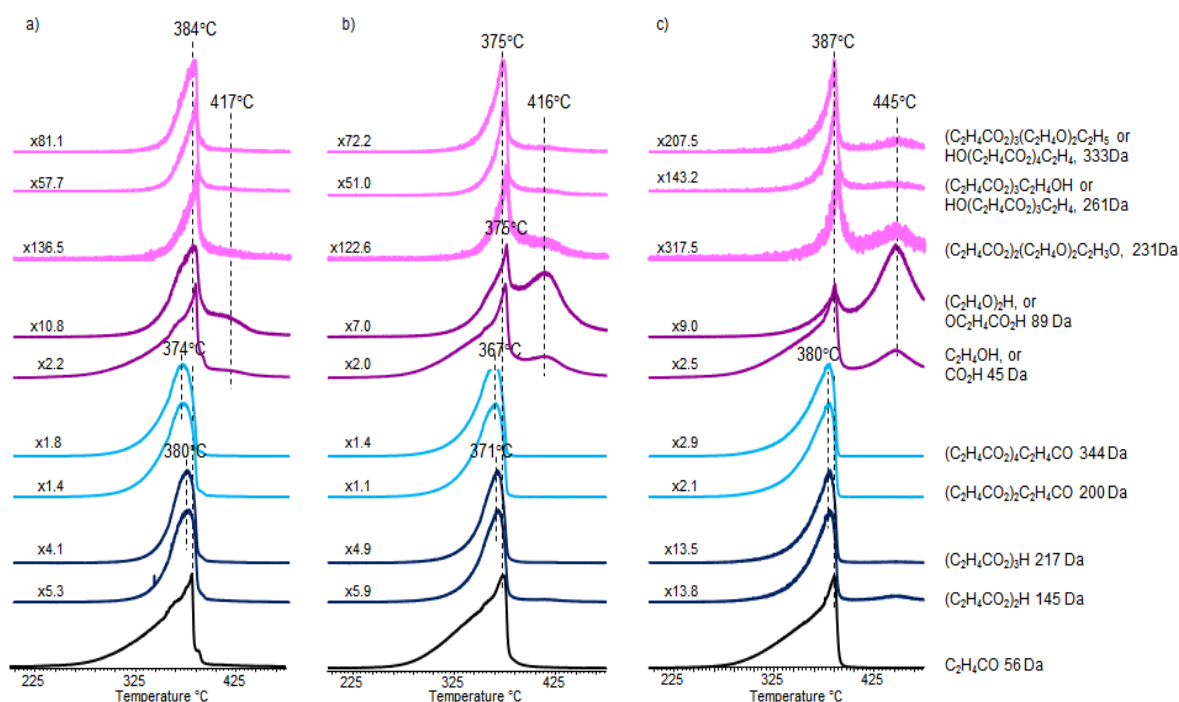


**Figure 40:** Single ion evolution profiles of the selected products of electrospun fibers of PLA-PEG blends involving a) 10 wt% b) 15 wt% c) 20 wt% PEG.

#### 3.1.2.4. Electrospun Fibers of PLA-PEG Composites Involving C30B

Electrospun fibers of PLA-PEG blends involving 10, 15 and 20 wt % PEG and 3 wt% Cloisite 30B were prepared and characterized. The experimental parameters used for generation of PLA-PEG fibers as 15% (w/v) PLA-PEG in  $\text{CHCl}_3/\text{DMF}$  90:10 (v/v) solvent system were also applied to produce PLA-PEG composite fibers.



### 3.1.2.4.1. Morphological Analyses

XRD measurements were used to determine the dispersion of Cloisites 30B in the PLA-PEG composite fibers. As mentioned in the previous sections before, Cloisite 30B presents a distinct maximum around  $2\Theta=5.0^\circ$  corresponding to an inter-reticular distance of  $d_{001}=1.8$  nm in XRD analysis, Figure 41. The characteristic peak of C30B was almost totally disappeared for PLA90-PEG10-C30B (90/10; PLA/PEG) and PLA85-PEG15-C30B (85/15; PLA/PEG) composite fibers involving 3 wt% C30B, whereas a weak peak was located at around  $2\Theta=4.5^\circ$  corresponding to an inter-reticular distance of  $d_{001}=2.0$  nm in the XRD of PLA80-PEG20-C30B (80/20%; PLA/PEG) composite fiber.

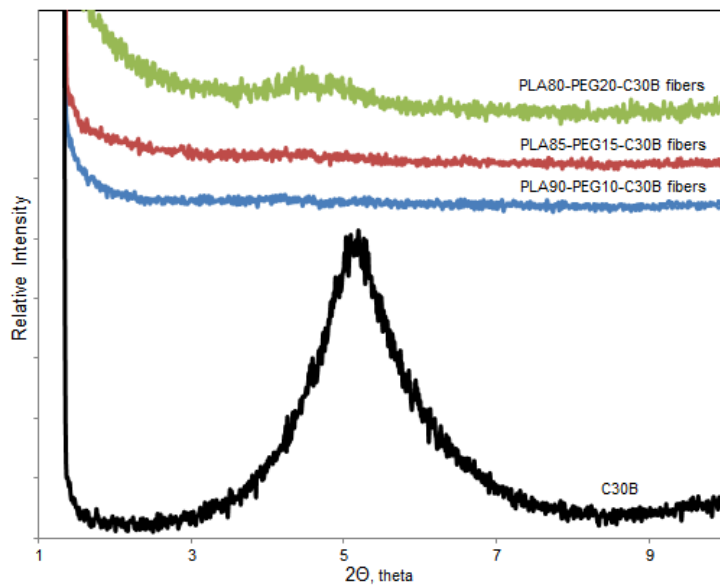


**Figure 41:** XRD diffractogram of C30B and PLA-PEG composite fibers involving C30B.

In Figure 42, SEM images of electrospun fibers of PLA-PEG blends and corresponding composites are shown. The generation of narrower fibers in the presence of C30B compared to their corresponding blends were attributed to the enhancement in the electrical conductivity during electrospinning process due to the presence of quaternary ammonium salt present as an organic modifier in the nanoclay. These results compromise with those obtained for PLA composite fibers involving C15A, C20A and C30B (*described in section 3.1.2.2*). For PLA-PEG composite fibers, it is also important to point out that as the amount of PEG incorporated increased, thinner fibers were collected. In Figure 43, size distribution of randomly selected fibers were given.

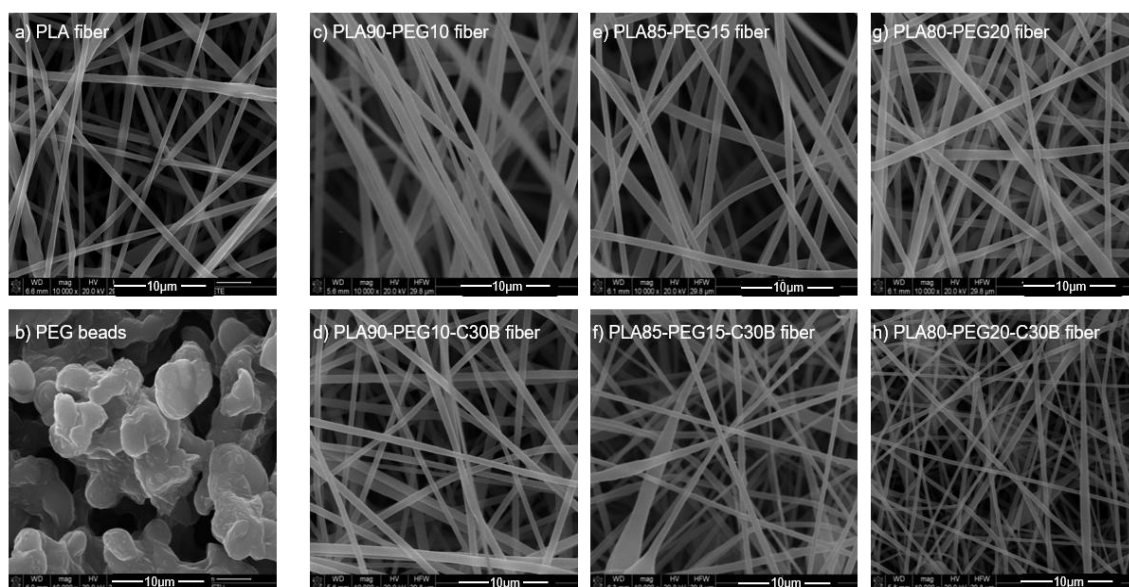


**Figure 42:** SEM images of a) PLA fibers, b) PEG beads and electrospun fibers of PLA-PEG blends and composites involving c,d) 10wt%, e,f) 15wt% and g,h) 20 wt% PEG.

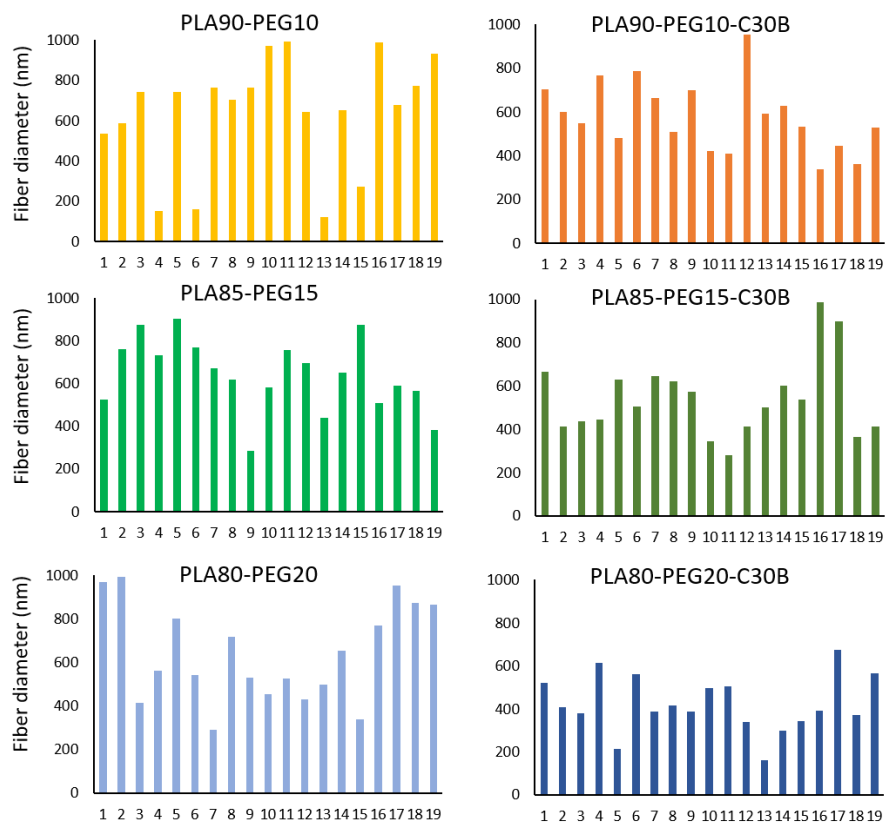


**Figure 43:** Size distributions of 19 randomly selected fibers of blends and composites

#### 3.1.2.4.2. Thermal Analyses

Thermal characteristics of PLA-PEG composite fibers involving 10, 15 and 20 wt % PEG and 3 wt % Cloisite 30B were investigated by DTA, TGA and DP-MS analyses.

### **3.1.2.4.2.1. Differential Thermal and Thermogravimetry Analyses**

DTA curves of neat PLA, PLA-PEG blends, PLA-PEG fibers and composite fibers involving 3 wt% C30B are given in Figure 44. After the incorporation of PEG, the melting peak of PLA was decreased for blends and electrospun fibers due to the plasticizing effect of PEG as mentioned before. The melting point of PLA-PEG fibers and PLA-PEG-C30B composite fibers showed no noticeable change compared to their corresponding blends.

The cold crystallization temperature ( $T_{cc}$ ) of PLA appeared at 86.2, 77.3 and 88.4°C after the incorporation of 10 wt%, 15 wt% and 20 wt% PEG, respectively. Upon fiber generation,  $T_{cc}$  values were shifted to 77.0, 68.9, and 87.4 °C for the samples involving 10 wt%, 15 wt% and 20 wt% PEG, respectively. On the other hand, upon addition of C30B, slight variations in  $T_{cc}$  values were detected.  $T_{cc}$  value of the composite fiber decreased to 75.1 for the sample involving 10wt% PEG but increased to 71.7 and 90.0°C for the samples involving 15 and 20 wt% PEG, respectively. The increase in  $T_{cc}$  values again can be associated with the nanofiller-induced nucleation effect of the organoclay.

In Figure 45, TGA curves of PLA-PEG fibers and composite fibers are collected and the relevant data are listed in Table 11. As mentioned before, thermal degradation of PLA-PEG blends occurred in two steps, the first step being due to the degradation of PLA and the second due to the degradation of PEG. However, the second step cannot be recorded for the fibers of composites involving C30B. In addition, a slight decrease in the thermal stability of fibers compared to neat PLA, PLA fiber and PLA-PEG blends were recorded. Finally, an increase in the char yield after incorporation of inorganic C30B were detected, as expected.

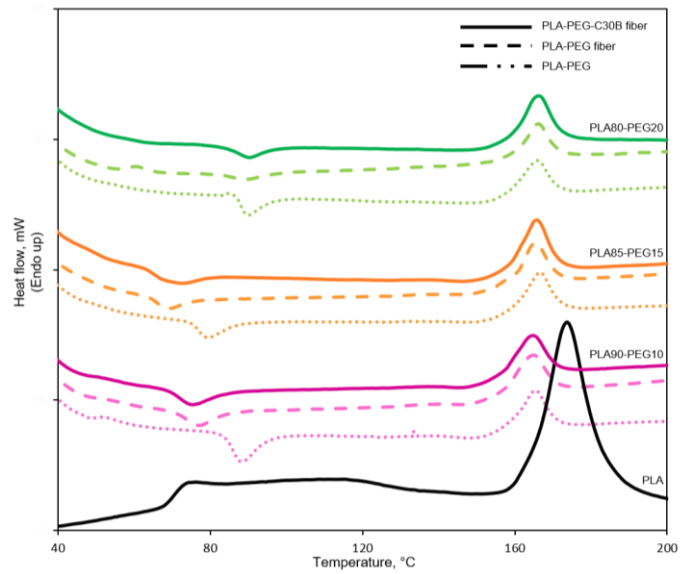


**Figure 44:** DTA curves of neat PLA, PLA-PEG blends, PLA-PEG fibers and composite fibers involving 3 wt% C30B.

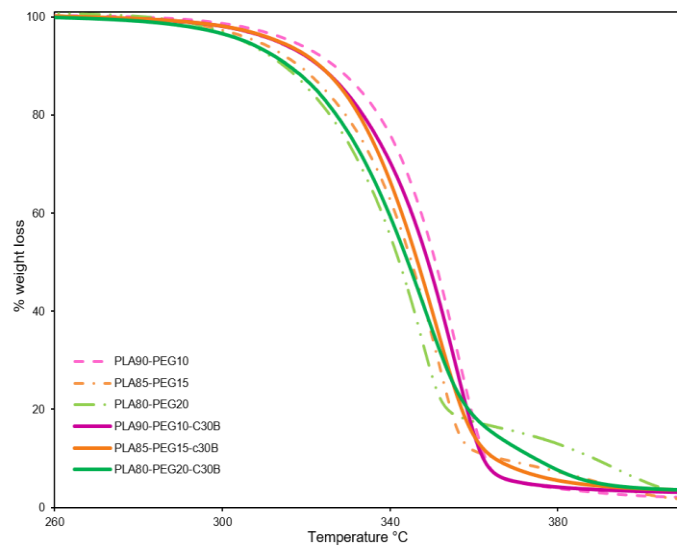


**Figure 45:** TGA curves of electrospun fibers PLA-PEG blends and composites involving C30B.

**Table 11:** TGA data of neat PLA, neat PEG, PLA fiber, PLA-PEG blends and composites involving C30B and their corresponding fibers.

	<b>T<sub>5%</sub></b>	<b>T<sub>10%</sub></b>	<b>T<sub>max1</sub></b>	<b>T<sub>max2</sub></b>	<b>%char yield</b>
<b>neat PLA</b>	329.1	337.0	366.9	-	0.8
<b>neat PEG</b>	338.4	354.9	-	395.3	1.0
<b>PLA-fiber</b>	322.6	33.4	362.6	-	0.4
<b>PLA90-PEG10</b>	315.8	326.9	358.3	-	0.8
<b>PLA90-PEG10-fiber</b>	316.5	326.6	357.8	-	0.7
<b>PLA90-PEG10-C30B-fiber</b>	312.3	322.7	356.0	-	1.7
<b>PLA85-PEG15</b>	308.8	320.8	358.6	394.3	1.2
<b>PLA85-PEG15-fiber</b>	308.0	318.1	352.5	394.5	0.3
<b>PLA85-PEG15-C30B-fiber</b>	312.9	323.0	352.1	-	2.6
<b>PLA80-PEG20</b>	310.5	320.6	351.0	397.7	0.9
<b>PLA80-PEG20-fiber</b>	304.7	314.3	348.3	396.6	1.3
<b>PLA80-PEG20-C30B-fiber</b>	305.5	315.6	349.2	-	2.8

#### 3.1.2.4.2.2. Direct Pyrolysis Mass Spectrometry Analyses

In Figure 46, TIC curves of electrospun fibers of PLA-PEG composites and the pyrolysis mass spectra recorded at the peak maxima are given. Contrary to the results obtained for fibers of blends, a single peak was present in the TIC curves of composite fibers. The pyrolysis mass spectra were mainly dominated with peaks due

to the degradation products of PLA. The most abundant pyrolysis product was  $C_2H_4CO$  and/or  $C_3H_4O$  fragments with  $m/z=56$  Da. The relative intensities of the peaks due to low mass fragment ions were increased after the addition of C30B. Thermal stability of PEG decreased while that of PLA chains increased remarkably in the presence of C30B as the amount of PEG increased. Thermal stability of PLA chains of PLA-PEG composite fibers in the presence of C30B was noticeably higher than the corresponding blends and composites [162].

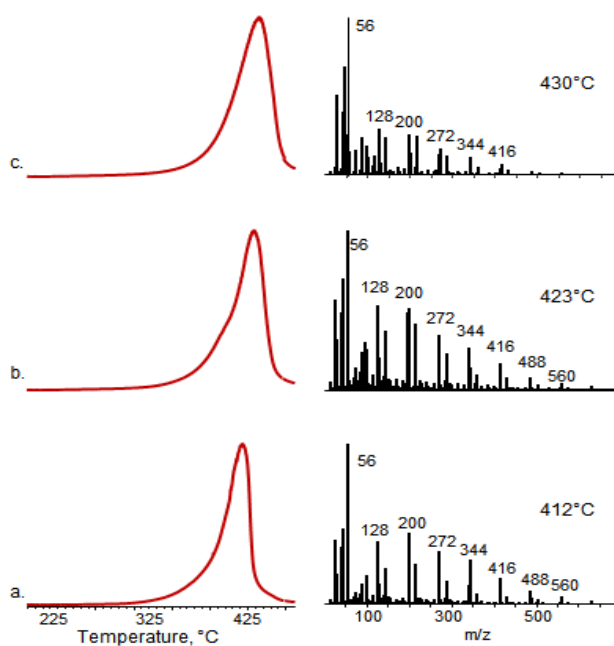


**Figure 46:** The TIC curves and the pyrolysis mass spectra recorded at peak maxima detected during the pyrolysis of PLA-PEG-C30B composite fibers involving a) 10 wt% b) 15 wt% c) 20 wt% PEG.

In Figure 47, single ion evolution profiles of the characteristic degradation products of PLA i.e. fragments with  $m/z= 56$  Da, 145 Da, 217 Da and 200 Da, degradation products of PEG i.e. fragments with  $m/z= 45$  Da and 89 Da and decomposition products of fragments generated by the interactions between PLA and PEG chains i.e. fragments with  $m/z= 231$  Da, 261 Da and 333 Da recorded during the pyrolysis of PLA-PEG composite fibers are given. Single ion pyrograms of the characteristic degradation products of the organic modifier  $C_{16}H_{31}N(CH_2)C_2H_4OH$  (296 Da) and OH (17 Da) are also included.

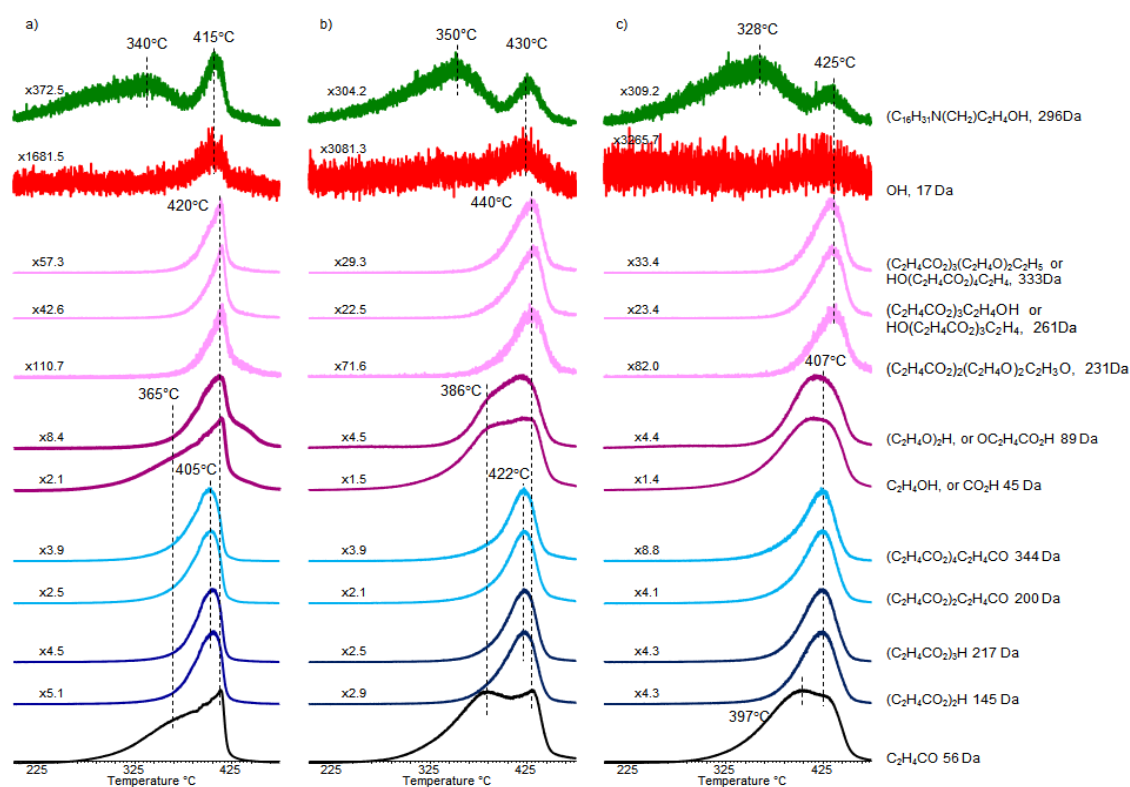


**Figure 47:** Single ion evolution profiles of the selected products of electrospun fibers of PLA-PEG-C30B composites involving a) 10 wt%, b) 15 wt% and c) 20 wt% PEG.



The single ion pyrograms detected during the pyrolysis of the composite fibers involving C30B showed drastic differences compared to the corresponding fibers of blends. Firstly, the thermal degradation of PLA and PEG chains occurred almost in the same temperature region. Secondly, the evolution of the products due to the decomposition of the units generated by the interactions between PLA and PEG chains was shifted to high temperatures and their yields increased significantly. For easier comparison, in Figure 48, the single ion evolution profiles of the electrospun fibers of PLA-PEG blend and composite involving 20 wt% PEG are given.

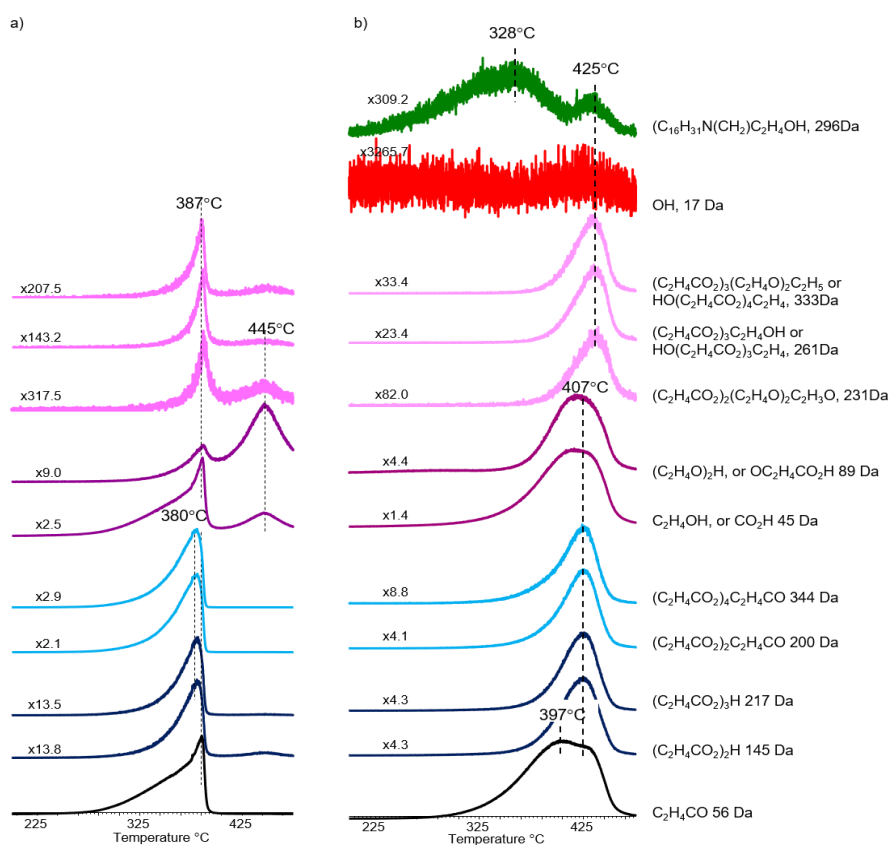


**Figure 48:** Single ion evolution profiles of the selected products of electrospun fibers of PLA-PEG a) blend and b) composite involving 20 wt% PEG.

The yields of the products due to the decomposition of the organic modifier of C30B were increased as the amount of PEG was increased similar to the results obtained for PLA-PEG composites involving C30B. Thus, it may be concluded that as a consequence of the diffusion of both PLA and PEG chains from the bulk polymer melt into the galleries between the silicate layers of the montmorillonite, the interactions between PLA and PEG chains were enhanced. This also led to the decomposition of both PLA and PEG chains in the same temperature region. In addition, as the relative intensity of the high temperature peak in the evolution profiles of the degradation products of the organic modifier, decreased noticeably, it can further be concluded that the reactions between the PLA and the organic modifier of C30B were inhibited due to the interactions of PLA with PEG chains.

### **3.2. Direct Pyrolysis Mass Spectrometry to Characterize Morphology of The Polymer/Organoclay Systems**

In general, direct pyrolysis mass spectrometry, DP-MS is used to study thermal behavior of polymers such as thermal stability thermal degradation products and thermal degradation mechanism. In this part of the work, the application of DP-MS to investigate the characteristics of polymer/organoclay systems, namely morphology and interactions between organic modifier and polymer matrix was discussed. For this purpose, various quaternary ammonium salt modified montmorillonites, commercially named as Cloisite 15A, 20A, 25A, 93A and 30B were incorporated into poly(lactic acid), PLA, poly(methyl methacrylate), PMMA, and polyethylene, PE, matrices and analyzed via DP-MS technique. In order to determine the merits and limitations of the technique, the results were correlated with the TEM images and X-ray diffractograms.

In order to visualize the dispersion states and separation of clay layers, TEM analyses of PLA, PMMA and PE composites involving several organically modified montmorillonites were conducted.

TEM images of PLA, PMMA and PE composites involving Cloisite 15A are presented in Figure 49. Since the organic modifier of C15A and C20A are the same, the TEM images of the PLA composite involving C20A were also included in the figure. The images showed almost a homogenous dispersion of C15A and C20A in PLA matrix with both intercalated and exfoliated regions. On the other hand, for both PMMA-C15A, and PE-C15A mainly intercalated platelets can be identified.

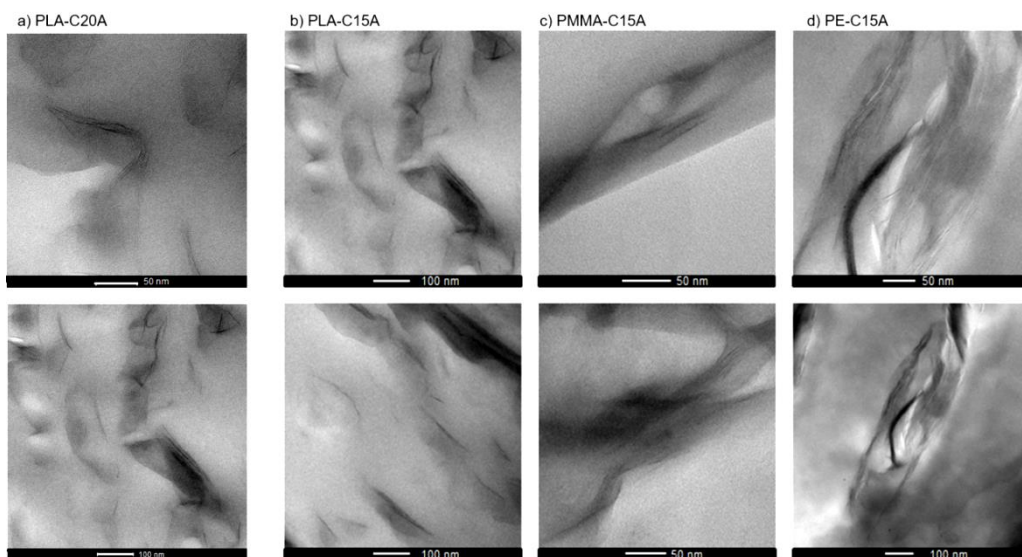


**Figure 49:** TEM images of PLA composite involving C20A and C15A, and PMMA and PE composites involving C15A.

In Figures 50 and 51, TEM images of the composites involving C25A and C93A are presented, respectively. For both PLA and PMMA composites, mainly intercalation of clay platelets was clearly detected. However, in contrast, trimming of bulk PE specimens by ultramicrotomy process for sample preparation caused slight fluctuations, making difficult to visualize the morphology of these composites. Yet, high magnifications of images showed intercalated platelets.

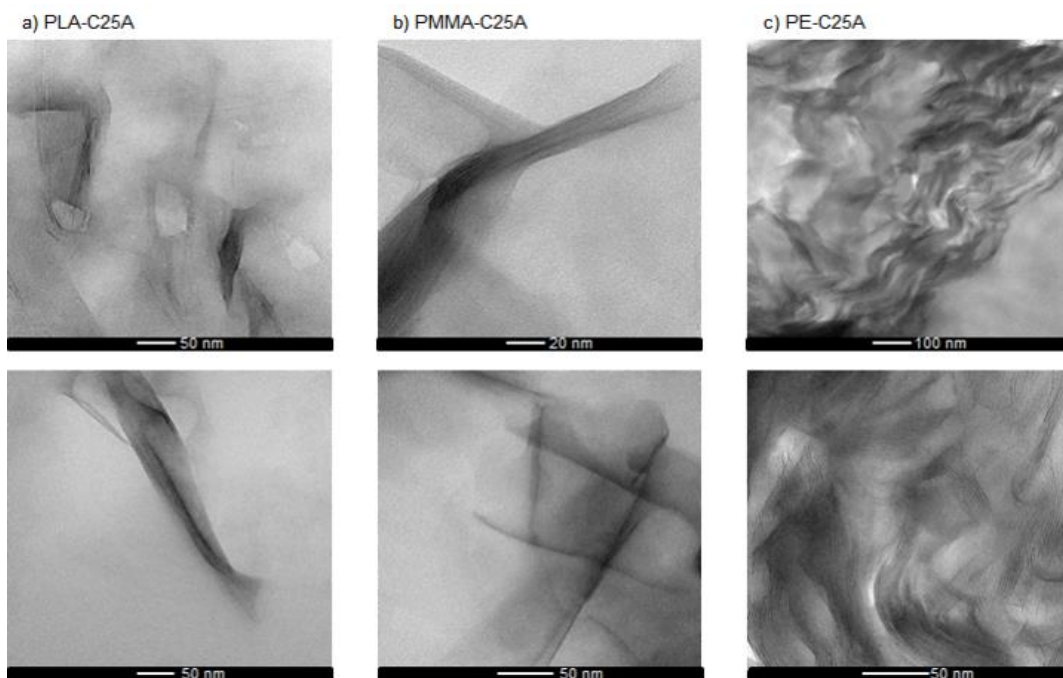


**Figure 50:** TEM images of PLA, PMMA and PE composites involving C25A.

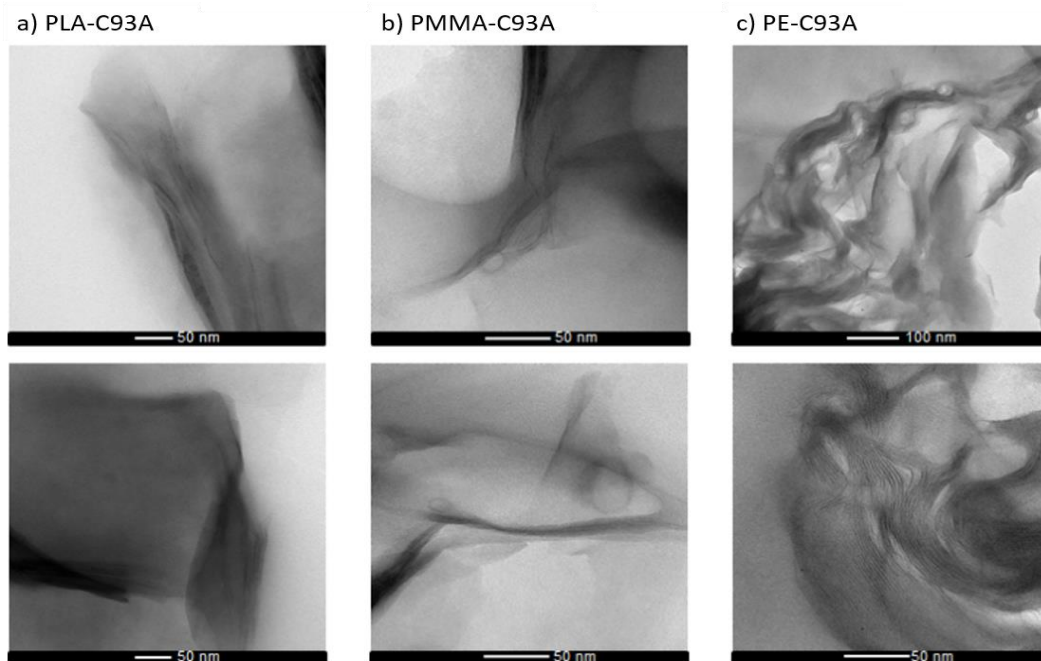


**Figure 51:** TEM images of PLA, PMMA and PE composites involving C93A.

In Figure 52, TEM images of PLA, PMMA and PE composites involving C30B are given. TEM images of PLA-C30B composite showed mainly exfoliated, well separated clay layers. For PMMA-C30B composite, even though there were separated clay platelets, mainly intercalated platelets were detected. Finally, for PE-C30B composite, intercalation of layers was observed.

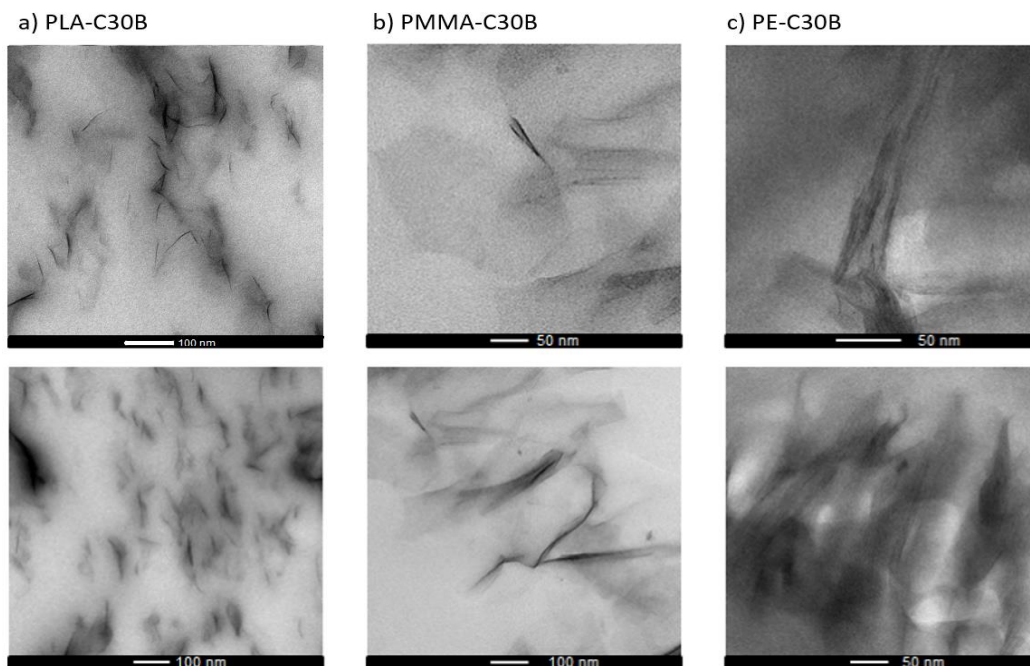


**Figure 52:** TEM images of PLA, PMMA and PE composites involving C30B.

### 3.2.1. X-Ray Diffractometry Analysis

XRD patterns of pure clays and composites of PLA, PMMA and PE involving C15A, C20A, C25A, C93A and C30B are given in Figure 53. Due to dilution, the peaks in the X-ray diffractograms of the organoclay composites were significantly weak compared to the corresponding pure clays.

XRD analysis of Cloisite 15A revealed three peaks at  $2\Theta=3.3, 5.2$  and  $7.7^\circ$  corresponding to inter-reticular distances of  $d_{001}= 2.64, 1.70$  and  $1.14$  nm, respectively, indicating a mixed-layering in the pure clay (Figure 53.a). In the diffractogram of PLA-C15A composite, two peaks located at around  $2.15$  and  $4.2^\circ$

corresponding to inter-reticular distances of  $d_{001}=4.1$  and  $2.1$  nm were detected. The increase in the inter-reticular distance indicated the intercalation of clay layers. The diffractogram of PMMA-C15A composite showed a peak at  $2\Theta=2.3^\circ$  corresponding to inter-reticular distance of  $d_{001}=3.87$  nm again pointing out delamination of the clay layers. For the PE-C15A composite, only a weak peak located at  $2\Theta=4.2^\circ$  corresponding to inter layer spacing of  $d_{001}=2.2$  nm was detected.

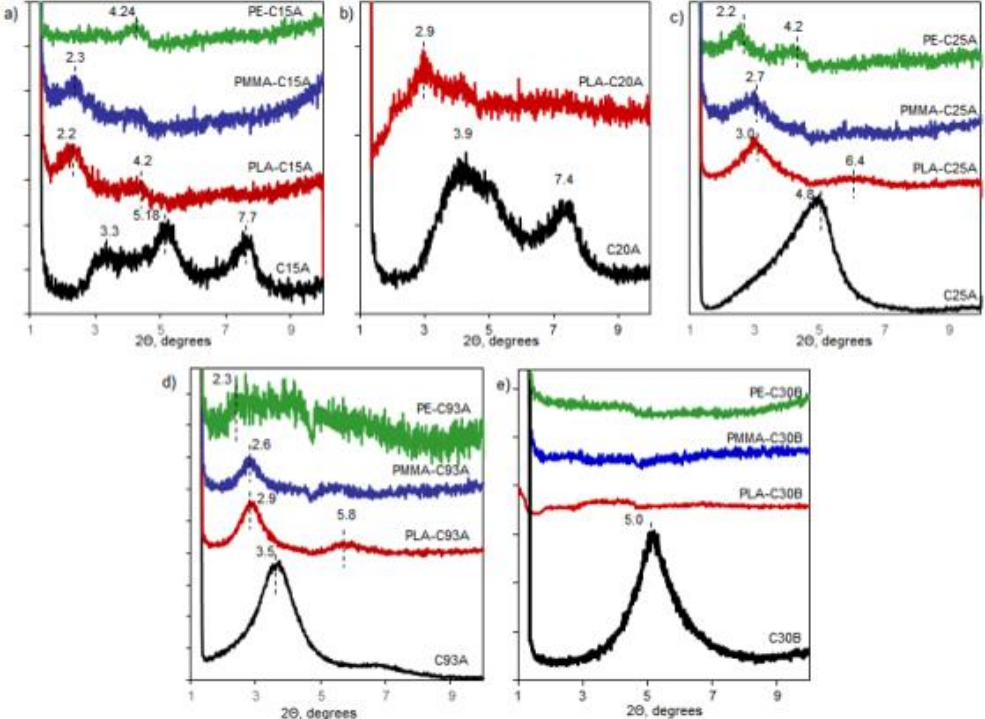
In Figure 53.b, XRD patterns of C20A and PLA-C20A composite are given. In the diffractogram of C20A, two broad peaks at around  $2\Theta=3.9$  and  $7.4^\circ$  corresponding to inter-reticular distances of  $d_{001}= 2.3$  and  $1.19$  nm were recorded. A weak peak appeared at  $2.9^\circ$  indicating an inter-reticular distance of  $d_{001}=3.04$  nm in the XRD of PLA-C20A nanocomposite.

Figure 53.c. represents the XRD patterns for neat Cloisite 25A and composites involving C25A. The diffractogram of C25A showed a characteristic intense and broad peak at  $4.7^\circ$  corresponding to interlayer spacing of  $d_{001}= 1.88$  nm. The diffractogram of PLA-C25A showed weak peaks at  $2\Theta= 2.9$  and  $64^\circ$  corresponding to inter-reticular distances of  $d_{001}=2.94$  and  $1.38$  nm indicating both partial increase and partial reduction of interlayer spacing between the platelets. A weak peak at  $2\Theta= 2.7^\circ$  corresponding to interlayer spacing of  $d_{001}= 3.27$  nm was detected in the diffractogram of PMMA-C25A. In the case of PE-C25A, two weak peaks at  $2\theta=2.2$  and  $4.2^\circ$  were observed, indicating delamination of clay galleries.

In Figure 53.d, XRD diffractograms of Cloisite 93A, and PLA, PE and PMMA composites involving C93A are given. The diffractogram of C93A showed an intense peak at  $2\Theta= 3.5^\circ$  corresponding to interlayer spacing of  $d_{001}=2.52$  nm. That of PLA-C93A showed two peaks located at  $2\Theta = 2.9$  and  $5.8^\circ$ . These values corresponded to  $3.04$  and  $1.52$  nm spacing. Thus, it can be concluded that during the blending process the reduction of interlayer spacing also took place as in case of PLA-C25A. The diffractogram of PMMA-C93A composite showed a weak peak

located at  $2\Theta = 2.6^\circ$  ( $d_{001}=3.4$  nm), again pointing out separation of clay layers. For the PE-C93A composite, only a very weak peak at around  $2.3^\circ$ , indicating inter layer spacing of 3.84 nm, was detected.

Finally, in Figure 53.e, XRD patterns for Cloisite 30B and composites involving C30B are drawn. The diffractogram of Cloisite 30B has a distinct maximum at around  $2\Theta=5.0^\circ$  corresponding to an inter-reticular distance of  $d_{001}=1.8$  nm. The characteristic peak of C30B was almost totally disappeared in the XRD patterns for PLA, PMMA and PE composites involving C30B.



**Figure 53:** X-ray diffractogram of composites of PLA, PMMA and PE involving a) C15A, b) C20A, c) C25A, d) C93A and e) C30B.



### 3.2.2. Direct Pyrolysis Mass Spectrometry Analyses

DP-MS analyses of the organic modifier, dimethyl hydrogenated ditallow ammonium, and all organoclays, namely C15A, C20A, C25A, C93A and C30B and the polymers used as the matrix, PLA, PMMA and PE and the polymer organoclay composites were done systematically to investigate the characteristics of the composites.

#### 3.2.2.1. Organoclays; C15A, C20A, C25A, C93A and C30B

In Figure 54, the TIC curves and the mass spectra recorded at the peak maxima of the organic modifier of Cloisite 15A and Cloisite 20A and organically modified montmorillonites, Cloisite 15A, Cloisite 20A, Cloisite 25A, Cloisite 93A and Cloisite 30B are given. C30B involve methyl tallow bis-2-hydroxyethyl ammonium salt. C15A and C20A involve the same organic modifier, dimethyl dehydrogenated tallow ammonium salt and the organic modifiers of C15A, C25A and C93A are very similar. In the case of C25A, one of the methyl groups present in the quaternary ammonium salt is replaced by 2-ethylhexyl group, and in the case of C93A one of the two dihydrogenated tallow groups is replaced by hydrogen. Therefore, even though the TIC curves showed noticeable differences, their mass spectra were almost identical. The single ion evolution profiles of the most abundant products,  $C_2H_4NH(CH_3)$  ( $m/z=58$  Da),  $C_{17}H_{34}NH(CH_3)$  or  $C_{16}H_{33}NHC_2H_4$  ( $m/z=268$  Da) and  $C_{18}H_{37}N(CH_3)CH_2$  or  $C_{18}H_{37}NHC_2H_4$  ( $m/z=296$  Da), are also given in Figure 54. The mass spectra of C30B also involved peaks at  $m/z=58$  Da,  $C_2H_4NH(CH_3)$ , and  $m/z=88$  Da,  $HOC_2H_4NH(C_2H_4)$ . For all the samples, the relative intensity of the fragment with  $m/z$  value 58 Da was increased at elevated temperatures.

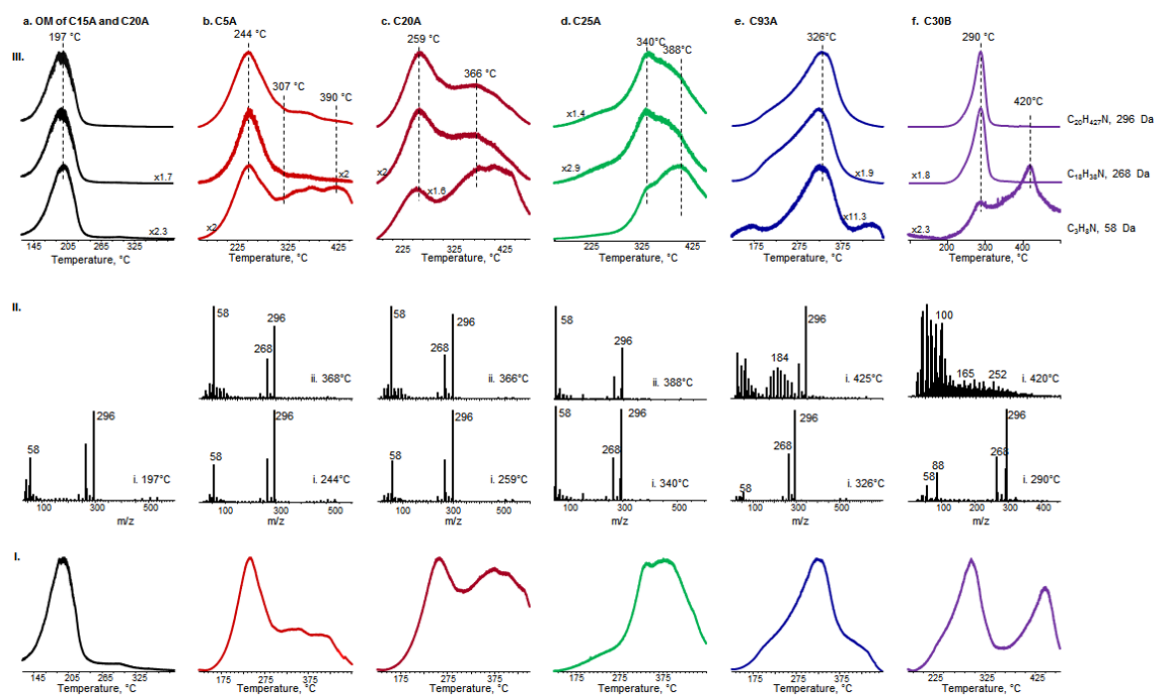


**Figure 54:** i. the TIC curves, ii. pyrolysis mass spectra at peak maxima and iii. single ion pyrograms of abundant fragments recorded during the pyrolysis of a) organic modifier of C15A and C20A, b) C15A, c) C20A, d) C25A, e) C93A and f) C30B.

The single ion evolution profiles of organic modifier of C15A and C20A indicated the elimination of the organic modifier during the pyrolysis at around 197 °C and similar behavior for all abundant fragments. On the other hand, the loss of organic modifier shifted to higher temperatures around 244 °C during the pyrolysis of C15A. This shift can be associated with the barrier effect of inorganic clay layers. Both high mass fragments, i.e. 268 and 296 Da fragments, and low mass fragments such as the one with  $m/z=58$  Da were mainly eliminated at around 244 °C, yet, the elimination of low mass fragments was also noticeable at higher temperatures, at around 307 °C and 390 °C. During the pyrolysis of C20A, the single ion evolution profiles of the most abundant products of the same organic modifier showed two peaks at around

259 °C and 366 °C. Again, the elimination of low mass fragments continued at elevated temperatures. The most abundant degradation product of the organic modifier of C25A was  $C_2H_4NH(CH_3)$  ( $m/z=58$  Da) contrary to the rest of the montmorillonites. This can be correlated with the presence of only one tallow substituent in its organic modifier. The high mass fragments were mainly detected at around 340 °C, whereas, low mass fragments showed two peaks at around 340 °C and 388 °C. Furthermore, the single ion profiles of high mass products of the organic modifier of C93A showed a peak at around 326 °C and noticeable diminish in the relative yield of low mass fragment was detected. Elimination of low mass fragments was less pronounced and again observed at higher temperatures.

It may be thought that a correlation between the temperature at which the organic modifier of the clay lost and the interlayer spacing of the clay layers should be present. Therefore, the elimination of the organic modifier may be expected to shift to higher temperatures as the interlayer spacing decreases due to the barrier effect of clays. According to XRD analyses of organoclays with similar organic modifiers, interlayer spacing of C25A, C93A and C15A, were determined as  $d_{00}=1.88$ , 2.52 and 2.68 nm, respectively. During the pyrolysis analyses, the temperature at which the ion yields maximized,  $T_{max}$ , was observed at 340 °C, 326 °C and 244 °C for C25A, C93A and C15A respectively and the free organic modifier was lost at around 197 °C. Thus, the shift of the  $T_{max}$  to high temperatures with the decrease in interlayer spacing supports the above proposal.

It may further be thought that if the interlayer spacing is very narrow, the loss of the organic modifier should shift to higher temperatures and extensive degradation of the organic modifier into small fragments should take place. The detection of only low mass fragments at relatively high temperatures for C93A and C30B supports this expectation.

### 3.2.2.2. Polymers; PLA, PMMA and PE

The TIC curves, pyrolysis mass spectra at peak maxima and single ion pyrograms of the abundant fragments recorded during the pyrolysis of poly(lactic acid), PLA, poly(methyl methacrylate), PMMA, and poly(ethylene), PE used as matrix materials were given in Figure 55.

The TIC curve of PLA has a maximum at around 362 °C (Figure 55a). As mentioned before, the pyrolysis mass spectrum of PLA showed series of peaks due to fragments generated by elimination of the neutral molecules like CO<sub>2</sub> and acetaldehyde during ionization of the cyclic oligomers (i.e. fragment with  $m/z=200$  Da), fragments produced by cis-elimination reactions (i.e. 217 Da) and low mass fragments produced by random chain homolysis reactions (i.e. fragment with  $m/z=56$  Da). The evolution of products due to cis-elimination reactions was observed at slightly higher temperatures, yet, this shift was almost negligible

As can be seen in the Figure 55b, the TIC curve of PMMA showed a peak with a maximum at 403°C and the pyrolysis mass spectrum of PMMA involved characteristics peaks of methylmethacrylate (100 Da) generated by depolymerization of PMMA. All the fragments detected during the pyrolysis showed identical evolution profiles as expected. A single peak at around 493 °C was present in the TIC curve of PE (Figure 55c). The pyrolysis mass spectrum of PE was dominated with relatively low mass fragment peaks as expected due to the random cleavage of hydrocarbon chains during the pyrolysis and ionization. Again, the single ion evolution pyrograms of all fragments showed identical trends.

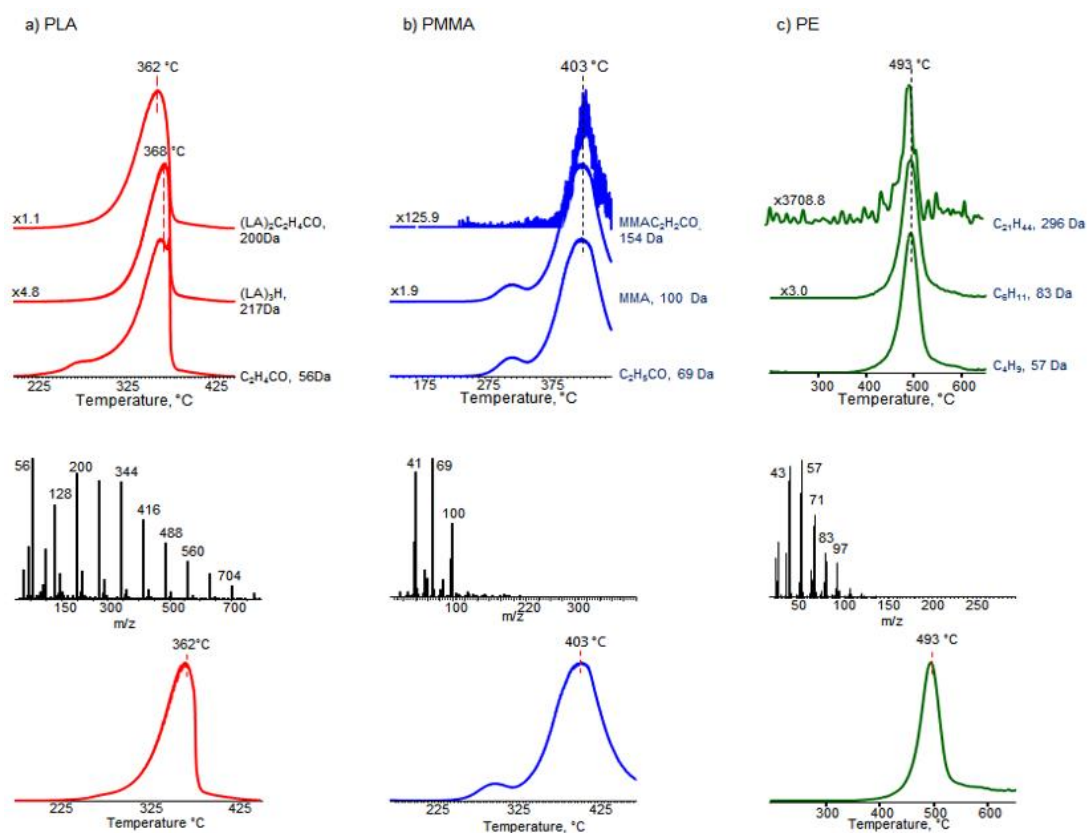


**Figure 55:** The TIC curves, pyrolysis mass spectra at peak maxima and single ion pyrograms of abundant fragments recorded during the pyrolysis of a) PLA, b) PMMA and c) PE.

DP-MS results indicated that none of the peaks presents in the pyrolysis mass spectra of PLA and PMMA, overlaps with the high mass peaks present in the pyrolysis mass spectra of the organoclays. In contrast, the pyrolysis mass spectra of PE showed several peaks overlapping with those present in the pyrolysis mass spectra of the organoclays as expected due to the presence of tallow as substituent in the organic modifier, yet, these fragments were eliminated at different temperature regions.

### 3.2.2.3. PLA, PMMA and PE Composites

Thermal degradation products of the composites were almost identical to those recorded during the pyrolysis of the corresponding polymers, yet; the relative yields of the thermal degradation products of the organic modifiers were quite weak since the composites involved only very small amounts of organoclays. To investigate the correlation between thermal behaviors and morphology, the single ion evolution pyrograms of composites with the characteristic pyrolysis products of the organic modifiers and host polymers were investigated. For this purpose, the fragment with  $m/z$  value 296 Da being the most abundant product was selected as the reference fragment for all organoclays.  $(C_2H_4CO_2)_2C_2H_4CO$  ( $m/z=200$  Da) fragment for PLA composites, the monomer,  $C_3H_5CO_2CH_3$  ( $m/z=100$  Da) for PMMA composites and the most abundant fragment,  $C_4H_9$  ( $m/z=57$  Da) for PE composites were selected as the diagnostic fragments. The single ion evolution profiles of these selected reference fragments detected during the pyrolysis of the composites involving C15A-C20A, C25A, and C93A are given in Figure 56, 57 and 58, respectively. The chemical structures and  $m/z$  values of the reference fragments were not given in the figures for simplicity. The thicker lines represent composites whereas, the corresponding ones for the organoclays and the neat polymers are shown as thin lines. In general, increase in the thermal stabilities of PLA and PMMA and slight decrease in the thermal stability of PE upon incorporation of organoclays were recorded.

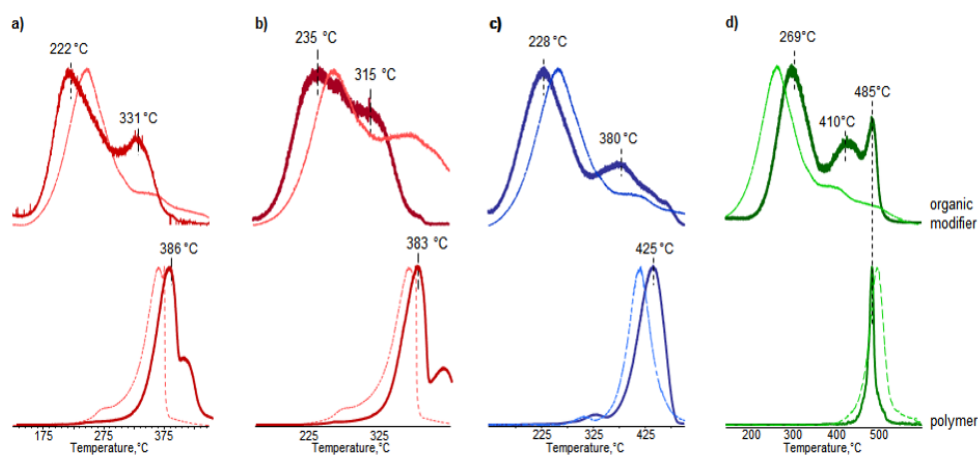


**Figure 56:** Single ion evolution profiles of the organic modifier and the polymers detected during the pyrolysis of a) PLA-C15A, b) PLA-C20A, c) PMMA-C15A and d) PE-C15A.

\*The corresponding ones for the organoclays and the neat polymers are shown as thin lines.

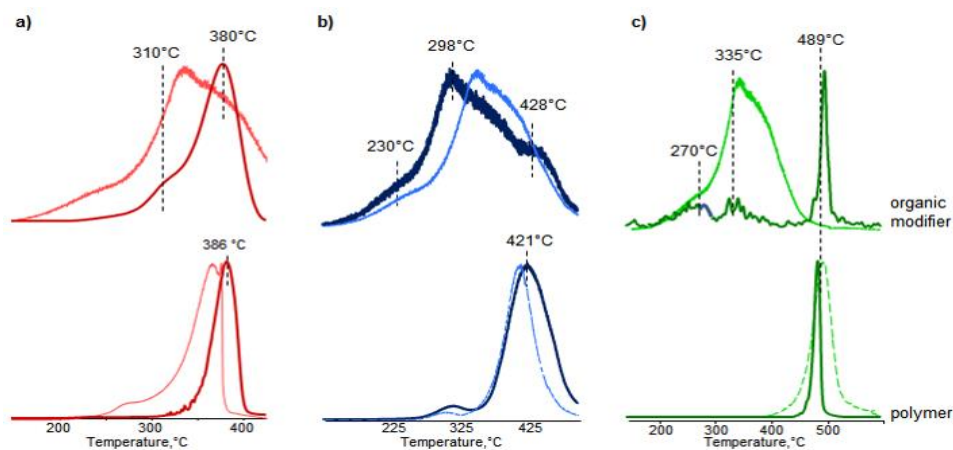


**Figure 57:** Single ion evolution profiles of the organic modifier and the polymers detected during the pyrolysis of a) PLA-C25A, b) PMMA-C25A and c) PE-C25A.

\*The corresponding ones for the organoclays and the neat polymers are shown as thin lines.

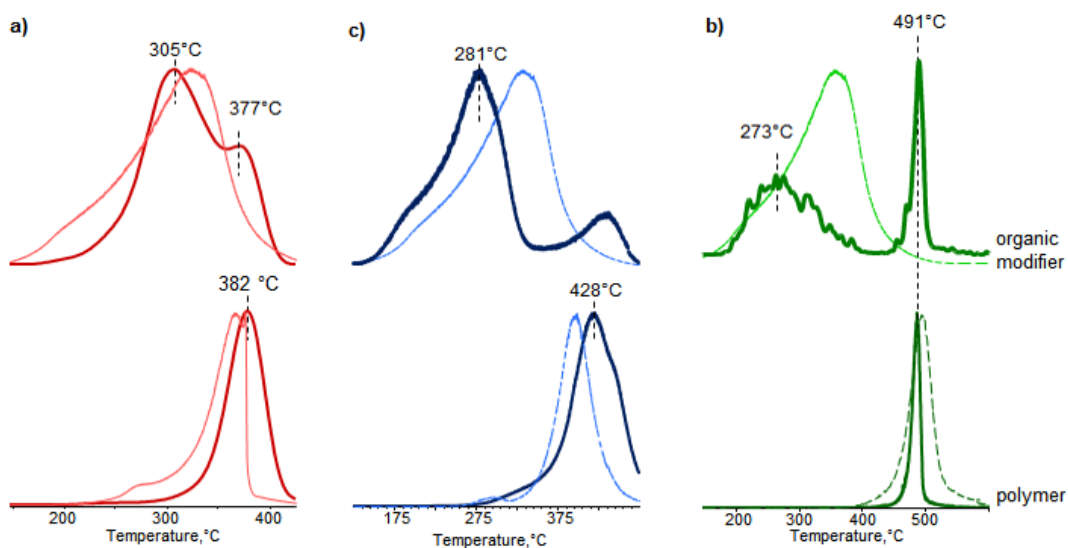


**Figure 58:** Single ion evolution profiles of the organic modifier and the polymers detected during the pyrolysis of a) PLA-C93A, b) PMMA-C93A and c) PE-C93A.

\*The corresponding ones for the organoclays and the neat polymers are shown as thin lines.

The single ion pyrograms of the organic modifiers detected during the pyrolysis of PLA and PMMA composites showed more than one peak, one being at lower temperature regions compared to the ones detected during pyrolysis of organoclays and the other being in the temperature regions where the matrix polymer decomposition took place. On the other hand, the single ion pyrograms of the organic modifier of PE composite showed multiple overlapping peaks. The sharp peak was recorded at high temperature regions where characteristic degradation product of PE detected and thus associated with  $C_{21}H_{44}$  fragment of PE. And, the relatively low temperature peaks were associated with the organic modifier.

In Table 12, the maximum of the peaks present in the evolution profiles of the characteristic degradation products of the organic modifiers, C15A, C20A, C25A and



C93A, and degradation products of the corresponding composites of PLA, PMMA and PE recorded during the pyrolysis are collected. XRD data for the organoclays and composites are also given in Table 12.

**Table 12:** DP-MS and XRD data for the organoclays and corresponding composites.

	<b>T<sub>max</sub>, °C, based on the products of organoclays</b>	<b>Interlayer spacing, d<sub>001</sub>, nm</b>	<b>T<sub>max</sub>, °C, based on the products of polymers</b>
<b>Organic modifier of C15A and C20A</b>	197	-	-
<b>C15A, C20A and Corresponding Composites</b>			
<b>C15A</b>	244, 307, 390	2.64, 1.67, 1.16	-
<b>PLA-C15A</b>	222, 331	4.1, 2.1,	386
<b>PMMA-C15A</b>	228, 380	3.84	425
<b>PE-C15A</b>	269, 410	2.2	485
<b>C20A</b>	259, 366	2.3, 1.19	-
<b>PLA-C20A</b>	235, 315	3.04	383
<b>C25A and Corresponding Composites</b>			
<b>C25A</b>	340	1.88	-
<b>PLA-C25A</b>	310, 380	2.94, 1.38	386
<b>PMMA-C25A</b>	298, 428	3.27	421
<b>PE-C25A</b>	270, 335	4.01, 2.1	489
<b>C93A and Corresponding Composites</b>			
<b>C93A</b>	326	2.52	-
<b>PLA-C93A</b>	305, 377	3.04, 1.52	382
<b>PMMA-C93A</b>	281, 425	3.40	428
<b>PE-C93A</b>	273	3.84	491

The temperatures at which the yield of  $C_{18}H_{37}N(CH_3)CH_2$  (296 Da) fragment maximized,  $T_{max}$ , recorded during the pyrolysis of each organoclay and the corresponding composites were correlated with XRD data, thus,  $T_{max}$  values are plotted as a function of interlayer spacing.

In Figure 59,  $T_{max}$  values recorded in the evolution profiles of decomposition products of C15A, C20A and composites involving these organoclays are plotted as a function of interlayer spacing for C15A, C20A and the corresponding composites. The  $T_{max}$  value for the free organic modifier is shown as a star for comparison. As it can clearly be seen from Table 12 that the number of peaks present in the XRD diffractograms and the number of peaks detected in the evolution profiles of characteristic degradation products detected during the pyrolysis of C15A, C20A and PLA-C15A were identical. Therefore, the correlations made for C15A, C20A, and PLA-C15A were straight forward; yet, for PLA-C20A, PMMA-C15A and PE-C15A composites, the correlations were done considering the trends observed for C15A, C20A, and PLA-15A.

In Figure 60 and 61, similarly,  $T_{max}$  values are plotted as a function of the inter-layer spacing values for C25A and C93A and for the corresponding composites involving C25A and C93A, respectively. The correlations made for PMMA composites involving C25A and C93A were done considering the trends observed for corresponding organoclays and PLA and PE composites.

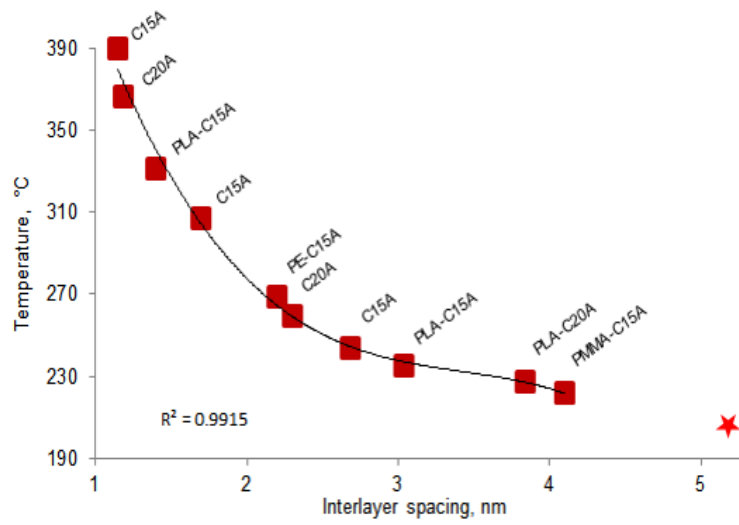


**Figure 59:** Variation of  $T_{max}$  as a function of inter-layer spacing for C15A, C20A and for the composites involving C15A and C20A.

\*The star represents  $T_{max}$  value for the free organic modifier.

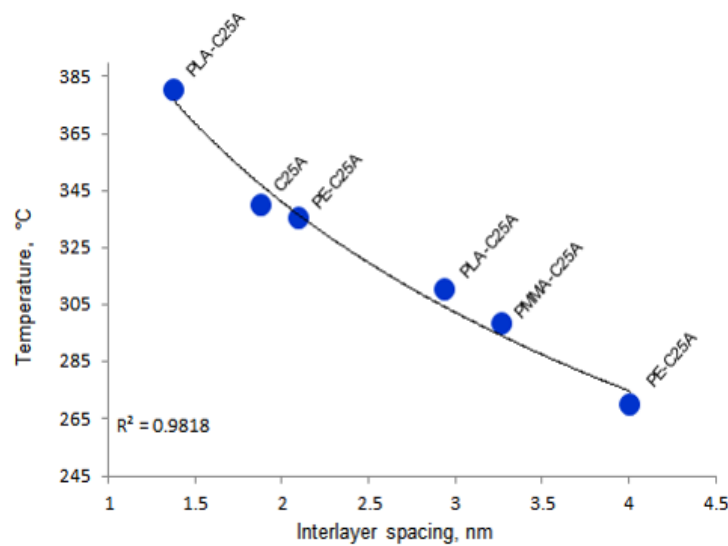


**Figure 60:** Variation of  $T_{max}$  as a function of inter-layer spacing for C25A and for the composites involving C25A.

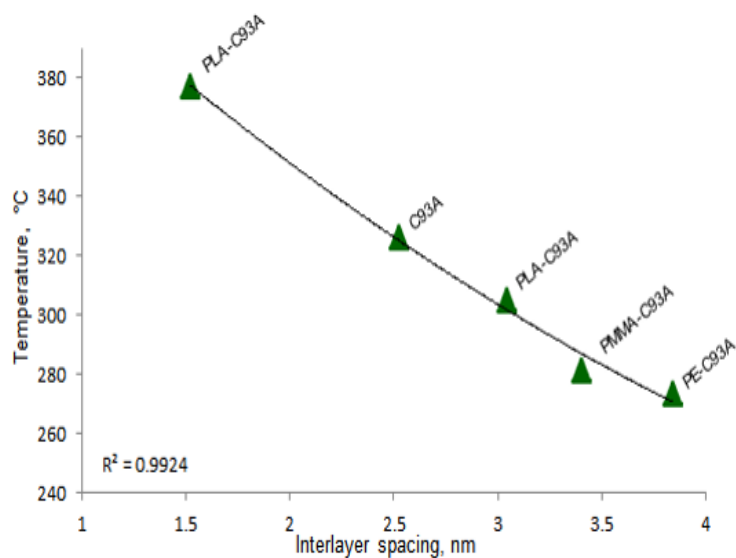
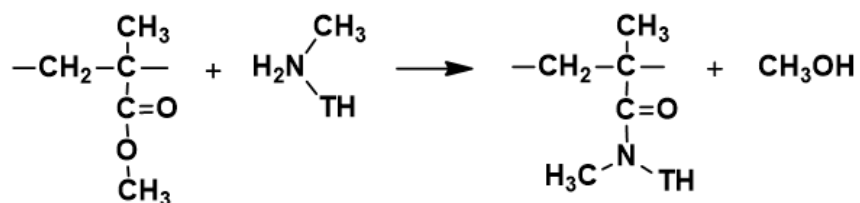


**Figure 61:** Variation of  $T_{\max}$  as a function of inter-layer spacing for C93A and for the composites involving C93A.

It is clear that as the separation between the clay layers increases the loss of organic modifier shifts to lower temperatures. The correlation coefficients calculated for a second order polynomial are also given in the figures indicated a non-linear or complex relation. One of the possible reasons for this complex relation may be the interactions between the organic modifier and the polymer matrix. For both PLA and PMMA composites, evolution of the characteristic fragments of the organic modifier was also detected at relatively high temperature regions, which supports this idea. The possible reaction between the amine group of the organic modifier and the ester groups of PMMA to generate amide functional groups and methanol are given in Scheme IV.

**Scheme IV:** Generation of amide units by interaction of fragments of the organic modifier with ester groups of PMMA.



Elimination of fragments involving amide functional groups and methanol at elevated temperatures confirmed the interactions of the organic modifier with PMMA composites involving C15A, C25A and C93A (Figure 62) [177]. Although, PLA is also a polyester, generation of amide units was only detected for PMMA composites most probably due to the significantly higher reactivity of methyl ester group present as a side group in case of PMMA.

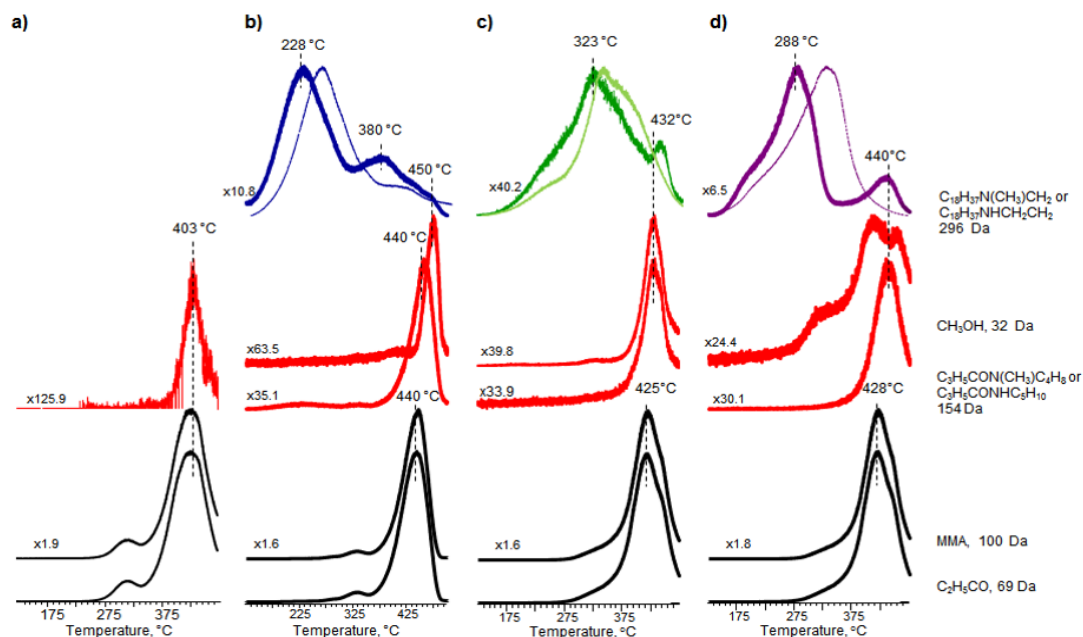


**Figure 62:** Single ion profiles of selected products detected during the pyrolysis of a) PMMA, b) PMMA-C15A, c) PMMA-C25A and d) PMMA-C93A.

\*The corresponding ones for the pure organoclays are shown as thin lines.

In Figure 63, the single ion evolution profiles of the organic modifier and the polymers detected during the pyrolysis of PLA-C30B, PMMA-C30B and PE-C30B composites are given. Increase in the thermal stabilities of PLA and PMMA, and in contrast, a decrease in the thermal stability of PE upon incorporation of C30B into polymer matrix was detected. In addition, a significant increase in the thermal stability of the organic modifier during the pyrolysis of PLA and PMMA composites was detected. During the pyrolysis of PE-C30B composite, elimination of the organic modifier was detected at around 292 °C, similar to loss of the organic modifier during the pyrolysis of pure C30B. This indicated that the interlayer spacing of C30B

was not changed during the blending process, although the characteristic peak of C30B was not detected in the XRD diffractogram of PE-C30B composite.

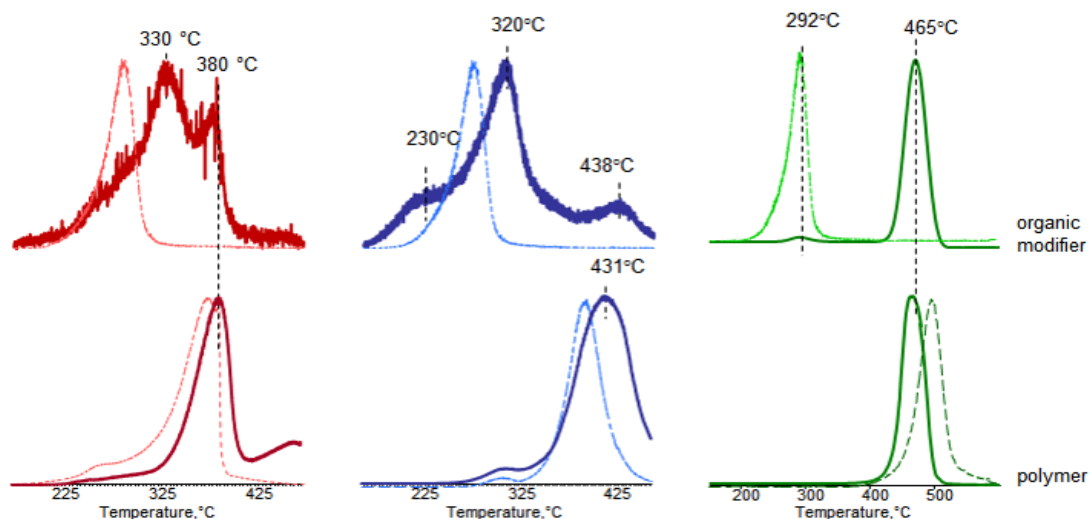


**Figure 63:** Single ion evolution profiles of the organic modifier and the polymers detected during the pyrolysis of a) PLA-C30B, b) PMMA-C30B and c) PE- C30B.

\*The corresponding ones for the organoclays and the neat polymers are shown as thin lines.

On the other hand, similar to the interactions between PLA and C30B, pyrolysis analyses of PMMA composite also revealed the generation of new products and elimination of  $\text{CH}_3\text{OH}$  indicating interactions between the ester groups of the PMMA and hydroxyl groups of organic modifier of C30B. In Figure 64 and 65, single ion evolution profiles of related fragments detected during the pyrolysis of PMMA, PLA and composites involving C30B are given. The reaction mechanisms of PMMA and PLA with C30B are shown in Scheme V and VI [162], [177].

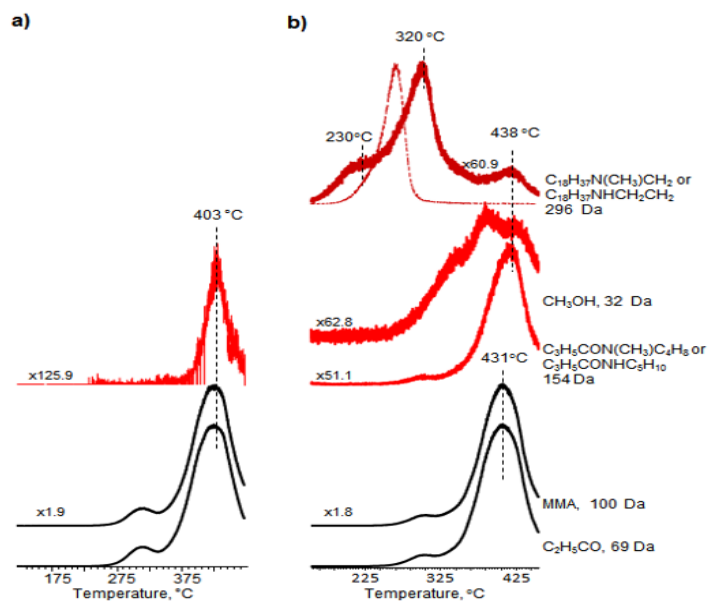


**Figure 64:** Single ion profiles of selected products detected during the pyrolysis of a)PMMA, b)PMMA-C30B.

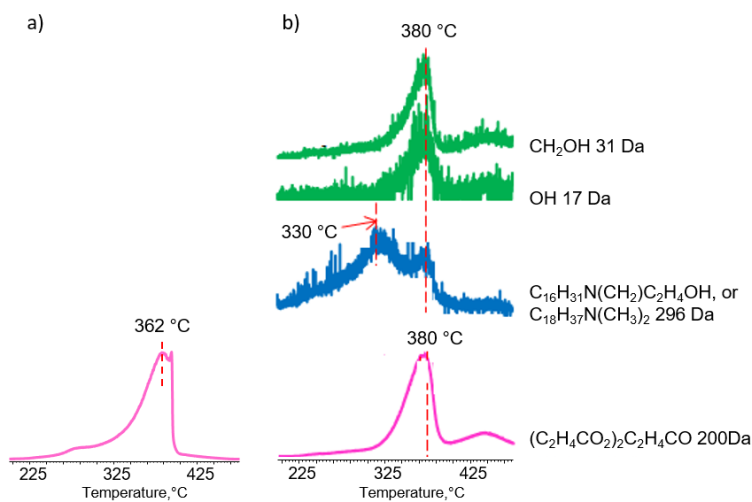
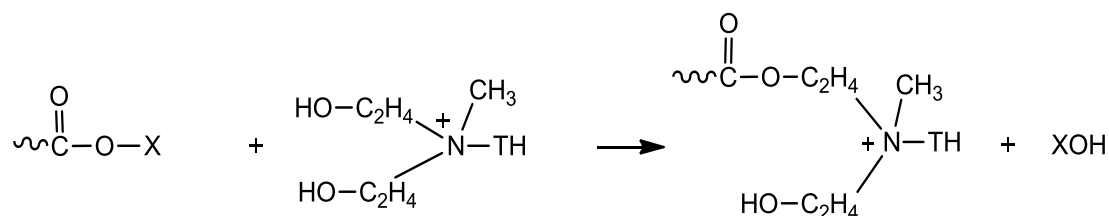


**Figure 65:** Single ion profiles of selected products detected during the pyrolysis of a)PLA, b) PLA-C30B.

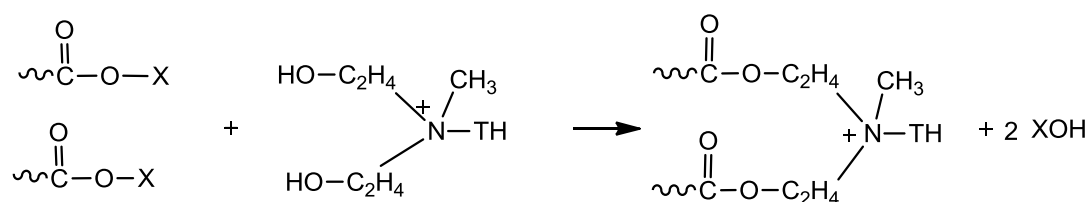


**Scheme V:** Trans-esterification reaction between the hydroxyl groups of the organic modifier and the ester groups of PMMA.



where X is CH(CH<sub>3</sub>)COO- for PLA and CH<sub>3</sub> for PMMA

**Scheme VI:** Crosslinking reactions due to trans-esterification reactions between the hydroxyl groups of the organic modifier and the ester groups of PMMA.



where X is CH(CH<sub>3</sub>)COO- for PLA and CH<sub>3</sub> for PMMA

Therefore, it can be concluded that DP-MS results supply information not only on the dispersion states of organoclays but also on the possible interactions between the organic modifier and polymer matrix based on the trends present in the single ion evolution profiles of the characteristic degradation products of the organic modifier.



## CHAPTER 4

### 4. CONCLUSION

#### *PLA BASED BLENDS, COMPOSITES AND FIBERS*

In the first part of this thesis, morphological, thermal and mechanical characterizations of poly(lactic acid)-poly(ethylene glycol), PLA-PEG, blends and their organoclay composites were investigated. In addition, morphological and thermal properties of electrospun fibers of PLA and of several PLA systems including PLA-organoclay composites, PLA-PEG blends and PLA-PEG composites were studied.

#### ➤ *PLA-PEG Blends and Composites Involving Cloisite 30B*

PLA-PEG blends involving 10, 15 and 20 wt% PEG, were prepared and characterized. Addition of PEG into PLA matrix reduced the endothermic melting peak of PLA due to the plasticizing effect of PEG. Both TGA and DP-MS analyses of PLA-PEG blends pointed out that the thermal decomposition occurred mainly in two steps. In addition, pyrolysis mass spectrometry analyses revealed interactions of COOH groups of PLA and ether linkages of PEG during the blending and/or

pyrolysis process. Consequently, decrease in the thermal stability of PEG chains was detected. The blends prepared by solution mixing method with variable mixing periods confirmed that the interactions took place mainly during the blending process. Addition of 20 wt% PEG decreased the tensile strength and tensile modulus of PLA while improving its ductility due to its plasticization effect, as expected.

PLA-PEG composites, involving 3 wt% C30B and 10, 15 and 20 wt% PEG, were prepared by melt blending and characterized. The morphological analyses of PLA-PEG composites via XRD and TEM methods indicated successful blend compatibilization due to the dispersion and localization of clay platelets at the PEG droplet interfaces. The tensile strength, % elongation at break and Young's modulus were increased upon incorporation of C30B into blends. The most significant increase in elongation was observed for the composite involving 20 wt% PEG. The onset of the decomposition temperature of PLA shifted to lower temperatures in the presence of PEG composites. However, DP-MS analyses pointed out that the generation of thermally more stable units, cross-linked by the chemical interactions between PLA and low mass PEG based fragments decomposed at low temperature regions were enhanced in the presence of C30B. The increase in Mw values of the blends in the presence of C30B and the unexpectedly high %elongation for PLA80-PEG20-C30B composite supports this proposal.

#### ➤ *Electrospun Fibers of PLA Based Systems*

Electrospun fibers of PLA, PLA composites, PLA-PEG blends and composites were prepared and characterized. CHCl<sub>3</sub>/DMF solvent system with 90:10 (v/v) solvent ratio was chosen as the most suitable solvent for obtaining thin PLA fibers. As the concentration of PLA was increased to 15% (w/v) in CHCl<sub>3</sub>/DMF 90:10 (v/v)

solvent, bead-free fibers having fiber diameter around 500 nm were obtained. DP-MS analyses of PLA fibers revealed that the thermal stability of PLA decreased upon fiber formation. The products generated by trans-esterification reactions became more pronounced pointing out that the probability of intermolecular trans-esterification reactions was increased upon nanofiber formation.

PLA composite fibers involving variable amounts of C15A, C20A, and C30B were prepared by electrospinning successfully. Slightly narrower fibers were created compared to neat PLA fibers upon incorporation of organoclays. As the amount of clay incorporated was increased, the fiber diameter became slightly narrower due to increase in electrical conductivity as a consequence of presence ammonium salts as an organic modifier in the montmorillonites. The diameters of the fibers were smallest for PLA-C15A composite and largest for PLA-C30B composite. DP-MS analyses of PLA fibers involving C15A, C20A and C30B indicated an increase in the thermal stability of PLA fiber upon incorporation of organoclays into PLA. The significant increase in the thermal stability of PLA composite fibers compared to their corresponding composites was correlated with the better delamination and intercalation of PLA chains into clay layers upon fiber formation. Also, the relative yields of high mass products generated by trans-esterification and cis-elimination reactions were significantly decreased indicating reduction in the intermolecular interactions in the presence of nano-clays.

Moreover, fibers of PLA-PEG blends were spun at higher voltage and their morphological and thermal analyses were carried out. SEM images of electrospun fibers of PLA-PEG blend revealed generations of bead-free and slightly thicker fibers compared to neat PLA fibers and correlated with the increase in the applied voltage. Similar to the blends, the melting temperatures of PLA-PEG fiber was shifted to lower temperatures compared to neat PLA fiber due to the plasticizing effect of PEG. Again, thermal degradations occurred in two steps, the first step being due to the degradation of PLA and the second due to the degradation of PEG

chains. During the pyrolysis of PLA-PEG fibers, the relative yields of the products related to the decomposition of the units generated by interactions between PLA and PEG were decreased and the decomposition of PEG chains was detected in the temperature region where pure PEG degraded. This behavior was associated with phase separation during electrospinning process.

In the presence of C30B narrower PLA-PEG fibers were generated, and again attributed to the enhancement in the electrical conductivity. In addition, significant increase in the thermal stability of PLA chains was detected not only compared to the neat blends and fibers but also compared to PLA-PEG organoclay composites. It may be concluded that as a consequence of the diffusion of both PLA and PEG chains into the galleries between the silicate layers, the interactions between PLA and PEG chains were enhanced and the phase separation during the electrospinning process detected for PLA-PEG fibers was not detected for PLA-PEG composite fibers.

### ***DIRECT PYROLYSIS MASS SPECTROMETRY (DP-MS) TO CHARACTERIZE THE POLYMER/ORGANOCLAY SYSTEMS***

In this part of the work, the application of DP-MS to investigate the characteristics of polymer/organoclay systems was studied. To investigate the correlation between thermal behavior and morphology, the single ion evolution pyrograms of characteristic pyrolysis products of the organic modifiers, host polymers and corresponding composites were evaluated. The temperature at which the loss of organic modifier was detected by DP-MS analyses was correlated with the inter-layer spacing of the platelets of organoclays determined via XRD measurements. It was clear from DP-MS analyses of PLA, PMMA and PE composites involving organically modified montmorillonites Cloisite 15A, 20A, 25A, 93A or 30B that as

the separation between the clay layers increases the loss of organic modifier shifts to lower temperatures. Besides the extent and type of dispersion of clay layers in the polymer matrices, DP-MS also allows the identification of possible interactions between the polymer and the organic modifier. The possible reaction between the amine group of the organic modifier of C15A, C25A or C93A and the ester group of PMMA, trans-esterification reaction between the hydroxyl groups of the organic modifier of C30B and the ester groups of PMMA or PLA and crosslinking reactions due to this trans-esterification reaction were given.





## REFERENCES

- [1] L.-T. Lim, R. Auras, and M. Rubino, "Processing technologies for poly(lactic acid)," *Prog. Polym. Sci.*, vol. 33, no. 8, pp. 820–852, 2008.
- [2] M. Jamshidian, E. A. Tehrany, M. Imran, M. Jacquot, and S. Desobry, "Poly-Lactic Acid: Production, Applications, Nanocomposites, and Release Studies," *Compr. Rev. Food Sci. Food Saf.*, vol. 9, no. 5, pp. 552–571, Aug. 2010.
- [3] M. Bijarimi, S. Ahmad, and R. Rasid, "Mechanical, thermal and morphological properties of poly(lactic acid)/natural rubber nanocomposites," *J. Reinf. Plast. Compos.*, vol. 32, no. 21, pp. 1656–1667, Nov. 2013.
- [4] F. Carrasco, P. Pagès, J. Gámez-Pérez, O. O. Santana, and M. L. MasPOCH, "Processing of poly(lactic acid): Characterization of chemical structure, thermal stability and mechanical properties," *Polym. Degrad. Stab.*, vol. 95, no. 2, pp. 116–125, 2010.
- [5] Q. Meng, M.-C. Heuzey, and P. J. Carreau, "Control of thermal degradation of polylactide/clay nanocomposites during melt processing by chain extension reaction," *Polym. Degrad. Stab.*, vol. 97, no. 10, pp. 2010–2020, 2012.
- [6] A. K. Mohapatra, S. Mohanty, and S. K. Nayak, "Effect of PEG on PLA/PEG blend and its nanocomposites: A study of thermo-mechanical and morphological characterization," *Polym. Compos.*, vol. 35, no. 2, pp. 283–293, Feb. 2014.
- [7] R. Wang, C. Wan, S. Wang, and Y. Zhang, "Morphology, mechanical properties, and durability of poly(lactic acid) plasticized with Di(isononyl) cyclohexane-1,2-dicarboxylate," *Polym. Eng. Sci.*, vol. 49, no. 12, pp. 2414–

2420, Dec. 2009.

- [8] G. Perego and G. D. Cella, "Mechanical Properties," in *Poly(Lactic Acid)*, Hoboken, NJ, USA: John Wiley & Sons, Inc., 2010, pp. 141–153.
- [9] L. Fambri and C. Migliaresi, "Crystallization and Thermal Properties," in *Poly(Lactic Acid)*, Hoboken, NJ, USA: John Wiley & Sons, Inc., 2010, pp. 113–124.
- [10] M. L. Di Lorenzo, "Crystallization behavior of poly(l-lactic acid)," *Eur. Polym. J.*, vol. 41, no. 3, pp. 569–575, Mar. 2005.
- [11] D. W. Grijpma, H. Altpeter, M. J. Bevis, and J. Feijen, "Improvement of the mechanical properties of poly(D,L-lactide) by orientation," *Polym. Int.*, vol. 51, no. 10, pp. 845–851, Oct. 2002.
- [12] J. R. Dorgan, "Rheology of Poly(Lactic Acid)," in *Poly(Lactic Acid)*, Hoboken, NJ, USA: John Wiley & Sons, Inc., 2010, pp. 125–139.
- [13] H. J. Lehermeier, J. R. Dorgan, and J. D. Way, "Gas permeation properties of poly(lactic acid)," *J. Memb. Sci.*, vol. 190, no. 2, pp. 243–251, Sep. 2001.
- [14] H. Tsuji, R. Okino, H. Daimon, and K. Fujie, "Water vapor permeability of poly(lactide)s: Effects of molecular characteristics and crystallinity," *J. Appl. Polym. Sci.*, vol. 99, no. 5, pp. 2245–2252, Mar. 2006.
- [15] F.-D. Kopinke, M. Remmler, K. Mackenzie, M. Möder, and O. Wachsen, "Thermal decomposition of biodegradable polyesters—II. Poly(lactic acid)," *Polym. Degrad. Stab.*, vol. 53, no. 3, pp. 329–342, Sep. 1996.
- [16] R. Auras, B. Harte, and S. Selke, "An Overview of Polylactides as Packaging Materials," *Macromol. Biosci.*, vol. 4, no. 9, pp. 835–864, Sep. 2004.
- [17] M. C. Gupta and V. G. Deshmukh, "Thermal oxidative degradation of poly-

- lactic acid,” *Colloid Polym. Sci.*, vol. 260, no. 3, pp. 308–311, Mar. 1982.
- [18] R. Al-Itry, K. Lamnawar, and A. Maazouz, “Improvement of thermal stability, rheological and mechanical properties of PLA, PBAT and their blends by reactive extrusion with functionalized epoxy,” *Polym. Degrad. Stab.*, vol. 97, pp. 1898–1914, 2012.
- [19] F.-J. Li, S.-D. Zhang, J.-Z. Liang, and J.-Z. Wang, “Effect of polyethylene glycol on the crystallization and impact properties of polylactide-based blends,” *Polym. Adv. Technol.*, vol. 26, no. 5, pp. 465–475, May 2015.
- [20] L. Ying, Z. Kun-Yu, D. Zhong-Min, L.-S. Dong, and L. Yue-Sheng, “Study of Hydrogen-Bonded Blend of Polylactide with Biodegradable Hyperbranched Poly(ester amide),” *Macromolecules*, vol. 40, no. 17, pp. 6257–6267, 2007.
- [21] J.-F. Zhang and X. Sun, “Physical Characterization of Coupled Poly(lactic acid)/Starch/Maleic Anhydride Blends Plasticized by Acetyl Triethyl Citrate,” *Macromol. Biosci.*, vol. 4, no. 11, pp. 1053–1060, Nov. 2004.
- [22] M. Nofar, M.-C. Heuzey, P. J. Carreau, and M. R. Kamal, “Effects of nanoclay and its localization on the morphology stabilization of PLA/PBAT blends under shear flow,” *Polymer (Guildf.)*, vol. 98, pp. 353–364, 2016.
- [23] J. Anakabe, A. M. Zaldua Huici, A. Eceiza, and A. Arbelaiz, “The effect of the addition of poly(styrene- *co* -glycidyl methacrylate) copolymer on the properties of polylactide/poly(methyl methacrylate) blend,” *J. Appl. Polym. Sci.*, vol. 133, no. 37, Oct. 2016.
- [24] Y. Hu, M. Rogunova, V. Topolkaraev, A. Hiltner, and E. Baer, “Aging of poly(lactide)/poly(ethylene glycol) blends. Part 1. Poly(lactide) with low stereoregularity,” *Polymer (Guildf.)*, vol. 44, no. 19, pp. 5701–5710, 2003.
- [25] J. Ahmed, S. K. Varshney, R. Auras, and S. W. Hwang, “Thermal and

- Rheological Properties of L-Polylactide/Polyethylene Glycol/Silicate Nanocomposites Films,” *J. Food Sci.*, vol. 75, no. 8, pp. N97–N108, Oct. 2010.
- [26] J. Parameswaranpillai, S. Thomas, and Y. Grohens, “Polymer Blends: State of the Art, New Challenges, and Opportunities,” in *Characterization of Polymer Blends*, Weinheim, Germany: Wiley-VCH Verlag GmbH & Co. KGaA, 2014, pp. 1–6.
- [27] Buthaina A. and K. M.Kadum, “Influence of Polymer Blending on Mechanical and Thermal Properties,” *Mod. Appl. Sci.*, vol. 4, no. 9, p. 157, 2010.
- [28] R. P. Patel and J. Shin, “Compounding and Processing of Plastic/Rubber Blends,” in *Encyclopedia of Polymer Blends*, Weinheim, Germany: Wiley-VCH Verlag & Co. KGaA, 2016, pp. 109–162.
- [29] N. C. Liu and H. Huang, “Types of Reactive Polymers Used in Blending,” in *Reactive Polymer Blending*, München: Carl Hanser Verlag GmbH & Co. KG, 2001, pp. 13–42.
- [30] S. Sánchez-Valdes, L. F. Ramos-De Valle, and O. Manero, “Polymer Blends,” in *Handbook of Polymer Synthesis, Characterization, and Processing*, Hoboken, NJ, USA: John Wiley & Sons, Inc., 2013, pp. 505–517.
- [31] G. L. Rempel and H. Wang, “Nitrile Rubber Latex Blends: Preparation, Characterization and Applications,” in *Rubber Nano Blends Preparation, Characterization and Applications*, Gordana Marković and Visakh P.M., Eds. Springer International Publishing AG, 2017, pp. 67–88.
- [32] J. Fawaz and V. Mittal, “Synthesis of Polymer Nanocomposites: Review of Various Techniques,” in *Synthesis Techniques for Polymer Nanocomposites*, Weinheim, Germany:Wiley-VCH Verlag GmbH & Co. KGaA, 2014, pp.1–30.

- [33] J. Feng, M. A. Winnik, R. R. Shivers, and B. Clubb, "Polymer Blend Latex Films: Morphology and Transparency," *Macromolecules*, vol. 28, no. 23, pp. 7671–7682, Nov. 1995.
- [34] E. Meaurio, N. Hernandez-Montero, E. Zuza, and J.-R. Sarasua, "Miscible Blends Based on Biodegradable Polymers," in *Characterization of Polymer Blends*, Weinheim, Germany: Wiley-VCH Verlag GmbH & Co. KGaA, 2014, pp. 7–92.
- [35] E. Ozdemir, T. Tinçer, and J. Hacaloglu, "Characterization of polylactide/poly(ethylene glycol) blends via direct pyrolysis mass spectrometry," *J. Anal. Appl. Pyrolysis*, vol. 122, pp. 315–322, Nov. 2016.
- [36] I. Pillin, N. Montrelay, and Y. Grohens, "Thermo-mechanical characterization of plasticized PLA: Is the miscibility the only significant factor?," *Polymer (Guildf)*, vol. 47, no. 13, pp. 4676–4682, Jun. 2006.
- [37] B.-S. Park, J. C. Song, D. H. Park, and K.-B. Yoon, "PLA/chain-extended PEG blends with improved ductility," *J. Appl. Polym. Sci.*, vol. 123, no. 4, pp. 2360–2367, Feb. 2012.
- [38] M. Sheth, R. A. Kumar, V. Dave, R. A. Gross, and S. P. McCarthy, "Biodegradable polymer blends of poly(lactic acid) and poly(ethylene glycol)," *J. Appl. Polym. Sci.*, vol. 66, no. 8, pp. 1495–1505, Nov. 1997.
- [39] K.-S. Kim, I.-J. Chin, J. S. Yoon, H. J. Choi, D. C. Lee, and K. H. Lee, "Crystallization behavior and mechanical properties of poly(ethylene oxide)/poly(L-lactide)/poly(vinyl acetate) blends," *J. Appl. Polym. Sci.*, vol. 82, no. 14, pp. 3618–3626, Dec. 2001.
- [40] M. Baiardo, G. Frisoni, M. Scandola, M. Rimelen, D. Lips, K. Ruffieux, and E. Wintermantel, "Thermal and mechanical properties of plasticized poly(L-lactic acid)," *J. Appl. Polym. Sci.*, vol. 90, no. 7, pp. 1731–1738, Nov. 2003.

- [41] Z. Kulinski and E. Piorkowska, "Crystallization, structure and properties of plasticized poly(l-lactide)," *Polymer (Guildf)*., vol. 46, no. 23, pp. 10290–10300, Nov. 2005.
- [42] N. Stoehr, B. Baudrit, E. Haberstroh, M. Nase, P. Heidemeyer, and M. Bastian, "Properties and weldability of plasticized polylactic acid films," *J. Appl. Polym. Sci.*, vol. 131, no. 12, p. n/a-n/a, Jun. 2014.
- [43] N. López-Rodríguez, A. López-Arraiza, E. Meaurio, and J. R. Sarasua, "Crystallization, morphology, and mechanical behavior of polylactide/poly( $\epsilon$ -caprolactone) blends," *Polym. Eng. Sci.*, vol. 46, no. 9, pp. 1299–1308, Sep. 2006.
- [44] J.-T. Yeh, C.-J. Wu, C.-H. Tsou, W.-L. Chai, J.-D. Chow, C.-Y. Huang, K.-N. Chen, and C.-S. Wu, "Study on the Crystallization, Miscibility, Morphology, Properties of Poly(lactic acid)/Poly( $\epsilon$ -caprolactone) Blends," *Polym. Plast. Technol. Eng.*, vol. 48, no. 6, pp. 571–578, May 2009.
- [45] M. Broz, D. . VanderHart, and N. . Washburn, "Structure and mechanical properties of poly(D,L-lactic acid)/poly( $\epsilon$ -caprolactone) blends," *Biomaterials*, vol. 24, no. 23, pp. 4181–4190, Oct. 2003.
- [46] R. Malinowski, "Mechanical properties of PLA/PCL blends crosslinked by electron beam and TAIC additive," *Chem. Phys. Lett.*, vol. 662, pp. 91–96, 2016.
- [47] Y. Yang, Z. Tang, Z. Xiong, and J. Zhu, "Preparation and characterization of thermoplastic starches and their blends with poly(lactic acid)," *Int. J. Biol. Macromol.*, vol. 77, pp. 273–279, 2015.
- [48] J. Wootthikanokkhan, N. Wongta, N. Sombatsompop, A. Kositchaiyong, J. Wong-On, S. Isarankura na Ayutthaya, and N. Kaabbuathong, "Effect of blending conditions on mechanical, thermal, and rheological properties of

- plasticized poly(lactic acid)/maleated thermoplastic starch blends,” *J. Appl. Polym. Sci.*, vol. 124, no. 2, pp. 1012–1019, Apr. 2012.
- [49] L. Yu, E. Petinakis, K. Dean, H. Liu, and Q. Yuan, “Enhancing compatibilizer function by controlled distribution in hydrophobic polylactic acid/hydrophilic starch blends,” *J. Appl. Polym. Sci.*, vol. 119, no. 4, pp. 2189–2195, Feb. 2011.
- [50] J. L. Eguiburu, J. J. Iruin, M. J. Fernandez-Berridi, and J. San Román, “Blends of amorphous and crystalline polylactides with poly(methyl methacrylate) and poly(methyl acrylate): a miscibility study,” *Polymer (Guildf.)*, vol. 39, no. 26, pp. 6891–6897, Dec. 1998.
- [51] T. Shirahase, Y. Komatsu, Y. Tominaga, S. Asai, and M. Sumita, “Miscibility and hydrolytic degradation in alkaline solution of poly(l-lactide) and poly(methyl methacrylate) blends,” *Polymer (Guildf.)*, vol. 47, no. 13, pp. 4839–4844, Jun. 2006.
- [52] J. Anakabe, A. M. Zaldúa Huici, A. Eceiza, and A. Arbelaiz, “Melt blending of polylactide and poly(methyl methacrylate): Thermal and mechanical properties and phase morphology characterization,” *J. Appl. Polym. Sci.*, vol. 132, no. 42, p. n/a-n/a, Nov. 2015.
- [53] R.-M. Wang, S.-R. Zheng, and Y.-P. Zheng, “Introduction to polymer matrix composites,” in *Polymer matrix composites and technology*, Woodhead Publishing, 2011, pp. 1–548.
- [54] M. Bar, R. Alagirusamy, and A. Das, “Flame retardant polymer composites,” *Fibers Polym.*, vol. 16, no. 4, pp. 705–717, Apr. 2015.
- [55] V. Ojijo and S. S. Ray, “Nano-biocomposites based on synthetic aliphatic polyesters and nanoclay,” *Prog. Mater. Sci.*, vol. 62, pp. 1–57, 2014.
- [56] S. A. Attaran, A. Hassan, and M. U. Wahit, “Materials for food packaging

- applications based on bio-based polymer nanocomposites,” *J. Thermoplast. Compos. Mater.*, vol. 30, no. 2, pp. 143–173, Feb. 2017.
- [57] S. Pavlidou and C. D. Papaspyrides, “A review on polymer-layered silicate nanocomposites,” *Prog. Polym. Sci.*, vol. 33, no. 12, pp. 1119–1198, Dec. 2008.
- [58] H. A. Patel, R. S. Somani, H. C. Bajaj, and R. V. Jasra, “Nanoclays for polymer nanocomposites, paints, inks, greases and cosmetics formulations, drug delivery vehicle and waste water treatment,” *Bull. Mater. Sci.*, vol. 29, no. 2, pp. 133–145, Apr. 2006.
- [59] L. Peponi, D. Puglia, L. Torre, L. Valentini, and J. M. Kenny, “Processing of nanostructured polymers and advanced polymeric based nanocomposites,” *Mater. Sci. Eng. R Reports*, vol. 85, pp. 1–46, 2014.
- [60] P. Bordes, E. Pollet, and L. Averous, “Nano-biocomposites: Biodegradable polyester/nanoclay systems,” *Prog. Polym. Sci.*, vol. 34, no. 2, pp. 125–155, Feb. 2009.
- [61] M. Alexandre and P. Dubois, “Polymer-layered silicate nanocomposites: preparation, properties and uses of a new class of materials,” *Mater. Sci. Eng. R Reports*, vol. 28, no. 1–2, pp. 1–63, Jun. 2000.
- [62] D. Porter, E. Metcalfe, and M. J. K. Thomas, “Nanocomposite fire retardants—a review,” *Fire Mater.*, vol. 24, no. 1, pp. 45–52, Jan. 2000.
- [63] J. Ma, J. Xu, J.-H. Ren, Z.-Z. Yu, and Y.-W. Mai, “A new approach to polymer/montmorillonite nanocomposites,” *Polymer (Guildf.)*, vol. 44, no. 16, pp. 4619–4624, Jul. 2003.
- [64] S. Sinha Ray and M. Okamoto, “Polymer/layered silicate nanocomposites: a review from preparation to processing,” *Prog. Polym. Sci.*, vol. 28, pp. 1539–



1641, 2003.

- [65] G. Beyer, "Flame retardancy of nanocomposites - from research to reality - Review," *Polym. Polym. Compos.*, vol. 13, no. 529–537, 2005.
- [66] R. A. Vaia and E. P. Giannelis, "Polymer Melt Intercalation in Organically-Modified Layered Silicates: Model Predictions and Experiment," *Macromolecules*, vol. 30, no. 25, pp. 8000–8009, Dec. 1997.
- [67] A. B. Morgan and J. W. Gilman, "Characterization of polymer-layered silicate (clay) nanocomposites by transmission electron microscopy and X-ray diffraction: A comparative study," *J. Appl. Polym. Sci.*, vol. 87, no. 8, pp. 1329–1338, Feb. 2003.
- [68] D. L. VanderHart, A. Asano, and J. W. Gilman, "NMR Measurements Related to Clay-Dispersion Quality and Organic-Modifier Stability in Nylon-6/Clay Nanocomposites," *Macromolecules*, vol. 34, no. 12, pp. 3819–3822, Jun. 2001.
- [69] D. L. VanderHart, A. Asano, and J. W. Gilman, "Solid-State NMR Investigation of Paramagnetic Nylon-6 Clay Nanocomposites. 2. Measurement of Clay Dispersion, Crystal Stratification, and Stability of Organic Modifiers," *Chem. Mater.*, vol. 13, no. 10, pp. 3796–3809, Oct. 2001.
- [70] S. Bourbigot, D. L. VanderHart, J. W. Gilman, W. H. Awad, R. D. Davis, A. B. Morgan, and C. A. Wilkie, "Investigation of nanodispersion in polystyrene-montmorillonite nanocomposites by solid-state NMR," *J. Polym. Sci. Part B Polym. Phys.*, vol. 41, no. 24, pp. 3188–3213, Dec. 2003.
- [71] F. Samyn, S. Bourbigot, C. Jama, S. Bellayer, S. Nazare, R. Hull, A. Castrovinci, A. Fina, and G. Camino, "Crossed characterisation of polymer-layered silicate (PLS) nanocomposite morphology: TEM, X-ray diffraction, rheology and solid-state nuclear magnetic resonance measurements," *Eur.*

- Polym. J.*, vol. 44, no. 6, pp. 1642–1653, Jun. 2008.
- [72] M. Iturrondobeitia, T. Guraya, A. Okariz, V. Srot, P. A. van Aken, and J. Ibarretxe, “Quantitative electron tomography of PLA/clay nanocomposites to understand the effect of the clays in the thermal stability,” *J. Appl. Polym. Sci.*, vol. 134, no. 15, Apr. 2017.
- [73] L. S. Loo and K. K. Gleason, “Fourier Transform Infrared Investigation of the Deformation Behavior of Montmorillonite in Nylon-6/Nanoclay Nanocomposite,” *Macromolecules*, vol. 36, no. 8, pp. 2587–2590, Apr. 2003.
- [74] M. Yoonessi, H. Toghiani, T. L. Daulton, J.-S. Lin, and C. U. Pittman, “Clay Delamination in Clay/Poly(Dicyclopentadiene) Nanocomposites Quantified by Small Angle Neutron Scattering and High-Resolution Transmission Electron Microscopy,” *Macromolecules*, vol. 38, no. 3, pp. 818–831, Feb. 2005.
- [75] P. C. LeBaron, Z. Wang, and T. J. Pinnavaia, “Polymer-layered silicate nanocomposites: an overview,” *Appl. Clay Sci.*, vol. 15, no. 1, pp. 11–29, 1999.
- [76] D. Schmidt, D. Shah, and E. P. Giannelis, “New advances in polymer/layered silicate nanocomposites,” *Curr. Opin. Solid State Mater. Sci.*, vol. 6, no. 3, pp. 205–212, 2002.
- [77] F. Hussain, M. Hojjati, M. Okamoto, and R. Gorga, “Review article: Polymer-matrix Nanocomposites, Processing, Manufacturing, and Application: An Overview,” *J. Compos. Mater.*, vol. 40, no. 17, pp. 1511–1575, Jan. 2006.
- [78] S. Ray and M. Bousmina, “Biodegradable polymers and their layered silicate nanocomposites: In greening the 21st century materials world,” *Prog. Mater. Sci.*, vol. 50, no. 8, pp. 962–1079, Nov. 2005.
- [79] S. S. Ray, P. Maiti, M. Okamoto, K. Yamada, and K. Ueda, “New

- Poly lactide/Layered Silicate Nanocomposites. 1. Preparation, Characterization, and Properties,” *Macromolecules*, vol. 35, no. 8, pp. 3104–3110, Apr. 2002.
- [80] D. R. Paul and L. M. Robeson, “Polymer nanotechnology: Nanocomposites,” *Polymer (Guildf.)*, vol. 49, no. 15, pp. 3187–3204, Jul. 2008.
- [81] S. C. Tjong, “Structural and mechanical properties of polymer nanocomposites,” *Mater. Sci. Eng. R Reports*, vol. 53, no. 3–4, pp. 73–197, Aug. 2006.
- [82] M. R. Bockstaller, R. A. Mickiewicz, and E. L. Thomas, “Block Copolymer Nanocomposites: Perspectives for Tailored Functional Materials,” *Adv. Mater.*, vol. 17, no. 11, pp. 1331–1349, Jun. 2005.
- [83] G. Choudalakis and A. D. Gotsis, “Permeability of polymer/clay nanocomposites: A review,” *Eur. Polym. J.*, vol. 45, no. 4, pp. 967–984, Apr. 2009.
- [84] A. Okada and A. Usuki, “Twenty Years of Polymer-Clay Nanocomposites,” *Macromol. Mater. Eng.*, vol. 291, no. 12, pp. 1449–1476, Dec. 2006.
- [85] J. P. Chimanowsky Junior, I. L. Soares, L. Luetkmeyer, and M. I. B. Tavares, “Preparation of high-impact polystyrene nanocomposites with organoclay by melt intercalation and characterization by low-field nuclear magnetic resonance,” *Chem. Eng. Process. Process Intensif.*, vol. 77, pp. 66–76, 2014.
- [86] J. Tan, X. Wang, Y. Luo, and D. Jia, “Rubber/clay nanocomposites by combined latex compounding and melt mixing: A masterbatch process,” *Mater. Des.*, vol. 34, pp. 825–831, 2012.
- [87] Z. Gu, G. Song, W. Liu, B. Wang, and J. Li, “Preparation and properties of organo-montmorillonite/cis-1,4-polybutadiene rubber nanocomposites by

- solution intercalation,” *Appl. Clay Sci.*, vol. 45, no. 1, pp. 50–53, 2009.
- [88] S. Labidi, N. Azema, D. Perrin, and J.-M. Lopez-Cuesta, “Organo-modified montmorillonite/poly( $\epsilon$ -caprolactone) nanocomposites prepared by melt intercalation in a twin-screw extruder,” *Polym. Degrad. Stab.*, vol. 95, no. 3, pp. 382–388, 2010.
- [89] L. Unnikrishnan, S. Mohanty, S. K. Nayak, and A. Ali, “Preparation and characterization of poly(methyl methacrylate)–clay nanocomposites via melt intercalation: Effect of organoclay on thermal, mechanical and flammability properties,” *Mater. Sci. Eng. A*, vol. 528, no. 12, pp. 3943–3951, 2011.
- [90] Z. Shen, G. P. Simon, and Y.-B. Cheng, “Comparison of solution intercalation and melt intercalation of polymer–clay nanocomposites,” *Polymer (Guildf.)*, vol. 43, no. 15, pp. 4251–4260, 2002.
- [91] D. J. Pochan and K. Vahik, “Poly (l-Lactic Acid)/Layered Silicate Nanocomposite: Fabrication, Characterization, and Properties,” *Chem. Mater.*, vol. 15, no. 22, pp. 4317–4324, 2003.
- [92] J. Liu, K. Zhou, P. Wen, B. Wang, Y. Hu, and Z. Gui, “The influence of multiple modified MMT on the thermal and fire behavior of poly (lactic acid) nanocomposites,” *Polym. Adv. Technol.*, vol. 26, no. 6, pp. 626–634, Jun. 2015.
- [93] M. Pluta, J. K. Jeszka, and G. Boiteux, “Polylactide/montmorillonite nanocomposites: Structure, dielectric, viscoelastic and thermal properties,” *Eur. Polym. J.*, vol. 43, no. 7, pp. 2819–2835, Jul. 2007.
- [94] M. Pluta, A. Galeski, M. Alexandre, M.-A. Paul, and P. Dubois, “Polylactide/montmorillonite nanocomposites and microcomposites prepared by melt blending: Structure and some physical properties,” *J. Appl. Polym. Sci.*, vol. 86, no. 6, pp. 1497–1506, Nov. 2002.

- [95] J.-H. Chang, Y. U. An, and G. S. Sur, "Poly(lactic acid) nanocomposites with various organoclays. I. Thermomechanical properties, morphology, and gas permeability," *J. Polym. Sci. Part B Polym. Phys.*, vol. 41, no. 1, pp. 94–103, Jan. 2003.
- [96] P. Maiti, K. Yamada, M. Okamoto, K. Ueda, and K. Okamoto, "New Polylactide/Layered Silicate Nanocomposites: Role of Organoclays," *Chem. Mater.*, vol. 14, no. 11, pp. 4654–4661, Nov. 2002.
- [97] M.-A. Paul, M. Alexandre, P. Degée, C. Henrist, A. Rulmont, and P. Dubois, "New nanocomposite materials based on plasticized poly(l-lactide) and organo-modified montmorillonites: thermal and morphological study," *Polymer (Guildf.)*, vol. 44, no. 2, pp. 443–450, Jan. 2003.
- [98] L. Di Maio, E. Garofalo, P. Scarfato, and L. Incarnato, "Effect of polymer/organoclay composition on morphology and rheological properties of polylactide nanocomposites," *Polym. Compos.*, vol. 36, no. 6, pp. 1135–1144, Jun. 2015.
- [99] K. Piekarska, P. Sowinski, E. Piorkowska, M. M.-U. Haque, and M. Pracella, "Structure and properties of hybrid PLA nanocomposites with inorganic nanofillers and cellulose fibers," *Compos. Part A Appl. Sci. Manuf.*, vol. 82, pp. 34–41, Mar. 2016.
- [100] R. Arjmandi, A. Hassan, S. J. Eichhorn, M. K. Mohamad Haafiz, Z. Zakaria, and F. A. Tanjung, "Enhanced ductility and tensile properties of hybrid montmorillonite/cellulose nanowhiskers reinforced polylactic acid nanocomposites," *J. Mater. Sci.*, vol. 50, no. 8, pp. 3118–3130, Apr. 2015.
- [101] J. Trifol, D. Plackett, C. Sillard, P. Szabo, J. Bras, and A. E. Daugaard, "Hybrid poly(lactic acid)/nanocellulose/nanoclay composites with synergistically enhanced barrier properties and improved thermomechanical

- resistance,” *Polym. Int.*, vol. 65, no. 8, pp. 988–995, Aug. 2016.
- [102] R. Arjmandi, A. Hassan, M. K. M. Haafiz, Z. Zakaria, and M. S. Islam, “Effect of hydrolysed cellulose nanowhiskers on properties of montmorillonite/polylactic acid nanocomposites,” *Int. J. Biol. Macromol.*, vol. 82, pp. 998–1010, Jan. 2016.
- [103] B.-U. Nam, K.-D. Min, and Y. Son, “Investigation of the nanostructure, thermal stability, and mechanical properties of polylactic acid/cellulose acetate butyrate/clay nanocomposites,” *Mater. Lett.*, vol. 150, pp. 118–121, Jul. 2015.
- [104] H. Kaya, E. Ozdemir, C. Kaynak, and J. Hacaloglu, “Effects of nanoparticles on thermal degradation of polylactide/aluminium diethylphosphinate composites,” *J. Anal. Appl. Pyrolysis*, vol. 118, pp. 115–122, 2016.
- [105] R. Salehiyan, A. A. Yussuf, N. F. Hanani, A. Hassan, and A. Akbari, “Polylactic acid/polycaprolactone nanocomposite: Influence of montmorillonite and impact modifier on mechanical, thermal, and morphological properties,” *J. Elastomers Plast.*, vol. 47, no. 1, pp. 69–87, Feb. 2015.
- [106] R. Salehiyan and K. Hyun, “Effect of organoclay on non-linear rheological properties of poly(lactic acid)/poly(caprolactone) blends,” *Korean J. Chem. Eng.*, vol. 30, no. 5, pp. 1013–1022, May 2013.
- [107] Z. Yu, J. Yin, S. Yan, Y. Xie, J. Ma, and X. Chen, “Biodegradable poly(l-lactide)/poly( $\epsilon$ -caprolactone)-modified montmorillonite nanocomposites: Preparation and characterization,” *Polymer (Guildf.)*, vol. 48, no. 21, pp. 6439–6447, 2007.
- [108] W. H. Hoidy, E. A. J. Al-Mulla, and K. W. Al-Janabi, “Mechanical and Thermal Properties of PLLA/PCL Modified Clay Nanocomposites,” *J. Polym. Environ.*, vol. 18, no. 4, pp. 608–616, Dec. 2010.

- [109] S. S. Sabet and A. A. Katbab, "Interfacially compatibilized poly(lactic acid) and poly(lactic acid)/polycaprolactone/organoclay nanocomposites with improved biodegradability and barrier properties: Effects of the compatibilizer structural parameters and feeding route," *J. Appl. Polym. Sci.*, vol. 111, no. 4, pp. 1954–1963, Feb. 2009.
- [110] S. Rodriguez-Llamazares, B. L. Rivas, M. Perez, and F. Perrin-Sarazin, "Poly(ethylene glycol) as a compatibilizer and plasticizer of poly(lactic acid)/clay nanocomposites," *High Perform. Polym.*, vol. 24, no. 4, pp. 254–261, Jun. 2012.
- [111] S. Gumus, G. Ozkoc, and A. Aytac, "Plasticized and unplasticized PLA/organoclay nanocomposites: Short- and long-term thermal properties, morphology, and nonisothermal crystallization behavior," *J. Appl. Polym. Sci.*, vol. 123, no. 5, pp. 2837–2848, Mar. 2012.
- [112] National Research Council, *Polymer Science and Engineering: The Shifting Research Frontiers*. Washington, D.C.: National Academies Press, 1994.
- [113] Q. Baojun, P. Ding, and W. Zhenqiou, "The mechanism and characteristics of dry-jet wet-spinning of acrylic fibers," *Adv. Polym. Technol.*, vol. 6, no. 4, pp. 509–529, 1986.
- [114] A. Baji, Y.-W. Mai, S.-C. Wong, M. Abtahi, and P. Chen, "Electrospinning of polymer nanofibers: Effects on oriented morphology, structures and tensile properties," *Compos. Sci. Technol.*, vol. 70, no. 5, pp. 703–718, 2010.
- [115] D. Li and Y. Xia, "Electrospinning of Nanofibers: Reinventing the Wheel?," *Adv. Mater.*, vol. 16, no. 14, pp. 1151–1170, Jul. 2004.
- [116] R. Khajavi and M. Abbasipour, "Electrospinning as a versatile method for fabricating coreshell, hollow and porous nanofibers," *Sci. Iran.*, vol. 19, no. 6, pp. 2029–2034, 2012.

- [117] D. Li and Y. Xia, "Direct Fabrication of Composite and Ceramic Hollow Nanofibers by Electrospinning," *Nano Lett.*, vol. 4, no. 5, pp. 933–938, May 2004.
- [118] A. Greiner and J. H. Wendorff, "Electrospinning: A Fascinating Method for the Preparation of Ultrathin Fibers," *Angew. Chemie Int. Ed.*, vol. 46, no. 30, pp. 5670–5703, Jul. 2007.
- [119] J.-F. Zhang, D.-Z. Yang, F. Xu, Z.-P. Zhang, R.-X. Yin, and J. Nie, "Electrospun Core–Shell Structure Nanofibers from Homogeneous Solution of Poly(ethylene oxide)/Chitosan," *Macromolecules*, vol. 42, no. 14, pp. 5278–5284, Jul. 2009.
- [120] P. Heikkilä and A. Harlin, "Parameter study of electrospinning of polyamide-6," *Eur. Polym. J.*, vol. 44, no. 10, pp. 3067–3079, Oct. 2008.
- [121] J. . Deitzel, J. Kleinmeyer, D. Harris, and N. . Beck Tan, "The effect of processing variables on the morphology of electrospun nanofibers and textiles," *Polymer (Guildf.)*, vol. 42, no. 1, pp. 261–272, Jan. 2001.
- [122] J. Zhang and J. Nie, "Transformation of complex internal structures of poly(ethylene oxide)/chitosan oligosaccharide electrospun nanofibers," *Polym. Int.*, vol. 61, no. 1, pp. 135–140, Jan. 2012.
- [123] K. E. Perepelkin, "Polylactide Fibres: Fabrication, Properties, Use, Prospects. A Review," *Fibre Chem.*, vol. 34, no. 2, pp. 85–100, 2002.
- [124] B. Gupta, N. Revagade, N. Anjum, B. Atthoff, and J. Hilborn, "Preparation of poly(lactic acid) fiber by dry–jet–wet spinning. II. Effect of process parameters on fiber properties," *J. Appl. Polym. Sci.*, vol. 101, no. 6, pp. 3774–3780, Sep. 2006.
- [125] B. Gupta, N. Revagade, and J. Hilborn, "Poly(lactic acid) fiber: An overview,"



- Prog. Polym. Sci.*, vol. 32, no. 4, pp. 455–482, 2007.
- [126] L. Fambri, A. Pegoretti, R. Fenner, S. D. Incardona, and C. Migliaresi, “Biodegradable fibres of poly(l-lactic acid) produced by melt spinning,” *Polymer (Guildf.)*, vol. 38, no. 1, pp. 79–85, Jan. 1997.
- [127] X. Yuan, A. F. T. Mak, K. W. Kwok, B. K. O. Yung, and K. Yao, “Characterization of poly(L-lactic acid) fibers produced by melt spinning,” *J. Appl. Polym. Sci.*, vol. 81, no. 1, pp. 251–260, Jul. 2001.
- [128] O. Baykuş, Ş. D. Dogan, U. Tayfun, A. Davulcu, and M. Dogan, “Improving the dyeability of poly (lactic acid) fiber using octa (aminophenyl) POSS nanoparticle during melt spinning,” *J. Text. Inst.*, vol. 108, no. 4, pp. 569–578, Apr. 2017.
- [129] I. Horáček and V. Kalíšek, “Polylactide. II. Discontinuous dry spinning–hot drawing preparation of fibers,” *J. Appl. Polym. Sci.*, vol. 54, no. 11, pp. 1759–1765, Dec. 1994.
- [130] B. Gupta, N. Revagade, N. Anjum, B. Atthoff, and J. Hilborn, “Preparation of poly(lactic acid) fiber by dry-jet-wet-spinning. I. Influence of draw ratio on fiber properties,” *J. Appl. Polym. Sci.*, vol. 100, no. 2, pp. 1239–1246, Apr. 2006.
- [131] K. Bruckmoser and K. Resch, “Effect of processing conditions on crystallization behavior and mechanical properties of poly(lactic acid) staple fibers,” *J. Appl. Polym. Sci.*, vol. 132, no. 33, p. n/a-n/a, Sep. 2015.
- [132] M. Ma and W. Zhou, “Improving the Hydrolysis Resistance of Poly(lactic acid) Fiber by Hydrophobic Finishing,” *Ind. Eng. Chem. Res.*, vol. 54, no. 10, pp. 2599–2605, Mar. 2015.
- [133] U. Tayfun and M. Dogan, “Improving the dyeability of poly(lactic acid) fiber

- using organoclay during melt spinning,” *Polym. Bull.*, vol. 73, no. 6, pp. 1581–1593, Jun. 2016.
- [134] R. Casasola, N. L. Thomas, A. Trybala, and S. Georgiadou, “Electrospun poly lactic acid (PLA) fibres: Effect of different solvent systems on fibre morphology and diameter,” *Polymer (Guildf.)*, vol. 55, no. 18, pp. 4728–4737, Sep. 2014.
- [135] F. Yang, R. Murugan, S. Wang, and S. Ramakrishna, “Electrospinning of nano/micro scale poly(l-lactic acid) aligned fibers and their potential in neural tissue engineering,” *Biomaterials*, vol. 26, no. 15, pp. 2603–2610, May 2005.
- [136] L. Li, R. Hashaikeh, and H. A. Arafat, “Development of eco-efficient micro-porous membranes via electrospinning and annealing of poly (lactic acid),” *J. Memb. Sci.*, vol. 436, pp. 57–67, Jun. 2013.
- [137] T. Lu, X. Jing, X. Song, and X. Wang, “Doxorubicin-loaded ultrafine PEG-PLA fiber mats against hepatocarcinoma,” *J. Appl. Polym. Sci.*, vol. 123, no. 1, pp. 209–217, Jan. 2012.
- [138] L. M. Buttaro, E. Drufva, and M. W. Frey, “Phase separation to create hydrophilic yet non-water soluble PLA/PLA-b-PEG fibers via electrospinning,” *J. Appl. Polym. Sci.*, vol. 131, no. 19, p. n/a-n/a, Oct. 2014.
- [139] X. Xu, X. Chen, Z. Wang, and X. Jing, “Ultrafine PEG–PLA fibers loaded with both paclitaxel and doxorubicin hydrochloride and their in vitro cytotoxicity,” *Eur. J. Pharm. Biopharm.*, vol. 72, no. 1, pp. 18–25, May 2009.
- [140] A. Toncheva, R. Mincheva, M. Kancheva, N. Manolova, I. Rashkov, P. Dubois, and N. Markova, “Antibacterial PLA/PEG electrospun fibers: Comparative study between grafting and blending PEG,” *Eur. Polym. J.*, vol. 75, pp. 223–233, Feb. 2016.

- [141] T. Nazari and H. Garmabi, "Thermo-rheological and interfacial properties of polylactic acid/polyethylene glycol blends toward the melt electrospinning ability," *J. Appl. Polym. Sci.*, vol. 133, no. 44, Nov. 2016.
- [142] W. Yang, N. He, J. Fu, Z. Li, and X. Ji, "Preparation of Porous Core–Shell Poly L-Lactic Acid/Polyethylene Glycol Superfine Fibres Containing Drug," *J. Nanosci. Nanotechnol.*, vol. 15, no. 12, pp. 9911–9917, Dec. 2015.
- [143] E. Llorens, L. J. del Valle, R. Ferrán, A. Rodríguez-Galán, and J. Puiggali, "Scaffolds with tuneable hydrophilicity from electrospun microfibers of polylactide and poly(ethylene glycol) mixtures: morphology, drug release behavior, and biocompatibility," *J. Polym. Res.*, vol. 21, no. 2, p. 360, Feb. 2014.
- [144] M. L. Dias, R. M. M. Dip, D. H. S. Souza, J. P. Nascimento, A. P. Santos, and C. A. Furtado, "Electrospun Nanofibers of Poly(lactic acid)/Graphene Nanocomposites," *J. Nanosci. Nanotechnol.*, vol. 17, no. 4, pp. 2531–2540, Apr. 2017.
- [145] M. Rahmat, M. Karrabi, I. Ghasemi, M. Zandi, and H. Azizi, "Silane crosslinking of electrospun poly (lactic acid)/nanocrystalline cellulose bionanocomposite," *Mater. Sci. Eng. C*, vol. 68, pp. 397–405, Nov. 2016.
- [146] N. Cai, Q. Dai, Z. Wang, X. Luo, Y. Xue, and F. Yu, "Preparation and properties of nanodiamond/poly(lactic acid) composite nanofiber scaffolds," *Fibers Polym.*, vol. 15, no. 12, pp. 2544–2552, Dec. 2014.
- [147] H. T. Au, L. N. Pham, T. H. T. Vu, and J. S. Park, "Fabrication of an antibacterial non-woven mat of a poly(lactic acid)/chitosan blend by electrospinning," *Macromol. Res.*, vol. 20, no. 1, pp. 51–58, Jan. 2012.
- [148] C. Liu, J. Shen, K. W. K. Yeung, and S. C. Tjong, "Development and Antibacterial Performance of Novel Polylactic Acid-Graphene Oxide-Silver

- Nanoparticle Hybrid Nanocomposite Mats Prepared By Electrospinning,” *ACS Biomater. Sci. Eng.*, vol. 3, no. 3, pp. 471–486, Mar. 2017.
- [149] O. J. Yoon, C. Y. Jung, I. Y. Sohn, H. J. Kim, B. Hong, M. S. Jhon, and N.-E. Lee, “Nanocomposite nanofibers of poly(d, l-lactic-co-glycolic acid) and graphene oxide nanosheets,” *Compos. Part A Appl. Sci. Manuf.*, vol. 42, no. 12, pp. 1978–1984, Dec. 2011.
- [150] T. Yang, D. Wu, L. Lu, W. Zhou, and M. Zhang, “Electrospinning of polylactide and its composites with carbon nanotubes,” *Polym. Compos.*, vol. 32, no. 8, pp. 1280–1288, Aug. 2011.
- [151] F. A. S. Pereira, G. N. Salles, B. V. M. Rodrigues, F. R. Marciano, C. Pacheco-Soares, and A. O. Lobo, “Diamond nanoparticles into poly (lactic acid) electrospun fibers: Cytocompatible and bioactive scaffolds with enhanced wettability and cell adhesion,” *Mater. Lett.*, vol. 183, pp. 420–424, Nov. 2016.
- [152] Y. Zhu, C. Li, and P. Cebe, “Poly(lactides) co-electrospun with carbon nanotubes: thermal and cell culture properties,” *Eur. Polym. J.*, vol. 75, pp. 565–576, Feb. 2016.
- [153] Y. Kong, J. Yuan, Z. Wang, and J. Qiu, “Study on the preparation and properties of aligned carbon nanotubes/polylactide composite fibers,” *Polym. Compos.*, vol. 33, no. 9, pp. 1613–1619, Sep. 2012.
- [154] F. Mei, J. Zhong, X. Yang, X. Ouyang, S. Zhang, X. Hu, Q. Ma, J. Lu, S. Ryu, and X. Deng, “Improved Biological Characteristics of Poly( l -Lactic Acid) Electrospun Membrane by Incorporation of Multiwalled Carbon Nanotubes/Hydroxyapatite Nanoparticles,” *Biomacromolecules*, vol. 8, no. 12, pp. 3729–3735, Dec. 2007.
- [155] S. Shao, S. Zhou, L. Li, J. Li, C. Luo, J. Wang, X. Li, and J. Weng,

- “Osteoblast function on electrically conductive electrospun PLA/MWCNTs nanofibers,” *Biomaterials*, vol. 32, no. 11, pp. 2821–2833, Apr. 2011.
- [156] Y. H. Lee, J. H. Lee, I.-G. An, C. Kim, D. S. Lee, Y. K. Lee, and J.-D. Nam, “Electrospun dual-porosity structure and biodegradation morphology of Montmorillonite reinforced PLLA nanocomposite scaffolds,” *Biomaterials*, vol. 26, no. 16, pp. 3165–3172, Jun. 2005.
- [157] A. M. Goes, S. Carvalho, R. L. Oréface, L. Avérous, T. A. Custódio, J. G. Pimenta, M. de B. Souza, M. C. Branciforti, and R. E. S. Bretas, “Cell Viability of Nanofibers from Biodegradable Polymers and their Nanocomposites with Montmorillonite,” *Polímeros*, vol. 22, no. 1, pp. 34–41, 2012.
- [158] J. Alongi and M. Poskovic, “Influence of nanoparticles on the morphology, thermal stability and air permeability of electrospun polylactic-acid fibres,” *e-Polymers*, vol. 11, no. 1, 2001.
- [159] N. Zhao, S. Shi, G. Lu, and M. Wei, “Polylactide (PLA)/layered double hydroxides composite fibers by electrospinning method,” *J. Phys. Chem. Solids*, vol. 69, no. 5–6, pp. 1564–1568, May 2008.
- [160] H. J. Haroosh, D. S. Chaudhary, and Y. Dong, “Electrospun PLA/PCL fibers with tubular nanoclay: Morphological and structural analysis,” *J. Appl. Polym. Sci.*, vol. 124, no. 5, pp. 3930–3939, Jun. 2012.
- [161] E. Ozdemir and J. Hacıoğlu, “Polylactide/organically modified montmorillonite composite fibers,” *J. Anal. Appl. Pyrolysis*, vol. 124, pp. 186–194, Mar. 2017.
- [162] E. Ozdemir, T. O. Lekeşiz, and J. Hacıoğlu, “Polylactide/organically modified montmorillonite composites; effects of organic modifier on thermal characteristics,” *Polym. Degrad. Stab.*, vol. 134, pp. 87–96, Dec. 2016.

- [163] “STA 6000 Simultaneous Thermal Analyzer.” [Online]. Available: [http://www.perkinelmer.com/Content/RelatedMaterials/Brochures/BRO\\_STA-6000.pdf](http://www.perkinelmer.com/Content/RelatedMaterials/Brochures/BRO_STA-6000.pdf). [Accessed: 28-May-2017].
- [164] J. Hacaloglu, “Direct Insertion Probe Mass Spectrometry of Polymers,” *Adv. Polym. Sci.*, vol. 248, pp. 69–103, 2011.
- [165] E. Ozdemir, T. Tinçer, and J. Hacaloglu, “Characterization of polylactide/poly(ethylene glycol) blends via direct pyrolysis mass spectrometry,” *J. Anal. Appl. Pyrolysis*, vol. 122, 2016.
- [166] E. Ozdemir and J. Hacaloglu, “Characterizations of PLA-PEG blends involving organically modified montmorillonite,” *J. Anal. Appl. Pyrolysis*, 2017.
- [167] E. Ozdemir and J. Hacaloglu, “Thermal degradation of polylactide and its electrospun fiber,” *Fibers Polym.*, vol. 17, no. 1, pp. 66–73, Jan. 2016.
- [168] B.-K. Chen, C.-C. Shih, and A. F. Chen, “Ductile PLA nanocomposites with improved thermal stability,” *Compos. Part A Appl. Sci. Manuf.*, vol. 43, no. 12, pp. 2289–2295, Dec. 2012.
- [169] M. M. Fares, J. Hacaloglu, and S. Suzer, “Characterization of degradation products of polyethylene oxide by pyrolysis mass spectrometry,” *Eur. Polym. J.*, vol. 30, no. 7, pp. 845–850, Jul. 1994.
- [170] T. Uyar, A. E. Tonelli, and J. Hacaloglu, “Thermal degradation of polycarbonate, poly(vinyl acetate) and their blends,” *Polym. Degrad. Stab.*, vol. 91, no. 12, pp. 2960–2967, Dec. 2006.
- [171] M. Pluta, M.-A. Paul, M. Alexandre, and P. Dubois, “Plasticized polylactide/clay nanocomposites. I. The role of filler content and its surface organo-modification on the physico-chemical properties,” *J. Polym. Sci. Part*

*B Polym. Phys.*, vol. 44, no. 2, pp. 299–311, Jan. 2006.

- [172] M. P. Arrieta, F. Parres, J. López, and A. Jiménez, “Development of a novel pyrolysis-gas chromatography/mass spectrometry method for the analysis of poly(lactic acid) thermal degradation products,” *J. Anal. Appl. Pyrolysis*, vol. 101, pp. 150–155, May 2013.
- [173] O. Ero-Phillips, M. Jenkins, and A. Stamboulis, “Tailoring Crystallinity of Electrospun Plla Fibres by Control of Electrospinning Parameters,” *Polymers (Basel)*., vol. 4, no. 4, pp. 1331–1348, Jun. 2012.
- [174] X. Zong, K. Kim, D. Fang, S. Ran, B. S. Hsiao, and B. Chu, “Structure and process relationship of electrospun bioabsorbable nanofiber membranes,” *Polymer (Guildf)*., vol. 43, no. 16, pp. 4403–4412, Jul. 2002.
- [175] W. Cui, X. Li, X. Zhu, G. Yu, S. Zhou, and J. Weng, “Investigation of Drug Release and Matrix Degradation of Electrospun Poly( dl -lactide) Fibers with Paracetamol Inoculation,” *Biomacromolecules*, vol. 7, no. 5, pp. 1623–1629, May 2006.
- [176] Xinhua Zong, Shaofeng Ran, Kwang-Sok Kim, Dufei Fang, and Benjamin S. Hsiao, and Benjamin Chu\*, “Structure and Morphology Changes during in Vitro Degradation of Electrospun Poly(glycolide-co-lactide) Nanofiber Membrane,” 2003.
- [177] E. Ozdemir and J. Hacaloglu, “Poly(methyl methacrylate) organoclay composites; interactions of organic modifier with the polymer effecting thermal degradation behavior,” *Eur. Polym. J.*, vol. 95, 2017.





## CURRICULUM VITAE

**Name and Surname** : Esra Özdemir  
**Date of Birth** : 20/09/1988  
**Sex** : Female  
**Marital Status** : Single  
**Nationality** : Republic of Turkey  
**Address** : Çankaya/Ankara/Turkey  
**Telephone** : +90 544 807 04 91  
**e-mail** : esraozdemir@gmx.com

### EDUCATION

**2014 –2017:** **Doctor of Philosophy, Ph.D**

Middle East Technical University, METU

*Polymer Science and Technology*

- Thesis Title: Poly(lactic acid) blends, composites and fibers and direct pyrolysis mass spectrometry for nanoclay composites mass spectrometry

**2012 –2014:** **Master of Science, MS**

Middle East Technical University, METU

*Polymer Science and Technology*

- Thesis Title: The effects of amount and type of organically modified montmorillonites on thermal degradation behaviors and mechanical properties of poly(lactic acid)

**2007 –2012:**       **Bachelor of Science, BS**  
Middle East Technical University, METU  
*Chemistry*

**2002 –2006:**       **High School Degree**  
Edirne Anatolian High School  
*Science and Mathematics*

## **RESEARCH EXPERIENCE**

**2017 –ongoing:**   **Project Researcher,**  
Scientific and Technological Research Council, TÜBİTAK

- Project Title: The use of boron compounds as a crosslinking-agent in polymers involving ester group, their nanocomposites and fibers

**2015 –2016:**       **Project Researcher,**  
Scientific and Technological Research Council, TÜBİTAK

- Project Title: Investigation the effect of pumice powders and synergistic effects of flame retardants on thermal properties of polymers

**2012 –2014:**       **Project Researcher,**  
Scientific and Technological Research Council, TÜBİTAK

- Project Title: Thermal and mechanical characterization of nanocomposites and nanocomposite fibers of poly(lactic acid) and poly(lactic acid)/poly(ethylene glycol)

## **INSTRUMENTAL EXPERIENCE**

- Twin-screw extruder
- Injection molding
- Compression molding
- Tensile tester instrument
- Charpy impact tester
- Direct pyrolysis mass spectrometry (DP-MS)
- Thermogravimetry (TGA)
- Differential scanning calorimetry (DSC)
- X-ray diffractometry (XRD)
- Gel permeation chromatography (GPC)

## **IT SKILLS**

**MS Office Programs**      ▪ Word, Excel, PowerPoint

**Scientific Tools**      ▪ ChemDraw  
                                  ▪ Pyris Manager  
                                  ▪ MassLynx DPMS  
                                  ▪ MSD ChemStation  
                                  ▪ IgorPro

## **PUBLICATIONS & PRESENTATIONS**

### **• Publications in Peer-Reviewed Journals**

1. Ozdemir, E. & Hacaloglu, J., The use of direct probe pyrolysis mass spectrometry to characterize the polymer/nanoclay composites, (manuscript in preparation).

2. Ozdemir, E. & Hacaloglu, J., Thermal degradation of polylactide/poly(ethylene glycol) fibers and composite fibers involving organoclay, *Journal of Analytical and Applied Pyrolysis*, (article in press).
3. Ozdemir, E. & Hacaloglu, J., Poly(methyl methacrylate) organoclay composites; interactions of organic modifier with the polymer effecting thermal degradation behavior, *European Polymer Journal*, 95 (2017) 474-481.
4. Ozdemir, E. & Hacaloglu, J., Characterizations of PLA-PEG blends involving organically modified montmorillonite, *Journal of Analytical and Applied Pyrolysis*, 127 (2017) 343-349.
5. Ozdemir, E. & Hacaloglu, J., Polylactide/organically modified montmorillonite composite fibers, *Journal of Analytical and Applied Pyrolysis*, 124 (2017) 186-194.
6. Ozdemir, E., Tinçer, T., & Hacaloglu, J., Characterization of polylactide/poly(ethylene glycol) blends via direct pyrolysis mass spectrometry, *Journal of Analytical and Applied Pyrolysis*, 122 (2016) 315–322.
7. Ozdemir, E., Lekesiz, T. O., & Hacaloglu, J., Polylactide/organically modified montmorillonite composites; effects of organic modifier on thermal characteristics, *Polymer Degradation and Stability*, 134 (2016) 87–96.
8. Ozdemir, E. & Hacaloglu, J., Thermal degradation of polylactide and its electrospun fiber, *Fibers and Polymers*, 17 (2016) 66–73.
9. Kaya, H., Ozdemir, E., Kaynak, C., & Hacaloglu, J., Effects of nanoparticles on thermal degradation of polylactide/aluminum diethylphosphate composites, *Journal of Analytical and Applied Pyrolysis*, 118 (2016) 115–122.

• **Oral Presentations in Conferences**

1. Ozdemir, E. & Hacaloglu, J., Use of Direct Pyrolysis Mass Spectrometry for Morphological Characterizations of Polymer/Nanoclay Composites, 29th National Chemistry Congress, 10-14 September 2017, Ankara, Turkey
2. Ozdemir, E., Ozkan, B. & Hacaloglu, J., The Effects of Nanoclays on Thermal Degradation of Polylactide via Direct Pyrolysis Mass Spectrometry, ISPAC 2014, 27th International Symposium on Polymer Analysis and Characterization, 16-18 June, 2014, Les Diablerets, Switzerland

- **Poster Presentations in Conferences**

1. Ozdemir, E., & Hacıoğlu, J., Nanocomposites and Nanocomposite Fibers of Poly(lactic acid) (PLA)/Polyethylene Glycol (PEG) Blends, Nanong'16 International Conference: Nanoscience and Nanotechnology for Next Generation, 20-22 October, 2016, Antalya, Turkey
2. Ozdemir, E., Tincer T., & Hacıoğlu, J., Thermal and Mechanical Characterizations of Poly(lactic acid)/nanoclay Composites, V. National Polymer Science and Technology Congress, 1-4 September, 2014, Tokat, Turkey
3. Orhan Lekesiz, T., Ozdemir, E., Tincer, T. & Hacıoğlu, J., Preparation and Characterization of Polylactide/Montmorillonite Composites, ICCE 22nd International Conference on Composites/Nano Engineering, 13-19 July, 2014, Malta.
4. Ozdemir, E., Ozkan, B., & Hacıoğlu, J., Analysis of Polylactide via Direct Pyrolysis Mass Spectrometry, ISPAC 2014 27th International Symposium on Polymer Analysis and Characterization, 16-18 June, 2014, Les Diablerets, Switzerland
5. Ozdemir, E., Ozkan, B., & Hacıoğlu, J., The Effects of Nanoclays on Thermal Degradation of Polylactide via Direct Pyrolysis Mass Spectrometry, ISPAC 2014 27th International Symposium on Polymer Analysis and Characterization, 16-18 June, 2014, Les Diablerets, Switzerland
6. Ozkan, B., Ozdemir, E., Orhan Lekesiz, T., & Hacıoğlu, J., Direct Pyrolysis Mass Spectrometry Analyses of Polylactide, PDDG Conference 2013 Polymer Degradation and Stability, 1-4 September, 2013, Paris, France
7. Yalcinkaya H., Ozdemir, E., Isitman, N.A., Kaynak, C., & Hacıoğlu, J., Poly(lactic acid)/Clay Nanocomposites, IUPAC 10th International Conference on Advanced Polymers via Macromolecular Engineering, 18-22 August 2013, Durham, England
8. Ozkan, B., Ozdemir, E., Orhan Lekesiz, T., & Hacıoğlu, J., Polylactide and Poly(ethylene glycol) Blends and Copolymers, IUPAC 10th International Conference on Advanced Polymers via Macromolecular Engineering, 18-22 August 2013, Durham, England
9. Ozkan, B., Ozdemir, E., & Hacıoğlu, J., Direct Pyrolysis Mass Spectrometry Analysis of Polymers, Copolymers and Fibers of Polylactide, Sustainable Polymers, 20-23 May 2013, Safety Harbor, Florida, USA